Summer 2019

Effect of TCDD, an Environmental Contaminant, on Activation of AHR Leading to Induction of Myeloid Derived Suppressor Cells (MDSCS) and the Ability of Resveratrol, a Botanical, to Neutralize this Effect

Wurood Hantoosh Neamah

EFFECT OF TCDD, AN ENVIRONMENTAL CONTAMINANT, ON ACTIVATION OF AHR LEADING TO INDUCTION OF MYELOID DERIVED SUPPRESSOR CELLLS (MDSCS) AND THE ABILITY OF RESVERATROL, A BOTANICAL, TO NEUTRALIZE THIS EFFECT

By

Wurood Hantoosh Neamah

Master of Agricultural Science
University of Basra 2010

Submitted in Partial Fulfillment of the Requirements

For the Degree of Doctor of Philosophy in

Biomedical Science

School of Medicine

University of South Carolina

2019

Accepted by

Mitzi Nagarkatti, Major Professor

Prakash Nagarkatti, Chairman, Examining Committee

Narendra Singh, Committee Member

Taixing Cui, Committee Member

Saurabh Chatterjee, Committee Member

Cheryl L. Addy, Vice Provost and Dean of the Graduate School

DEDICATION

I would like to dedicate this work to my country, my mentors, my family, my father's soul, my friends and to all those who were martyred in defense of Iraqi land.

ACKNOWLEDGEMENTS

As I near the achievement of part of my dream and graduate from the University of South Carolina School of Medicine, I would like to thank a multitude of people who helped me to accomplish my ambition and obtain a good education and good skills in the biomedical sciences field.

First, I would like to thank my sponsor, Ministry of Higher Education and Scientific Research (MOHESR) in Iraq for its support that has created a good ambiance for living and studying in US. I am thankful to my mentors, Dr. Mitzi Nagarkatti and Dr. Prakash Nagarkatti for their support and guidance. It is through their generosity and kindness bestowed upon a naïve person like me that provided the opportunity to learn and work in their labs. With that, I want to thank my committee members, Dr. Narendra Singh, Dr. Taixing Cui, and Dr. Saurabh Chatterjee for their guidance. I am thankful to all people who are currently working or have worked in the past, under the leadership of the Ngarkattis, including all the graduate students, Osama Abdudalla, Esraah Al-Harris, Zinah Al-Ghezi, Kathryn Miranda, Muthanna Sultan, William Baker, Haider Al-Rafas, Amira Mohammed, Nicolas Dopkins, Alkeiver Cannon and, Bryan Holloman as well as Post docs, Brandon Busbee, Marpe Bam, Xiaoming Yang, Alex Rutkovsky and, Courtney Culpepper. Thanks are also due to our technician, Yin Zhong. Special thanks to Dr. Singh, Dr. Hasan and previous PhD student, Jessica Sido.

I would like to thank people who are working in Iraqi Cultural Attaché for their support and assistance. Finally, I would like to thank from my deep heart each member in my

family, my mother, my brother, my sisters, my uncles, my aunts, my nephews and my nieces.

ABSTRACT

Aryl hydrocarbon receptor (AhR), is a ligand-activated transcription factor that integrates environmental, dietary, microbial and metabolic cues to control various cellular processes, such as the cell cycle, epithelial barrier function, cell migration and immune function. AhR was discovered as the receptor that binds with high affinity to 2,3,7,8-tetrachlorodibenzo-p-dioxin (TCDD) and leads to numerous of toxicological outcomes. In the current study, we discovered a critical role played by AhR, following activation by TCDD, in modulating a variety of immunological functions through regulation of epigenetic and microbial pathways. Our data demonstrated that AhR activation triggers MDSC mobilization from bone marrow to peritoneal cavity which correlated with increased levels various of chemokines and their receptors and induced epigenetic changes via modulation of small noncoding RNA molecules and targeted genes. These MDSCs had high levels of immunosuppressive activity and energy metabolic rate. Also, our data provided a novel link between gut microbiome alterations and MDSC induction and function in colon after TCDD administration. Additionally, we provide evidence that Resveratrol, a natural polyphenol compound is capable to attenuating the immunotoxicological effect of TCDD by altering the migration, differentiation, and suppressive function of MDSCs. Together, our studies demonstrate that AhR can be targeted to suppress inflammation and thus treat inflammatory and autoimmune diseases as well as cancer.

TABLE OF CONTENTS

Dedication iii

Acknowledgements iv

Abstract vi

List of Tables viii

List of Figures ix

Chapter 1: Introduction 1

Chapter 2: AhR activation leads to massive mobilization of myeloid derived suppressor cells (MDSCs) with immunosuppressive activity through regulation of CXCR2 and miR-150-5p and miR-543-3p that target anti-inflammatory genes 9

Chapter 3: AhR activation leads to alterations in the gut microbiome with consequent effect on induction of myeloid derived suppresser cells in a CXCR2-dependent manner. 47

Chapter 4: Resveratrol-mediated attenuation of TCDD-induced MDSCs mobilization, differentiation and suppressive function 80

Chapter 5: Summary and conclusion 94

References 96

LIST OF TABLES

Table 2.1: The forward and reverse primers for listed genes:……..……44

Table 2.2: Number of the sequences sites of the dioxin responsive element (DRE) on the promoter region of listed chemokines as well as accession and version for each chemokine.…….46

LIST OF FIGURES

Figure 2.1: TCDD induces MDSCs in naïve mice……..……...…35

Figure 2.2: AhR antagonist CH223191 treatment decreases TCDD-mediated MDSC induction 36

Figure 2.3: Identifying the source of TCDD-induce MDSCs……37

Figure 2.4: TCDD-induced MDSCs suppress T cell proliferation and exhibit different metabolic profile……....38

Figure 2.5: TCDD-induced MDSCs protect from ConA-induced liver damage and inflammation in vivo following adoptive transfer…….....…..39

Figure 2.6: TCDD treatment attenuates ConA-induced hepatitis and associated inflammation…….…..…40

Figure 2.7: TCDD-mediated alterations in miRNA expression in MDSCs ……....41

Figure 2.8: SVR and context alignment between miRNAs and targeted genes……42

Figure 2.9: Q-PCR analysis of miRNA-150-5p and miRNA-543-3p and specific targeted genes ……..…….……..43

Figure 3.1: TCDD treatment alters microbiome composition……...68

Figure 3.2: Mini blot bar from Nephele analysis showing 16s rRNA sequencing data depicting relative OTU abundance at the phylum level……69

Figure 3.3: Mini blot bar from Nephele analysis showing 16s rRNA sequencing data depicting relative OTU abundance at the class level……70

Figure 3.4: Mini blot bar from Nephele analysis showing 16s rRNA sequencing data depicting relative OTU abundance at the order level……...…....71

Figure 3.5: Mini blot bar from Nephele analysis showing 16s rRNA sequencing data depicting relative OTU abundance at the family level…….……..……72

Figure 3.6: Mini blot bar from Nephele analysis showing 16s rRNA sequencing data depicting relative OTU abundance at the genus level…….……..……73

Figure 3.7: Bacterial depletion in ABX mice……74

Figure 3.8: Effect of fecal microbiota transplantation on MDSCs and MDSC subset induction ……75

Figure 3.9: Effect of TCDD or FMT transfer into ABX mice on MDSC induction in ABX mice……76

Figure 3.10: Fecal transplantation from TCDD-treated mice to ABX mice leads to induction of Tregs……..77

Figure 3.11: Role of cysteine in TCDD-mediated immunomodulation……..……78

Figure 3.12: Role of CXCR2 in TCDD-mediated induction of MDSCs……..……..79

Figure 4.1: Resveratrol (RSV) attenuated MDSCs mobilization from bone marrow to the peritoneal cavity. ……..91

Figure 4.2: RSV impaired protein efflux rate (PER) and immunosuppressive function in MDSCs……...92

Figure 4.3: Flow gating strategy to identify immune cells in the peritoneal cavity……..93

CHAPTER 1

INTRODUCTION

1.1: ARYL HYDROCARBONE RECEPTOR (AhR)

Aryl hydrocarbon receptor (AHR) is a member of basic helix-loop-helix/Per-Arnt-Sim (bHLH/PAS) family of transcription factors that need ligand to be activated (1). The early studies about AhR were carried out in rat liver and described AhR as enzyme induced by foreign chemicals and inducible cytochrome P450 (CYP) monooxygenases (2, 3). However, AhR interacts with foreign chemicals (xenobiotics) but also plays a critical role in the regulation of immune functions. Use of Ahr(−/−) knockout mouse lines provided strong evidence of the wide importance of AhR in various critical-life processes (4).

AhR has numerous agonists ncluding xenobiotic such as TCDD, PCDDs, PCB, and 3-MC and non-xenobiotic such as Resveratrol, I3C, and l-Kynurenine. AhR, exists as a multiprotein complex, containing three molecules of the chaperone protein hsp90 (a heat shock protein of 90 kDa), the X-associated protein 2 (XAP2), and p23 (23-kDa co-chaperone protein). Following xenobiotic agonist binding, the complex translocates to the nucleus and AhR is dimerized with a related nuclear protein called Arnt and converts AhR into high affinity DNA binding form. AhR:Arnt complex binds to Dioxin Response Element (DRE) or Xenobiotic Response Elements (XRE) a specific DNA recognition site found on the promoters of various genes, thereby regulating the expression of these genes, such as CYP1A1 (5). In addition to XRE and DRE, AhR can also be recruited to

novel target DNA sequences by interaction with estrogen receptor, retinoic acid receptor (RAR) and retinoblastoma protein (RB) through Krüppel-like factor 6 (KLF6), controlling the expression of genes that do not bear XREs in their regulatory regions (6).

The important role of AhR in regulation of innate and adaptive immunity was performed by studies that used AhR knockout mice or mice carrying AhR variants with reduced affinity for its ligands (7-9). T helper (TH) cell subsets exhibit differential levels of AhR expression. Th17 cells and regulatory T (Treg) cells (including $FOXP3^+$ Treg cells and T regulatory type 1 cells (Tr1 cells)) express the highest AhR levels, whereas naive $CD4^+$ T cells, Th1 and Th2 cells exhibit no or negligible AhR expression (10, 11). In DC, AhR may contribute to the anti-inflammatory effects of certain cytokines such as TGF-β that increase Treg cell induction (12), or increase FOXP3 Treg generation (13).

Various studies in last decade have focused on Ahr role in gut specific intestinal epithelial cells (IECs). AhR plays important role in IEC regeneration following infectious or chemical injury (14). IEC-specific Ahr knockout ($Vil1^{Cre}Ahr^{fl/fl}$) mice failed to control infection by the pathogen *Citrobacter rodentium* due to impairment of intestinal stem cells (ISCs) differentiation into IECs which caused uncontrolled proliferation of these cells and increased malignant epithelial cell transformation (14). In addition, Ahr enhances epithelial barrier function and prevent infection through increase in the expression of tight junction proteins in response to IL-22 that is produced by DCs and $CD4^+$ T cells (15, 16), or through controlling the expression of antimicrobial proteins such as regenerating islet-derived protein 3β (REG3β) and REG3γ and limiting the pathogenicity of infections in colitis animal models (17).

1.2: MYELOID DERIVED SUPPRESSER CELLS (MDSC)

Myeloid derived suppressor cells (MDSCs) are a heterogeneous population of immature and mature myeloid cells exhibiting immunoregulatory activity in both arms of immune system, innate and adaptive immunity (18). The major population of bone marrow (BM)-derived myeloid cells are granulocytes and mononuclear cells (monocytes, terminally differentiated to macrophages and dendritic cells (DCs). In the steady condition, macrophage widely expand in situ, while DCs differentiate from their specific BM precursors (19). Under physiological conditions, the cell-signaling molecule GM-CSF drives myelopoiesis. G-CSF induces granulocyte differentiation and M-CSF induces macrophage differentiation (20). In chronic inflammation and cancer, these cell-signaling molecules are enhanced and induce MDSCs generation and expansion (21).

In mice, MDSCs consist of two phenotypes, Monocytic (M-MDSCs) are defined as $CD11b^{+}Ly6G^{-}Ly6Chi$ cells with low side scatter, and Granulocytic (G-MDSCs) or Polymorphonuclear (PMN-MDSCs) that can be defined as $CD11b^{+}Ly6G^{+}Ly6C^{low}$ cells with high side scatter (22). M-MDSCs have more suppressive function than PMN-MDSCs (23). Both of these phenotypes use different mechanism for suppression, The most distinct factors involved in MDSC suppressive activity include ARG1, ARG2, NO, upregulation of ROS (23-25). A recent study showed inhibition of fatty acid-β oxidation (FAO) used by tumor-infiltrating MDSCs as a primary source of energy, impaired the suppressive function of tumor-infiltrating MDSCs thereby leading to enhanced the immune response against cancer (26).

It has been reported that there are two groups of interconnected signals involved in MDSCs accumulation and activation. First group of signals is responsible for

immature myeloid cell expansion whereas, the second group of signal is responsible for their activation and promotion of pathologic activity (27). First group includes GM-CSF, M-CSF, G-CSF, IL-6, VEGF and polyunsaturated fatty acids and signals primarily via STAT3 and STAT5. However this signaling alone is not sufficient without second activating signal which is mainly provided by pro-inflammatory molecules such as interferon-γ (IFN-γ), IL-1β, IL-4, IL-6, IL-13, tumor necrosis factor (TNF), TLR ligand, and signals that utilize NF-κB, STAT1, and STAT6 transcription factors for their activation (27-29).

Numerous studies have been addressed that the proliferation, development, migration and function of MDSCs are controlled by epigenetic mechanisms such as DNA methylation which enhanced promoter methylation of DNMT3a and DNMT3b and improved ARG1 and STAT3 expression with THC treatment (30, 31). Histone modification, one of the epigenetic mechanisms, specifically histone deacetyltransferases (HDACs), including HDAC2 (32) and HDAC11 also plays a role in MDSC induction (33). In physiological conditions, miRNA regulate genes expression that is implicated in cell development and differentiation. Several miRNA have been reported that modify gene expression and enhance the suppressive function of MDSCs including miR-210, miR-494, miR-155, miR-21, and miR-34a (34-37).

1.3: 2,3,7,8-TETRACHLORODIBENZO-P-DIOXIN (TCDD)

2,3,7,8-Tetrachlorodibenzo-p-dioxin (TCDD) is a typical epitome for a group of environmental halogenated aromatic hydrocarbon contaminants which elicit immune toxicity and other toxic responses through activation of aryl hydrocarbon receptor (AhR). TCDD is infused into the environment by many sources including chemical industries

and burning processes. It is considered a byproduct of fossil fuels and wood combustion. Also, it is one of the manufacturing remnants of chlorinated hydrocarbons, paper, pulp bleaching (38). International Agency for Research on Cancer, WHO and US National Toxicology Program classified TCDD as human carcinogen (39). TCDD is similar to other chlorinated compounds and has bioaccumulation feature in food chain which causes food contamination. Ingestion the contaminated food is the most known way to TCDD exposure (40).

Thymic atrophy is the hallmark of TCDD-mediated immunotoxicity in different animal models. It is characterized by a marked reduction in the frequency of double positive ($CD4^+CD8^+$) thymocytes, as well as a relative increase in the frequency of double negative ($CD4^-CD8^-$) and single-positive of both $CD4^+$ and $CD8^+$ thymocytes, these shifts in thymocyte subset frequencies was accompanied by a significant decrease in the absolute number of thymocytes in each of the four subpopulations (41-44). It was noted recently that thymic atrophy is also caused by activation Ahr in $CD11c^+$ dendritic cells which may be responsible for TCDD-induced alterations in the development and differentiation of thymocytes (45). TCDD also suppresses the activation and differentiation of human B cells into Immunoglobulin-M (IgM) secreting cells (46, 47).

Activation AhR by its high affinity ligand TCDD in $CD4^+$ T cells directly alters gene expression and increases IL-10 producing and eventually T-cell differentiation to $FoxP3^-$ type 1 regulatory T cells (Tr1 cells) (48). TCDD through AhR activation, induces $FoxP3^+$ Treg which promote tolerogenic phenotype and suppress several immune-mediated diseases (13, 49-51).

In humans, ingestion of contaminated food is one of the most common source of TCDD exposure route (40). The gastrointestinal tract is the largest habitat of microbiota. The diversity of microbes within a given host can be defined as the number and abundance of distribution of distinct types of organisms such as bacteria, archaea, protists, fungi and viruses, which have been linked to immunologic, hormonal, and metabolic homeostasis of their host. Microbiome dysbiosis occurs due to a wide range of causes such as diseases, environmental contamination, diet, and stress (52-54). Emerging studies reported that TCDD after exposure is rapidly absorbed from the gastrointestinal and causing shift in gut commensals (55, 56).

1.4: 3,5,4'-TRIHYDROXYSTILBENE (RESVERATROL)

Resveratrol (RSV) is a natural polyphenolic products that is synthesized as a phytoalexin (compounds that are produced in plants as a defense mechanism against pathogenic and stressful environmental situations) in plants such as grapes, soy, nuts, and chocolate (57). The chemical structure of resveratrol (trans-3,5,4′-trihydroxystilbene) is identified in two isomeric forms, cis- and trans-resveratrol, both of isomeric forms have different biological activities (58). Because of anti-inflammatory, antioxidant, antibacterial, and anticancer properties of resveratrol, it has received recently significant scientific attention.

Plurality of anti-inflammatory features of RSV have been investigated widely in inflammatory bowel diseases, when 5-20 mg/kg of RSV doses reduced colitis symptoms by decreasing the production of inflammatory cytokines IL-1β, IL-12, IL-6, TNF-α, COX2, and prostaglandin D2 (PGD2) and increased the levels of IL-10 in rat colitis models (59-61). Numerous studies from our lab showed the protective role of RSV in

various inflammatory disease including lung injury (62, 63), kidney injury (64), liver injury (65), and colitis (66, 67). Also, RSV showed a marked protective effect on inflammatory and autoimmune disease such as allergic asthma (68), and multiple sclerosis (69).

In terms of its antioxidant capability, RSV has an aromatic ring structure and OH group that provides electrons which help to scavenge free radicals that are generated in the electron transport chain undergoing oxygen-consuming reaction (70). RSV protects hippocampal neuron from ROS by its scavenging properties (71). Interestingly, RSV inhibits QR2, a cytosolic enzyme which enhances the production of damaging ROS and involved in memory impairment. Inhibition of QR2 reduced hippocampal neuronal cell death– a brain area involved in learning and memory, in the rat model (72).

RSV is considered antibacterial because it is a molecule that has ability to interact with more than 20 proteins in eukaryotic organisms including *Mycobacterium smegmatis* and *Escherichia coli*, the interaction is accompanied with inhibition of both ATP hydrolysis and ATP synthesis functions which stop bacterial growth in media (73-75).

RSV was reported to exert multiple anticancer activity in various cancer cell lines through varied mechanisms. Treatment with resveratrol induced apoptotic cell death by increasing ROS in the human ovarian cancer cell lines, A2780 and SKOV3 (76). In gastric cancer cell line BGC823, RSV 200 μM inhibited the viability, migration, and invasion of cells and suppressed metastasis-associated lung adenocarcinoma transcript 1 (MALAT1) expression, which was overexpressed in gastric cancer cells (77). Furthermore, RSV inhibited the Interleukin-6 induced SGC7901 cell invasion and matrix

metalloproteinase activation through inhibition of Raf/MAPK pathway of activation (78). RSV inhibited lung cancer tumor growth that was induced by injection of LLC tumor cells in B6 mice through reduction of $F4/80^{+}$ expressing cells and M2 polarization in tumors (79). Studies from our lab have shown that RSV reduced colitis and prevented colon cancer through modulation of CD3(+) T cells that express tumor necrosis factor-alpha and IFN-gamma or through the up-regulation of SIRT-1 in immune cells in the colon (80, 81). Studies from our lab have also shown that RSV can serve as a ligand or agonist of AhR, based on the dose (82)

Hypothesis: In the current study, we tested the central hypothesis that activation of AhR by TCDD may induce significant alterations in the activation and migration of MDSCs and that this effect may result from modulation of gut microbiota. Interestingly, we noted that TCDD induced massive mobilization of MDSCs and MDSC subsets from bone marrow to peritoneal cavity which was regulated by the miRNA. Also, we found that TCDD caused gut microbiome dysbiosis, which also played a crucial role in the induction of MDSCs. Furthermore, we also observed that RSV attenuated immunomodulating properties of TCDD by reducing the mobilization, differentiation, suppressive functions of MDSCs.

CHAPTER 2

AHR ACTIVATION LEADS TO MASSIVE MOBILIZATION OF MYELOID DERIVED SUPPERSSOR CELLS (MDSCS) WITH IMMUNOSUPPRESSIVE ACTIVITY THROUGH REGULATION OF CXCR2 AND MIR-150-5P AND MIR-543-3P THAT TARGET ANTI-INFLAMMATORY GENES

2.1 ABSTRACT

TCDD (2,3,7,8-Tetrachlorodibenzo-p-dioxin), an environmental contaminant, is a potent ligand for Aryl hydrocarbon receptor (AhR). In the current study, we made an exciting observation that naïve C57BL6 mice exposed intraperitoneally to TCDD showed massive mobilization of MDSCs in the peritoneal cavity. These MDSCs were highly immunosuppressive and attenuated Con-A-induced hepatitis upon adoptive transfer. TCDD administration in naïve mice also led to induction of several chemokines and cytokines in the peritoneal cavity and serum (CCL2, CCL3, CCL4, CCL11, CXCL1, CXCL2, CXCL5, CXCL9, G-CSF, GM-CSF, VEGF and M-CSF), and chemokine receptors on MDSCs (CCR1, CCR5, and CXCR2). Treatment with CXCR2 or AhR antagonists in mice led to marked reduction in TCDD-induced MDSCs. TCDD-induced MDSCs had high mitochondrial respiration, glycolytic and ATP rates and exhibited differential miRNA expression profile. Specifically, there was significant down-regulation of miR-150-5p and miR-543-3p. These two miRNAs targeted and enhanced anti-inflammatory genes, including IL-10, PIM1, ARG2, and STAT3 as well as CCL11 and its receptors CCR3 and CCR5 as wells as CXCR2. The role of miRs in MDSC activation was confirmed by transfection studies. Together, the current study

demonstrates for the first time that activation of AhR in naïve mice triggers robust mobilization of MDSCs through induction of chemokines and their receptors, and MDSC activation through regulation of miRNA expression. AhR ligands include diverse compounds from environmental toxicants such as TCDD that are carcinogenic to dietary indoles that are anti-inflammatory. Our studies provide new insights on how such ligands may regulate health and disease through induction of MDSCs.

2.2 INTRODUCTION

TCDD (2,3,7,8-Tetrachlorodibenzo-p-dioxin) is a halogenated aromatic hydrocarbon found in the environment as a contaminant with immunotoxic and carcinogenic properties. It is well characterized for its ability to act as a high affinity ligand for AhR, a member of the basic helix-loop-helix/Per-Arnt-Sim (bHLH/PAS) family of transcription factors. In fact, AhR is required for induction of toxicity inasmuch as mice deficient in AhR are mostly resistant to TCDD-mediated toxicity (83). More recent studies have demonstrated that AhR may also play a crucial role in regulating various physiological and developmental processes including the functions of the immune system (84).

Extensive studies have shown that the immune system is one of most sensitive targets of TCDD. Multiple mechanistic pathways have been identified to delineate how AhR activation leads to regulation of the immune system. These include but not limited to: activation of Fas which expresses DREs leading to induction of apoptosis of activated T cells (84-87). induction of FoxP3 and Tregs by virtue of the fact that FoxP3 expresses DREs on its promoter (88, 89). promoting Tregs while suppressing Th17 cells through decreased methylation of CpG islands of Foxp3 and increased methylation of IL-17

promoter (50, 85) differential miRNA induction such as decreased expression of miR-31, miR-219, and miR-490 that targeted Foxp3, and increased expression of miR-495 and miR-1192 that were specific to IL-17 (90). AhR ligands also include dietary compounds such as indole-3-carbinol (I3C),3,3'-diindolylmethane (DIM), and resveratrol (37, 82, 91-93). The essential amino acid tryptophan, acquired from the diet, also serves as a source of AhR ligands (94). It is interesting to note that while some AhR ligands are considered to be highly toxic and carcinogenic, others constitute ligands that are endogenously produced or found in the diet that regulate immune response in health and disease. Also, while some AhR ligands such as TCDD are known to trigger Tregs, others such as 6-formyl indolo[3,2-b]carbazole (FICZ), induce Th17 cells (89, 90). Thus, the precise mechanisms through which AhR ligands regulate the immune response needs further investigation.

Myeloid-Derived Suppressor cells (MDSCs) are heterogeneous populations derived from bone marrow and comprised of myeloid progenitors that under normal conditions, differentiate into dendritic cells, granulocytes, and macrophages (95). In situations involving chronic infection, inflammation, trauma or malignancy, the associated chemokines and cytokines induce abnormal accumulation of such immature myeloid cells that are highly immunosuppressive (96). These cells in mice express $CD11b^+$ and $Gr\text{-}1^+$ surface markers (97, 98). MDSCs have contradictory roles in infection and immunity. They may act as a double-edged sword during the early and late stages of infection and inflammation, from promoting innate immunity in early stages to attenuating the immune system through inducing immunosuppressive conditions in late stages of infection (99). In some cases, increasing MDSCs during infection help to reduce

inflammatory extension and limit undesirable tissue damages (100). In cancers, MDSC accumulation can prevent anti-cancer immunity thereby facilitating the tumor growth. MDSCs have also been shown to induce Tregs and regulate macrophage (101, 102).

2.3 MATERIALS AND METHODS

Experimental Animals:

Female mice C57BL/6 mice (6-8) weeks old were purchased from Jackson laboratory, USA. All mice were housed in specific pathogen-free condition at the AAALAC-accredited University of South Carolina, School of Medicine, Animal Resource Facility. All experiments performed using mice were approved by the Institutional Animal Care and Use Committee (IACUC), University of South Carolina.

Chemicals and reagents

TCDD was a kind gift from Dr. Steve Safe (Institute of Biosciences & Technology, Texas A&M Health Sciences Center, College Station, Texas). RSV was purchased from Supelco (MO, USA). Concanavalin A (Con A), N acetyl-cysteine (NAC), AhR antagonist (CH223191) and CXR2 antagonist (Sch527123) were purchased from Sigma-Aldrich, N.C. Culture medium reagents (RPMI 1640, Penicillin-Streptomycin, HEPES, L-Glutamine, FBS, and PBS) were purchased from Invitrogen Life Technologies (Carlsbad, CA). The following antibodies were used for surface markers, and/or intra-nuclear staining and were purchased from BioLegend (San Diego, CA-USA): FITC or Alexa Fluor 700-conjugated anti-CD11b, PE or BV510-conjugated-GR-1, Alexa Fluor 488-conjugated anti-Ly6C, BV785-conjugated anti-Ly6G, PE or BV785-conjugated anti-CD4, PE-conjugated anti-CD3, and BV510-conjugated anti-NrP1. PE-conjugated anti-IL-17, BV605-conjugated anti-IL-10, BV650-conjugated anti-INF-g, PerCP-Cy™5.5-

conjugated anti-TGF-β, and Alexa Flour 488-conjugated anti-IL-4, Alexa Fluor 488-conjugated anti-FOXP3 and PE-Dazzle-conjugated anti-Helios. Fc Blocker reagent was procured from BD Biosciences (San Diego, USA). Monoclonal Mouse IgG anti Arg1 were purchased from BD Biosciences (San Diego, USA). Monoclonal Rat IgG antibodies of CD11b and Ly6G/Ly6C (GR-1) were purchased from R&D Systems Biotech Brand (Minneapolis, USA). Cytofix/CytopermTM Fixation/ Permeabilization kit was purchased from BD Biosciences (San Diego, USA). True-Nuclear™ Transcription Factor Buffer Set was from BioLegend. EasySep™ PE Positive Selection Kits were purchased from Stem cells Technologies (Vancouver, BC, Canada). RNeasy and miRNANeasy Mini kits, miScript primer assays kit, and miScript SYBR Green PCR kit were obtained from QIAGEN (QIAGEN, Valencia, CA). The following reagents: iScript and miScript cDNA synthesis kits were purchased from Bio-Rad (Madison, WI). Epicentre's PCR premix F and Platinum Taq DNA Polymerase kits from Invitrogen Life Technologies (Carlsbad, CA). ELISA kits for IL-4, IL-10 and TGF-b (ELISA MAXTM Standard SET Mouse) were bought from BioLegend. XFp glycolytic rate assay kit and XFP cell mito stress test kit were purchased from Agilent Technologies.

Induction of MDSCs in mice by TCDD.

Groups of 5 mice were injected intraperitoneally (i.p.) with TCDD (1-10µg/kg) or the vehicle, corn oil. At various days post exposure, mice were euthanized, peritoneal cells were collected, and washed twice with PBS. The cells were counted and stained for MDSC markers (CD11b and Gr-1), Granulocytic MDSCs (G-MDSCs: CD11b and Ly6-G), and Monocytic MDSCs (M-MDSCs: CD11b and Ly6-C) populations by flow cytometry (BD FACScelesta), as described (103). Feces were collected from two groups

as well as from naïve group and kept in -80 0C for later use. For RSV treatment, mice were given orally 50 mg/kg RSV prior one day from TCDD 10 µg/kg injection, upon one day of TCDD exposure, cells from peritoneal cavity were collected and stain with MDSCs and MDSCs subset phenotype markers.

Purification of MDSCs and their subsets M-MDSCs and G-MDSCs

TCDD-induced MDSCs were purified from exudates of peritoneal cavity, as described previously (31). In brief, peritoneal exudates were collected from TCDD-exposed mice and labeled with PE-conjugated Gr-1 antibody. PE-selection kit from Stem Cells Technologies was used for selection and following the protocol from company. After purification, flow cytometry (BD FACScelesta) was used to assess the purity of MDSCs. We purified M-MDSCs and G-MDSCs subsets of MDSCs using FACS Aria II sorter (BD FACS Aria II). Peritoneal exudate cells were stained with CD11b and LY6C for M-MDSCs or CD11b and LY6G for G-MDSCs.

AhR and CXCR2 antagonists

Mice were injected i.p with 10 mg/kg or 50 mg/kg of AhR antagonist (CH223191) or CXCR2 antagonist (Sch527123) respectively, one day before TCDD injection. Peritoneal exudates were collected in day 3 and stained with CD11b, Gr-1, LY6G and LY6C to detect MDSCs and subset of MDSCs.

Effect of TCDD-induced MDSCs and MDSCs subsets (M-MDSCs and G-MDSCs) on T-cell proliferation in vitro

To examine the suppressive effect of MDSCs on T-cell proliferation, splenocytes ($5x10^5$) from C57BL/6 naïve mice were cultured in the presence of Con-A (2µg/ml) together with different ratios of TCDD-generated MDSCs, M-MDSCs and G-MDCSs for

24 hrs, as described (104). [3H]thymidine (1μCi/well) was added to the cells cultures and after 18 hrs, radioactivity was measured using a liquid-scintillation counter (MicroBeta Trilux; PerkinElmer Life and Analytical Sciences).

Mitochondrial respiration, glycolytic rate, and ATP rate.

Oxygen consumption rates (OCR), proton efflux rate (PER), and ATP rate were measured in 2×10^5 of purified MDSCs from peritoneum of vehicle or TCDD-treated mice using XF Extracellular Flux Analyzer (Seahorse Bioscience). For OCR, MDSCs were plated in XF cell culture plate coated with 15 μg CellTak (BD Biosciences) in XF assay medium supplied with 1 mM pyruvate, 2 mM glutamine, and 10 mM glucose. MDSCs were analyzed under stressed conditions and in response to 1 μM oligomycin, 1 μM fluorocarbonyl-cyanide-phenylhydrazone (FCCP), and 0.5 μM rotenone and antimycin-A. For PER, MDSCs were plated in XF cell culture plate coated with 15 μg CellTak in phenol red-free Base Medium enriched with 2 mM glutamine, 10 mM glucose, 1 mM pyruvate, and 5 mM HEPES as initial conditions. Cells monitored under stressed conditions and in response to 0.5 μM Rotenone plus Antimycin A (Rot/AA) and 50 mM 2-Deoxy-D-glucose (2-DG). For ATP rate, MDSCs were plated in XF cells culture plate with 15 μg CellTak in DMEM Medium enriched with10 mM of glucose, 1 mM of pyruvate, 2 mM of glutamine. ATP rate production measured under stressed conditions in response to 1.5 μM of oligomycin and 0.5 μM Rotenone + Antimycin A. All three tests quantified by Seahorse Bioscience XFp Extracellular Flux Analyzer (Agilent Technologies).

Proliferation assessment by BrdU and Ki67 labeling in vivo

To characterize MDSCs proliferation in vivo, mice were injected with BrdU (100 mg/kg) two hours before TCDD treatment, as described (105, 106). Cells from the peritoneal exudate were harvested and were first stained using anti-mouse antibodies against CD11b and Gr-1. After fixation and permeabilization, the cells were stained with PerCP-Cy™5.5-conjugated anti-BrdU (BD Biosciences) and PE-conjugated anti-Ki67 antibodies (Biolegend) and using intranuclear staining protocol (BD Biosciences). Quad-stained cells were analyzed by flow cytometry (BD FACScelesta).

Con-A-induced hepatitis and adoptive transfer of MDSCs

To generate hepatic inflammation, (C57BL/6) mice were injected intravenously (iv) with Con-A (12.5mg/kg) as described (103). For adoptive transfer, Con-A injected mice received 5 million purified MDSCs from peritoneal cavity (PC-MDSCs) or bone marrow MDSCs (BM-MDSCs) from TCDD-treated mice 1 hr before Con-A injection. In experiments where TCDD was tested for its ability to attenuate ConA-induced hepatitis, mice received TCDD (10 µg/kg) by i.p. route, 1 hr before ConA injection. Mice were sacrificed after 48 hrs post treatment and spleens and livers were harvested as well as blood was collected. Single cell suspension of splenocytes was prepared and infiltrating mononuclear cells in the liver were isolated using Percoll gradient, as described (107). Harvested cells from spleens and liver mononuclear were stained with Abs against CD4 and INF-γ or IL-17 or IL-4 or IL-10 to determine Th1, Th-17, Th-2 and induced T-reg cell populations by flow cytometry (Beckman Coulter). IL-4 and TGF-b cytokines level were detected in sera by ELISA.

Enzyme-linked immunosorbent assay (ELISA)

Serum from individual mouse was collected and the concentration of various cytokines including, IL-4, and TGF-β was measured using ELISA MAXTM Standard SET Mouse kit for respective cytokines were purchased from Biolegend.

Chemokines analysis

Serum and peritoneal exudates were collected from individual mouse after 3 days of TCDD or vehicle injection. G-CSF, GM-CSF, M-CSF, Eotaxin (CCL11), LIF, LIX (CXCL5), KC (CXCL1), MCP-1 (CCL2), MIP-1A (CCL3), MIP-1B (CCL4), MIP-2 (CXCL2), MIG (CXCL9), RANTES (CCL5), and VEGF concentrations were determined by using Milliplex map kit (Sigma-Milipore, USA) according to the manufacturer protocol and analyzed by Bio-Plex chemiluminescence assay system (Bio-Rad).

Histopathology of liver

Livers were harvested from mice and fixed in formaldehyde (4%) overnight, then embedded in paraffin and cut to ~6 micron-thickness. The liver sections were then stained with hematoxylin and eosin (H&E) and analyzed by Cytation5 microscopic system (BioTek, USA).

microRNA Arrays and Analysis

miRNA analysis was carried out as describe (31). Total RNA including microRNA was isolated from peritoneal MDSCs post-TCDD administration using miRNAN easy kit from Qiagen and following the protocol of the company (Qiagen). miRNAs arrays were performed using Affymetrix miRNA array (version 4). Signal expression (fold change) of more than 3000 miRNAs were detected from the raw array data and only those miRNAs that were altered more than 2-fold, were considered for

further analysis. The selected miRNAs were further analyzed for their targets and alignments using TargetScan, microRNA.org, and miRNAWalk database. Furthermore, selected miRNAs were analyzed for their role in various diseases and pathways using Ingenuity pathway analysis (IPA) software. miRNAs from various groups were also analyzed for their relationship using LucidChart or Venn Diagram.

Real-Time (Q-PCR) to validate miRNAs and associated genes expression

Q-PCRs were performed to determine the expression of selected miRNAs (miRNA-150-5p, and miRNA-543-3p) on cDNAs synthesized from total RNAs including miRNAs isolated from peritoneal MDSCs post-TCDD or vehicle exposure. miScript primer assays kit (QIAGEN, Valencia, CA) and SSo advance SYBR Green PCR kit from Bio-Rad,were used and Q-PCR was performed following the protocol of the company. For Q-PCR run conditions to detect miRNA: 15min at 95°C (initial activation step), followed by 40 cycles of 15s at 94°C (denaturing temperature), 30s at 60°C (annealing temperature), and 30s at 70°C (extension temperature and fluorescence data collection) were used. Normalized expression (NE) of miRNAs was calculated using NE ¼ 2_DDCt, where Ct is the threshold cycle to detect fluorescence. The data were normalized to miRNAs against internal control miRNA (SNORD96A, Qiagen-Germany) and fold change of miRNAs was calculated against control miRNA (SNORD96A) and treatment group (TCDD) was compared with vehicle group.

Real time PCR (RT-PCR) to determine the expression of IL-10, ARG2, STAT3, INOS1 and PIM1 in MDSCs post-TCDD or vehicle treatment.

RT-PCR was performed to detect IL-10, ARG2, STAT3, PIM1, CCL11, CCR1, CCR3, CCR5, and CXCR2 expression. Primers of these genes are specifically designed

to above genes through IDT tools (Table 2.1). RT-PCR was performed for 40 cycles using the following conditions: at 98°C (denaturing temperature) for 30 s, at 98°C (annealing temperature) for 10 s, and at 60°C (extension temperature) for 30 s. The PCR products, generated from mouse gene-specific primer pairs, were visualized with UV light performing electrophoresis (1.2% agarose gel). The band intensity of PCR products was determined using ChemiDoc image analysis system from Bio-Rad (Bio-Rad, Hercules, CA). The expression of the above genes were normalized against PCR products generated from mouse housekeeping gene GAPDH (internal control).

Statistical analysis.

GraphPad Prism software version 6.01 (San Diego, CA) was used for statistical analysis. A standard t-test or multiple t-test with Holm-Sidak's multiple comparisons corrections was used when comparing two groups for significance. A one-way or two-way analysis of variance (ANOVA) with post hoc Tukey's multiple comparisons test was used to compare between the means of more than two groups. Error bars were expressed as Mean ± standard error of mean (±SEM), and significance was determined as having a p value less than 0.05. Each experiment was repeated at least twice with consistent results.

2.4 RESULTS

TCDD induces MDSCs in mice.

TCDD is a potent agonist of AhR and thus, we used TCDD to test if activation of AhR leads to induction of MDSCs. To this end, three doses of TCDD (1, 5, and 10 µg/kg body weight) or vehicle were injected (i.p.) into C57BL/6 mice and peritoneal exudates collected on day 3 post treatment. The presence of MDSCs in peritoneal cavity was

analyzed by staining the cells with fluorophore labeled anti-mouse CD11b and Gr-1 antibodies and using flow cytometry. There was a dose-dependent increase in both the percentages and numbers of $CD11b^{+}Gr\text{-}1^{+}$ cells in peritoneal cavity (Fig 2.1A-B) of mice that received TCDD, when compared to mice that received vehicle. Upon analysis of subsets of MDSCs (monocytic and granulocytic) by staining the cells with Abs against Ly6C and Ly6G, we observed significant increase in both monocytic MDSCs ($CD11b^{+}Ly6G^{-}Ly6C^{hi}$) and granulocytic MDSCs ($CD11b^{+}Ly6G^{+}Ly6C^{low}$) following TCDD treatment, when compared to vehicle controls (Fig 2.1C-D). However, the granulocytic MDSCs were significantly more in both the percentages and total numbers when compared to monocytic MDSCs. To study the time course, we injected mice with TCDD and collected peritoneal exudates on days 1, 2 and day 3 post-treatment. We observed significant induction of MDSCs on day 1 and their numbers continued to rise till day 3 (Fig 2.1E-F). Additionally, on day 3, we noted that the proportion of G-MDSC induction was significantly more than that of M-MDSCs (Fig 2.1G-H). Together, these data demonstrated that TCDD induces robust MDSCs in the peritoneal cavity.

TCDD induces MDSCs through activation of AhR

Because TCDD is a potent ligand for AhR, we tested the effect of AhR antagonist (CH223191) on the induction of MDSCs by TCDD. We found administration of AhR antagonist significantly reduced the number of MDSCs (Fig 2.2A-B) and MDSC subsets (Fig 2.2C-D), thereby suggesting that TCDD was inducing the MDSCs, at least in part, through activation of AhR.

TCDD promotes the migration of MDSCs from bone marrow to peritoneal cavity through chemokines induction.

Normal mouse bone marrow contains 20–30% $CD11b^+$ $Gr\text{-}1^+$ while their proportion is much smaller in the spleens (2–4%), and they are absent in the lymph nodes (95). Thus, we next determined if TCDD was promoting the migration of MDSCs from the bone marrow. To this end, we enumerated $CD11b^+$ $Gr\text{-}1^+$ cells in bone marrow and peritoneal exudate at 0 hr and 16 hrs post-TCDD treatment, by flow cytometry (FACScelesta). Interestingly. there was a significant decrease in the percentage of $CD11b^+$ $Gr\text{-}1^+$ cells in bone marrow after 16 hrs following TCDD treatment while there was a significant increase in MDSCs in peritoneal cavity (Fig 2.3A-B). These data suggested that $CD11b^+$ $Gr\text{-}1^+$ cells from the bone marrow may be migrating to the peritoneal cavity, the site of TCDD administration. Next, we investigated if specific chemokines have a role to recruit MDSCs from bone marrow to peritoneal cavity. To that end, we detected some chemokines and cytokines that regulate MDSCs, and found that the peritoneal fluid of TCDD-injected mice had significant levels of MCP-1 (CCL2), MIP-1A (CCL3), MIP-1B (CCL4), Eotaxin (CCL11), KC (CXCL1), MIP-2 (CXCL2), MIG (CXCL9), VEGF, and M-CSF when compared to controls. Also, we saw an increase in CCL2, CCL4, CXCL1, CXCL5, G-CSF and GM-CSF in the serum of TCDD-treated mice (Fig 2.3C-D). We also assessed chemokines receptors expression in MDSCs post-TCDD treatment. We found that three of the chemokine receptors increased in TCDD-induced MDSCs group (CCR1, CCR5, and CXCR2) when compared to vehicle-induced MDSCs group (Fig 2.3E). Next, we investigated if blocking CXCR2 would have an effect on MDSCs recruitment to peritoneal cavity. To this end, we injected CXCR2

antagonist Sch527123 in mice one day before TCDD treatment and after 3 days, MDSCs were assessed in peritoneal cavity. We observed that MDSC percentage and numbers were dramatically decreased following CXCR2 antagonist treatment when compared to controls (Fig 2.3F). We also examined whether TCDD induces only the migration of MDSCs from bone marrow to peritoneal cavity or it also induces MDSCs proliferation in the peritoneal cavity. To that end, we injected BrdU in mice 2 hrs before TCDD treatment. After 48 hrs, we stained the peritoneal cells using fluorophore labeled anti-mouse CD11b and Gr-1 antibodies as well as intranuclear BrdU, and intracellular Ki67. We observed no significant difference in BrdU and Ki67 positive cells between vehicle and TCDD groups demonstrating that TCDD does not induce proliferation of MDSCs in the periphery (Fig 2.3G).

TCDD-induced peritoneal MDSCs, M-MDSCs, and G-MDSCs mediate suppression of T cell activation in vitro

Immune suppression is the hall mark feature of MDSCs and thus, to determine if TCDD-induced MDSCs can suppress T cell activation, we performed T cell proliferation assays using ConA (2 µg/ml) in the presence or absence of TCDD-induced MDSCs collected from peritoneal cavity. We observed dose-dependent suppression of T cell activation in the presence of MDSCs and furthermore, while both G-MDSC and M-MDSCs were suppressive, the latter were found to be more effective (Fig 2.4A-C).

TCDD-induced peritoneal MDSCs have high mitochondrial respiration, glycolytic and ATP rates.

Tumor-infiltrating MDSCs (T-MDSCs) have been shown to have increased oxygen consumption rate (OCR) and extracellular acidification rate (ECAR), when

compared to splenic-MDSCs (29). To explore the nature of TCDD-induced MDSCs, we tested the Oxygen Consumption Rate (OCR) and Proton Efflux Rate (PER) as well as ATP rate using Seahorse Bioscience XFp Extracellular Flux Analyzer. We observed that TCDD-induced MDSCs from peritoneal cavity had higher OCR, PER and ATP production rate in comparison to vehicle- induced MDSCs (Fig 2.4D-F).

TCDD-induced MDSCs protect ConA-induced liver damage *in vivo*.

Next, we investigated whether TCDD-induced MDSCs are functional in vivo in suppressing T cell response. We have shown earlier that MDSCs can protect liver from ConA-mediated hepatitis in vivo (108). To that end, we injected naïve mice with purified TCDD-induced MDSCs from peritoneal cavity or bone marrow, i.v. followed 1 hr later with ConA. Spleens and livers of mice treated with peritoneal-MDSCs or BM-MDSCs were harvested 48 hrs after treatment. Upon histological analysis of liver, there was reduced liver inflammation in mice that received TCDD-peritoneal-MDSCs, when compared to mice that received MDSCs from BM (Fig 2.5A). Analysis of alanine transaminase (ALT) in sera showed significantly reduced ALT level in sera of mice that received TCDD-peritoneal MDSCs, when compared to mice that received MDSCs from BM (Fig 2.5B). Moreover, levels of IL-4 and TGF-β (anti-inflammatory cytokines) increased in sera of mice that received TCDD-peritoneal-MDSCs, when compared to mice that received BM-MDSCs (Fig 2.5C). These data suggested that TCDD-induced peritoneal MDSCs are more immunosuppressive in function in vivo, when compared to bone marrow-derived MDSCs from the same mice.

TCDD-induced MDSCs reduce inflammation in liver and spleen of ConA induced hepatitis mice.

To better understand the suppressive effect of TCDD-induced peritoneal MDSCs, we purified mononuclear cells from livers as well as spleen cells from mice treated with peritoneal-MDSCs and BM-MDSCs as described in Materials and Methods. The mononuclear cells and splenocytes were stained to determine Th1, Th17, Th2 and induced Tregs. There was significant reduction in $CD4^+IL\text{-}17^+$ in the liver and $CD4^+IFN\text{-}\gamma^+$ in the spleens of mice treated with TCDD-induced peritoneal MDSCs, when compared to cells treated with BM-MDSCs. In contrast, there was significant upregulation of $CD4^+IL\text{-}10^+$ in the liver and $CD4^+IL\text{-}4^+$ in the spleens of mice treated with peritoneal-MDSCs, when compared to cells from mice treated with BM-MDSCs (Fig 2.5D-E)

TCDD reduces inflammation in ConA-induced hepatitis in mice by generating MDSCs and Tregs.

To test if TCDD would directly suppress ConA-induced hepatitis and if this is regulated by MDSCs, we injected mice with TCDD (10µg/kg) or vehicle 1 hr before ConA (10mg/kg) injection (iv). We noted that TCDD was able to decrease ALT levels thereby showing protection of liver damage (Fig 2.6A). Next, we stained the spleen cells and liver mononuclear cells for MDSCs, various T helper cells (Th1, Th2, and Th3), and Treg subsets (tTreg, pTreg, and Tr1). We observed significant increase in MDSCs and G-MDSCs in spleens of mice exposed to TCDD, when compared to mice treated with vehicle (Fig 2.6B-C). Furthermore, there was significant reduction in the percentages of $CD3^+CD4^+$ cells and Th1 cells and an increase in the percentages of Th2 cells in TCDD-

treated mice when compared to vehicle-treated mice (Fig 2.6D-G). For Treg and its subsets (Fig 2.6H), there was significant increase in the percentages of $CD4^{+}FoxP^{+}$ population (Fig 2.6I) and in the percentages of pTregs, and Tr1, as well as in the percentage of Th3 cells in spleen of TCDD-treated mice in comparison to vehicle-treated mice (Fig 2.6K-L). However, the percentages of $CD4^{+}FoxP3^{-}$ (Fig 2.6J) and tTregs (Fig 2.6K) were significantly decreased in mice were treated with TCDD, when compared to mice treated with vehicle.

TCDD altered miRNAs expression in peritoneal MDSCs.

Our previous studies demonstrated that miRNA play a critical role in MDSC induction (65). To that end, we investigated the role of miRNA in the induction of MDSCs by TCDD, by performing miRNA microarray using MDSCs derived from vehicle or TCDD-treated groups. There were more than 3195 miRNAs that were analyzed by arrays (Fig 2.7A) of which the expression of only 141 miRNAs were altered by greater than two-fold in TCDD-treated groups when compared to vehicle-controls (Fig 2.7A). As shown in Venn diagram, there were 3054 miRNAs that showed no change (Fig 2.7B), while 97 miRNAs were upregulated, and 44 miRNAs were downregulated (Fig. 2.7B). Figure 2.7C depicts upregulated (n=97) and downregulated (n=44) miRNAs in TCDD-induced MDSCs, when compared to vehicle-induced MDSCs. Similarly, Fig 2.7D depicts TCDD-dysregulated (upregulated and downregulated) miRNAs in TCDD-induced peritoneal MDSCs. Furthermore, upon analysis of 141 dysregulated miRNAs using ingenuity pathway analysis (IPA) software, we observed a direct relationship between various miRNAs and the target genes including miR-150-5p and the target genes IL-10 and PIM1, and miR-543-3p and the target genes ARG2 and STAT3 as well as

CCL11, CCR3, CCR5 and CXCR2 (Fig 2.7E). These data suggested that TCDD-mediated alterations in the miRNAs may regulate the expression of various target molecules such as IL-10, PIMI, ARG2, STAT3, CCL11, CCR3, CCR5 , and CXCR2 that are prominently involved in the induction and functions of MDSCs.

Real-Time (Q-PCR) to validate selective miRNAs and the target genes.

Based on the complementary binding affinity of miR-150-5p with IL-10 and PIMI genes (Fig 2.8A) and miR-543-3p with ARG2, STAT3, and CXCR2 (Fig 2.8B) as well as with CCL11, CCR3, and CCR5 (Fig 2.8C), we selected miR-150-5p and miR-543-3p to validate their expression. Q-PCR data showed significant downregulation of both miR-150-5p and miR-543-3p in TCDD-induced peritoneal MDSCs, when compared to vehicle-induced MDSCs (Fig 2.9A). Next, we examined the expression of target genes IL-10 and PIM1 (miR-150-5p target genes), ARG2, STAT3, CCL11, and CCR5 (miR-154-3p target genes) by performing Q-PCR. We observed significant upregulation all these genes in TCDD-induced peritoneal MDSCs, when compared to vehicle-induced-MDSCs (Fig 2.9B). These data demonstrated that TCDD-alters the expression of miRNA in MDSCs which may lead to their induction and functions.

Analysis of miR-150-5p and miR-543-3p and specific targeted genes expression.

To further understand the role of miR-150-5p in IL-10 and PIM1 expression and miR-543-3p in ARG2, STAT3, CCL11, CCR3, CCR5, and CXCR2 expression, we performed a series of transfection assays. To that end, MDSCs were mock-transfected or transfected with mature miR-150-5p, mature miR-543-3p, anti-miR-150-5p inhibitor or anit-miR-543-3p inhibitor, and cultured for 24hrs. Next, the expression of various miRNAs and their target molecules was studied. Mock-transfected MDSCs showed basal

level expression of both miR-150-5p and miR-543-3p. MDSCs transfected with mature miR-150-5p and miR-543-3p showed significantly upregulated expression of both miRNAs in transfected MDSCs. However, transfection of MDSCs with anti-miR-150-5p and ani-miR-543-3p inhibitors showed downregulated expression of both miRNAs in MDSCs (Fig 2.9C,E). These data demonstrated that transfection of MDSCs with mature miRNAs or anti-miRNAs inhibitors showed expected results. To further understand the role of these two miRNAs, we performed q-PCR to determine the expression of IL-10, PIM1, STAT3, ARG2, CC11 genes and chemokines receptors CCR2, CCR5, and CXCR2. As shown in Fig 2.9D, the expression of IL-10 and PIM1 was significantly reduced in MDSCs in the presence of miR-150-5p. However, the expression of the above genes was significantly increased in MDSCs in the presence of anti-miRNA inhibitor. Figure 2.9F showed significant reduction in the expression of ARG2, STAT3 as well as chemokine CCL11 and chemokines receptors, CCR3, CCR5, and CXCR2 (Fig 2.9G) in MDSCs in the presence of miR-543-3p. However, there was a significant increase in the expression of these genes and chemokines receptors in the presence of anti-miRNA inhibitor. Together, these data demonstrated that TCDD-mediated alterations in the expression of miRNA may play a critical role in MDSC induction and functions.

2.5 DISCUSSION

In the current study we made an exciting observation that TCDD potently induces MDSCs at the site of administration even in naïve animals. Also, TCDD was able to induce MDSCs in an inflammatory model of ConA-induced hepatitis. We found that TCDD-induced MDSCs were highly immuosuppressive as demonstrated using in vitro and adoptive transfer experiments. TCDD induced both the subsets of MDSCs:

granulocytic G-MDSCs ($CD11b^{+}LY6G^{+}Ly6C^{low}$) and monocytic M-MDSCs ($CD11b^{+}Ly6G^{-}LY6C^{hi}$). Additionally, we found that TCDD caused alterations in the expression of miRNA in MDSCs that promote the immunosuppressive functions of MDSCs.

TCDD is well characterized for its immunosuppressive properties that are mediated through activation of AhR (109-112). TCDD-mediated immunosuppression may involve multiple pathways because AhR ligation leads to activation of DREs found on a significant number of genes (113-115). TCDD-mediated immunosuppression may involve multiple pathways because AhR ligation leads to activation of DREs found on a significant number of genes (36-38), including those involved in the regulation of immune response. Some mechanistic pathways that have been previously identified include: induction of Fas that expresses DRE on its promoter and upregulation of FasL leading to enhanced activation-induced cell death/apoptosis (84, 85, 87, 114, 116, 117), upregulation of FoxP3 which also expresses DREs thereby leading to induction of Tregs (88, 89) increased induction of Tregs while suppressing Th17 cells via epigenetic regulation (50), and the like. In addition to Tregs, it is increasingly becoming clear that MDSCs also play a critical role as regulators of inflammation (103, 118, 119). Whether AhR activation can lead to induction of MDSCs in naïve mice has not been investigated thus far, and therefore formed the rationale for the pursuit of the current study. Interestingly, we found that TCDD treatment led to robust induction of MDSCs in naïve animals in a dose-dependent manner and such an induction was AhR-dependent. It has been reported that there are two groups of interconnected signals in MDSCs accumulation and activation. First group of signals is responsible for immature myeloid

cells expansion whereas, the second group of signal is responsible for their activation and promotion of pathologic activity (27). First group includes GM-CSF, M-CSF, G-CSF, IL-6, VEGF and polyunsaturated fatty acids and signals primarily via STAT3 and STAT5. However this signaling alone is not sufficient without second activating signal which is mainly provided by pro-inflammatory molecules such as interferon-γ (IFN-γ), IL-1β, IL-4, IL-6, IL-13, tumor necrosis factor (TNF), TLR ligand, and signals that utilize NF-κB, STAT1, and STAT6 transcription factors for their activation (27-29). In the current study, we found that induction of MDSCs in the peritoneal cavity was associated with increases in several chemokines such as CCL2, CCL3, CCL4, CCL11, CXCL1, CXCL2, CXCL5 and CXCL9. Also, the observation that TCDD caused a decrease in MDSCs in the bone marrow while an increase in the peritoneal cavity suggested that TCDD-induced chemokines in the peritoneal cavity may have caused MDSC mobilization from bone marrow to peritoneal exudate. This was also supported by the observation that TCDD treatment led to a significant decrease in BM-MDSCs with a consequent increase in peritoneal MDSCs. Additionally, we found that the peritoneal MDSCs induced by TCDD were not actively dividing thereby supporting the migration rather than in situ proliferation of MDSCs. We noted that TCDD treatment also caused activation of MDSC and their functions. Energy metabolic pathway(s) used by MDSCs may play a critical role on the immunosuppressive functions of MDSCs and increase in this pathway is a sign for high immunosuppressive activity of cells (26). We observed that TCDD-induced MDSCs had higher oxygen consumption rates (OCR), proton efflux rate (PER) and ATP rate. TCDD-induced MDSCs also exhibited significant increase in cell lineage-specific transcription factors and cytokines including IL-10, PIM1, STAT3, and ARG2.

Chemokines and their receptors such as CCL5, CXCL17, CXCL2, CCR5 and CXCR2 play a critical role in MDSCs migration from bone marrow to tumor environment (120-122). Furthermore, we observed increased expression of chemokines receptors post-TCDD administration on MDSCs such as CCR1 (receptor for CCL3 and CCL4), CCR5 (receptor for CCL4 and CCL11) and CXCR2 (receptor for CXCL1, CXCL2 and CXCL5) (Fig 2.3E). One of the chemokine receptors that is expressed on MDSCs that has effective role in MDSC migration is CXCR2. Thus, CXCR2-deficient mice showed significantly decreased MDSC induction, in an inflammatory models of endometriosis when compared to wild-type mice (123). Also, we found in the current study that blocking CXCR2 using an antagonist Sch527123, reduced TCDD-mediated MDSC induction (Fig 2.3F). Importantly, a second signal that is involved in MDSC accumulation includes GM-CSF, G-CSF, M-CSF, and VEGF (23, 124), and we found an increase in these factors in both serum and peritoneal exudate of TCDD-treated group when compared to vehicle (Fig 2.3C-D). These data together suggested that TCDD-induced upregulation of chemokines and their receptors were responsible for the migration and accumulation of MDSCs in the peritoneal cavity. We were surprised to see that TCDD induced many chemokines and thus, we checked to see if such chemokines may be induced following AhR activation involving DREs. To that end, we performed in silico analysis to address if the chemokine promoters expressed DREs. Such an analysis demonstrated that several chemokines expressed DREs on their promoters (Table 2).

MDSCs constitute a heterogeneous population of cells representing a pathological state of activation of myeloid cells that have acquired a highly immunosuppressive

phenotype (125). These cells are of great interest in cancer as well as in inflammation as they potently suppress the cytotoxic activities of natural killer and natural killer T cells, and immune responses mediated by CD4 and CD8 T cells (120, 126). Under normal conditions, precursor myeloid cells from bone marrow differentiate into mature granulocytes, macrophages or dendritic cells as they home to peripheral organs. However, enhanced mediator production during pathological conditions such as cancer, infections, trauma, inflammation and autoimmunity, as well as sometimes in response to certain natural compounds, there is proliferation of immature myeloid cells while blocking their terminal differentiation resulting in the accumulation of immunosuppressive MDSCs phenotype (121). Recent studies from our laboratory have demonstrated the induction of MDSCs as an important mechanism through which several natural compounds exert immunosuppressive or anti-inflammatory properties, including marijuana cannabinoids, and resveratrol (103, 108, 122, 127)

Functional analysis of TCDD-induced MDSCs showed potent immunosuppressive effects on T cell proliferation in vitro. We noted that while both G-MDSC and M-MDSCs were immunosuppressive against T cell proliferation in vitro, the latter cells were more potent. In the current study, we also demonstrated that TCDD-induce MDSCs were functionally immunosuppressive in vivo as well. Thus, upon adoptive transfer of TCDD-induced MDSCs in to ConA-injected mice, there was significant protection of liver form acute inflammation. This was found to be associated with increased polarization of Th2 cells and Tregs and decreased induction of Th1 and Th17 cells, along with increased production of anti-inflammatory cytokines TGF-β and IL-4 levels in these mice (Fig 2.5A-E). These data are consistent with our previous

studies demonstrating that MDSCs induced by cannabinoids can suppress ConA-induce hepatitis in vivo upon adoptive transfer (103). Importantly, we also noted that administration of TCDD into ConA-injected mice also led to protection of liver and in such mice, we also saw similar cell phenotypes including increased presence of MDSCs, Th2 cells, Tregs, and subsets of Tregs but a decrease in the induction of Th1 cells (Fig 2.6). MDSCs can induce Tregs through disruption Th17/Treg balance because MDSCs have the potential to convert Th17 cells into $Foxp3^{+}$ Treg and enhance shifting the immune response from inflammation to tolerance (128), which can also be mediated by increase of IL-10 or TGF-β production (101, 129).

Several studies have shown that miRNA play an influential role in the toxicity of TCDD in animal models (116, 130-133). Studies have also shown that miRNA play a critical role in the regulation of MDSCs in different diseases models (65, 104, 134-136). For example, inhibition of miRNA-9 has been shown to promote the differentiation of MDSCs whereas, overexpression of miRNA-9 markedly enhanced the function of MDSCs (137). Also miRNA-155 and miRNA-21 were the two most upregulated miRNAs during the induction of MDSCs from the bone marrow cells by GM-CSF, IL-6 and TGF-B (36). Chen and his colleagues found that miRNA-17-5p, miRNA-20a, miRNA-223, miRNA-21, miRNA-155, miRNA-494, miRNA-690, and miRNA-101 are of particular interest for tumor MDSCs accumulation and function (138). In this study, we also observed that TCDD-induced MDSCs exhibited significant down-regulation in the expression of miRNA including miR-150-5p and miR-543-3p. Upon further characterization of these two miRNAs, we observed that these two miRNAs targeted several anti-inflammatory genes IL-10, PIM1, ARG2, STAT3, and CCL11 and

chemokines receptors CCR3, CCR5, and CXCR2. Transfection studies confirmed that these miRNAs caused upregulation of these anti-inflammatory genes. IL-10, ARG2, and STAT3 have been well characterized for their ability to downregulate the production of pro-inflammatory cytokines such as INF-γ, IL-2, IL-3, and TNF-α (122, 127). Additionally, STAT3, a transcription factor, is a hallmark of MDSCs, as STAT3 is directly involved in the accumulation and expansion of MDSCs in humans and mice. Arg2 found in MDSCs is directly involved in depleting l-arginine availability for T cells in the inflamed microenvironment and thus inhibit T-cell proliferation. MDSCs not only suppress T cell activation by IL-10 production but also by interacting with macrophages to increase IL-10 production and decrease IL-12 secretion (139-141). PIM1 is a member in serine/threonine kinases family that has two members, PIM2 and PIM3 in addition to PIM1 and have been implicated in the regulation of apoptosis, metabolism, cell cycle, and migration. PIMI was observed to be overexpressed in numerous solid tumors and was accompanied by MDSCs accumulation (142). From the current study, we noted that CCL11 and its receptors CCR3 and CCR5 were specifically embroiled in MDSCs migration from bone marrow to peritoneal exudate. Analysis using ingenuity pathway, shed light on the relationship of STAT3, IL-10, PIM1, ARG2, CCL11, CCR3, CCR5, and CXCR2 and the two downregulated miRNAs, miR-150-5p that targets IL-10 and PIM1 and miR-543-3p that targets ARG2, STAT3, CCL11, CCR3, CCR5, and CXCR2.

In summary, the present study demonstrates for the first time that activation of AhR triggers massive accumulation of MDSCs even in naïve mice without any inflammatory signal, resulting from induction of chemokines and their receptors. Furthermore, we observed that TCDD also causes changes in the expression of miRNA

within the MDSCs and alter gene expression that promote their anti-inflammatory functions. AhR activation is a double-edged sword. On one hand AhR plays a key role in intestinal homeostasis. Thus, deficits in AhR signaling have been linked to experimental and human intestinal bowel disease (143). On the other hand, AhR ligands such as the environmental contaminants, TCDD or methylcholanthrene (3-MC), are highly toxic and are considered to be carcinogens. Interestingly, this dual-action of AhR activation also correlates with that of MDSCs which are known to suppress inflammation and autoimmune disease (144) as well as promote tumor development and progression (145). Further studies aimed at addressing the nature of AhR-induced MDSCs in the regulation of health and disease should provide useful clues to regulate disease pathogenesis.

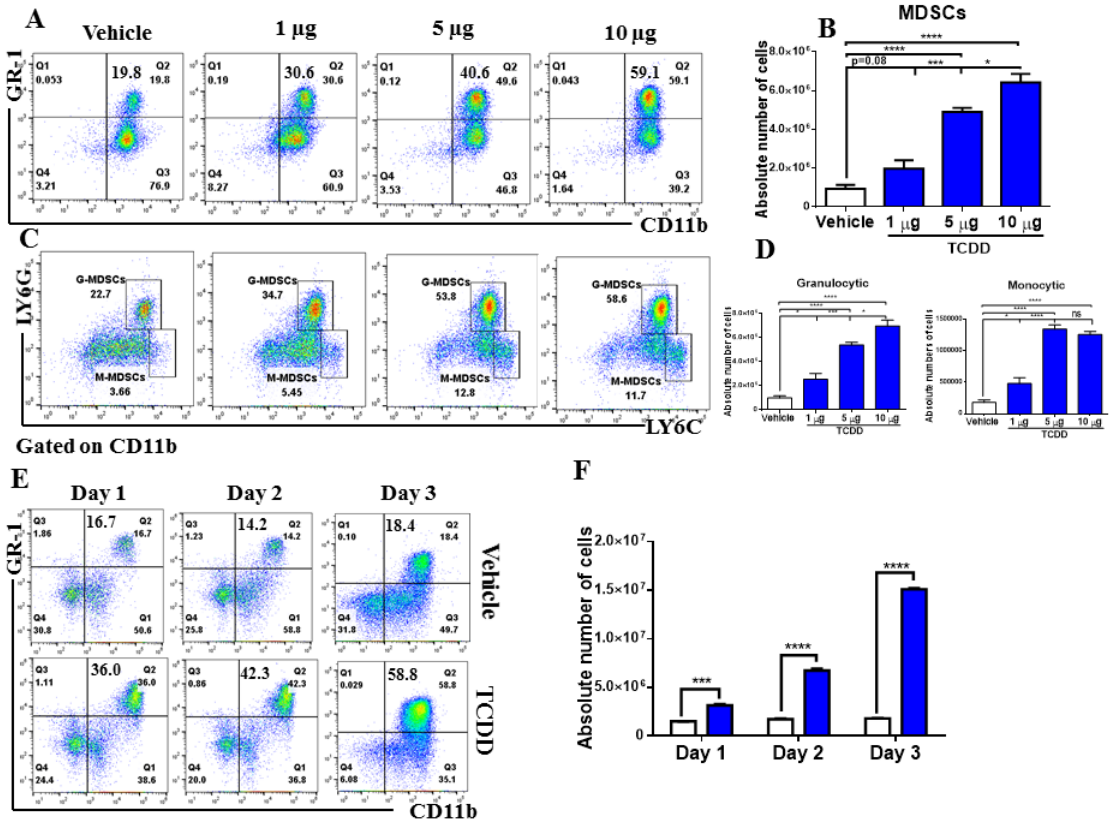

Figure 2.1: TCDD induces MDSCs in naïve mice. Naïve C57BL/6 mice were injected with TCDD or vehicle i.p. and at various days post-treatment, cells from the peritoneal cavity were harvested and analyzed for MDSCs. (A) Representative plots from flowjo software analysis of flow cytometry data showing induced in MDSC percentages following 1, 5, or 10 µg/kg TCDD administration when compared to vehicle. Cells were harvested on day three (B) Total number of MDSCs/mouse expressed as mean+/-SEM based on panel A description (C) Representative pseudocolor plots showing Monocytic MDSCs ($CD11b^{+}LY6G^{-}LY6C^{hi}$) and Granulocytic MDSCs ($CD11b^{+}LY6G^{+}LY6C^{low}$) percentages following administration of 1, 5, or 10 µg/kg TCDD when compared to vehicle. (D) Total number of monocytic and granulocytic MDSCs/mouse expressed as mean+/-SEM. (E) Time-course of induction of MDSCs. (F) Total number of MDSCs/mouse at different days expressed as mean+/-SEM. (G) Representative plots showing M-MDSCs and G-MDSCs after 3 days of 10 µg/kg TCDD treatment when compared to vehicle. (H). Total number of MDSCs/mouse after 3 days following 10 µg/kg TCDD administration, expressed as mean+/-SEM. Statistical analysis was performed using Student's t test and one-way analysis of variance (ANOVA) *$p < 0.05$; **$p < 0.01$; ***$p < 0.001$; ****$p < 0.0.0001$.

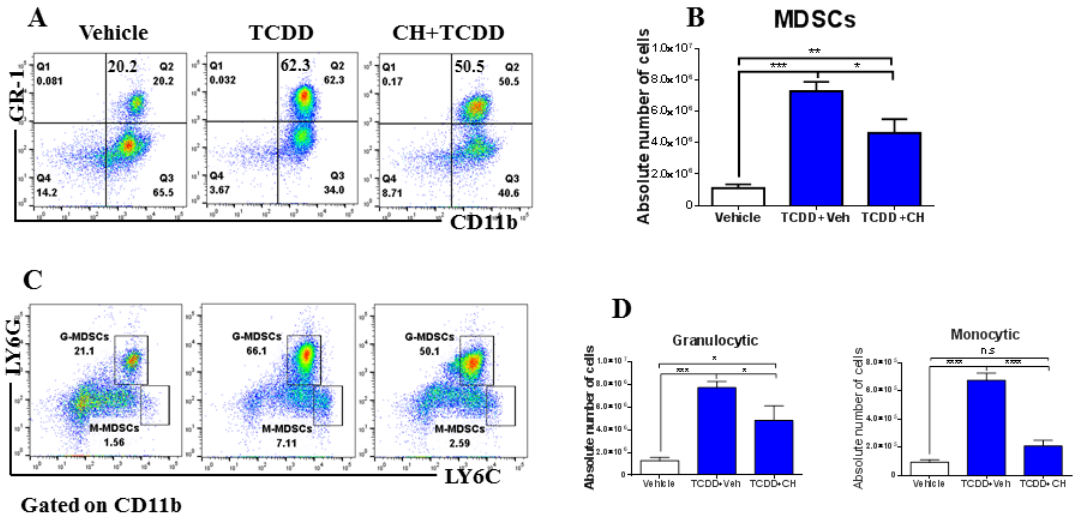

Figure 2.2: AhR antagonist CH223191 treatment decreases TCDD-mediated MDSC induction. Naïve C57BL/6 mice were injected with TCDD (10 µg/kg) i.p. as described in Fig 1 legend. These mice were injected i.p with 10 mg/kg of AhR antagonist (CH223191) one day before TCDD injection. Peritoneal exudates were collected in day 3 and stained for MDSCs. (A) Representative flow cytometric analysis showing MDSC percentages after treatment with AhR antagonist. (B) Total number of MDSCs/mouse expressed as mean+/-SEM following treatment with AhR antagonist, based on panel A description. (C) Representative flow cytometric analysis showing percentages of MDSC subsets after treatment with AhR antagonist. (D) Total number of MDSC subsets /mouse expressed as mean+/-SEM following treatment with AhR antagonist. One-way analysis of variance (ANOVA) was used to compare between the groups *$p < 0.05$; **$p < 0.01$; ***$p < 0.001$; ****$p < 0.0001$.

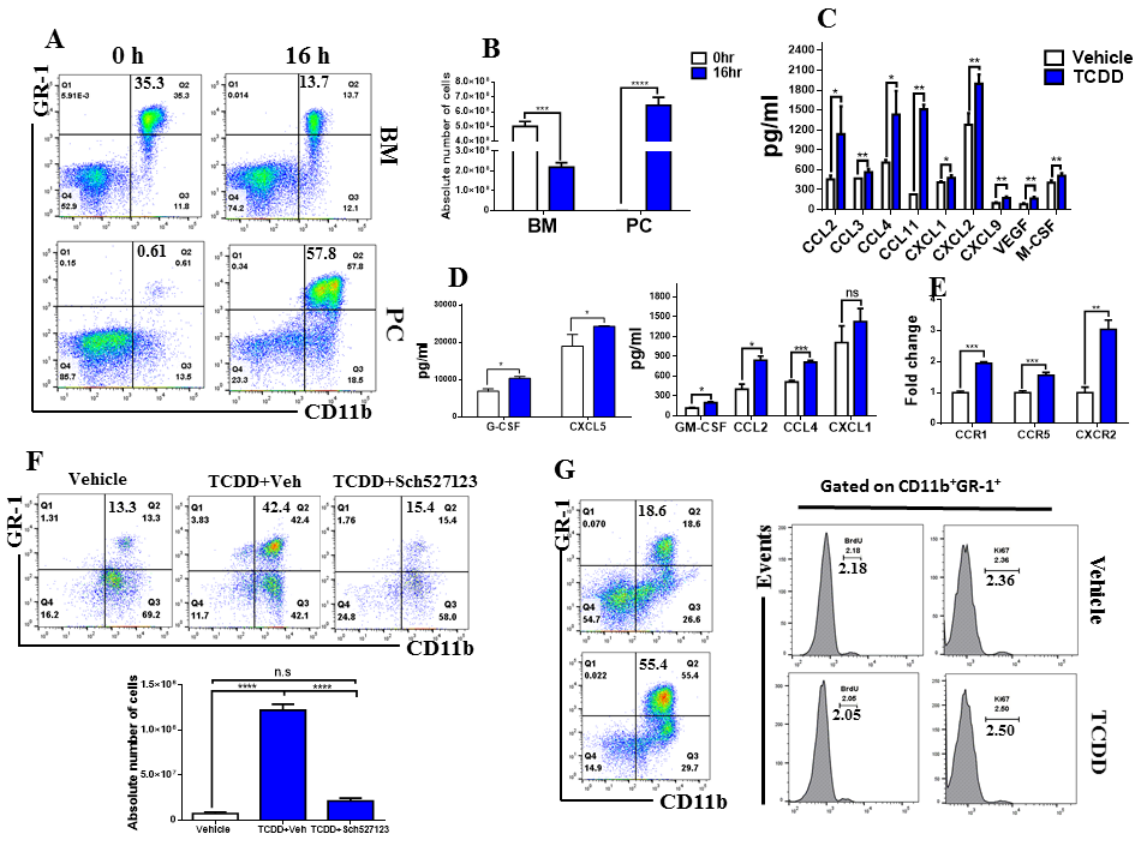

Figure 2.3: Identifying the source of TCDD-induce MDSCs. Naïve C57BL/6 mice were injected with TCDD (10 µg/kg) i.p. as described in Fig 1 legend. (A) Representative flow cytometric analysis showing that percentage of MDSCs in bone marrow 16 hrs after TCDD treatment when compared to 0 hr. Contrary, MDSCs percentage increased in peritoneal cavity after 16 hrs compared to 0 hr. (B) Total number of MDSCs/mouse expressed as mean+/-SEM based on panel A description (C) Measurement of chemokines in peritoneal exudate with data expressed as mean+/-SEM. (D) Detection of chemokines in the serum with data expressed as mean+/-SEM. (E) Q-PCR validation of CCR1, CCR5 and CXCR2 expression in TCDD compared to vehicle, with data expressed as mean+/-SEM. (F) Flow cytometric analysis of MDSC percentage and absolute numbers following treatment with TCDD and CXR2 antagonist. Vertical bars represent total cellularity/mouse expressed as mean+/-SEM. (G) Representative plots of BrdU labeling and anti-Ki67 staining at 48 h post-TCDD treatment. The left panel shows staining for MDSCs and right panel shows staining for BrdU and Ki67 on gated MDSCs. Vertical bars represent mean ± SEM. Student's t test and One-way analysis of variance (ANOVA) with *$p < 0.05$; **$p < 0.01$; ***$p < 0.001$; ****$p<0.0001$.

.

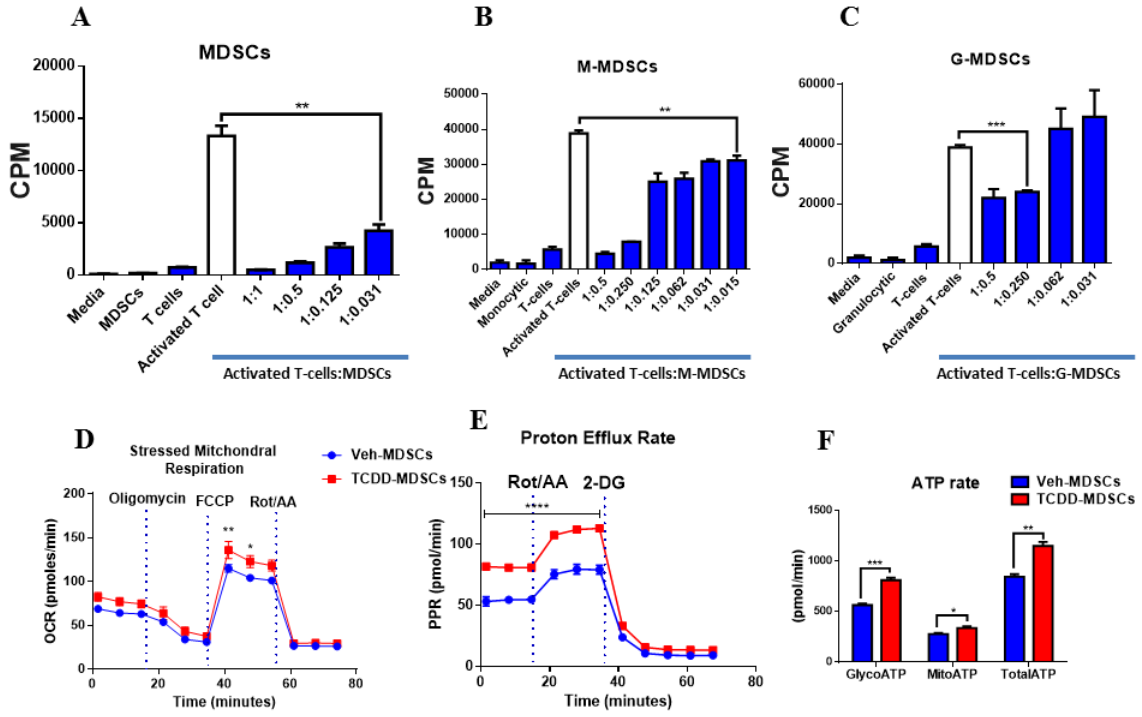

Figure 2.4: TCDD-induced MDSCs suppress T cell proliferation and exhibit different metabolic profile. (A-C) TCDD-induced purified peritoneal MDSCs as well as monocytic and granulocytic MDSCs were incubated with spleen cells activated with ConA at different ratios and T cell proliferation was assessed by 3H-thymidine incorporation assay. Data are depicted as mean ± SEM of triplicate cultures shown as counts per minute (CPM). (D,E) Oxygen consumption rate (OCR) and Glycolytic proton efflux rate (GRE) TCDD-induced MDSCs compared to vehicle-induced MDSCs. (F). ATP production rate in the experimental groups. Student's t test was used to compare between the groups in panels A-C $^{**}p < 0.01$; $^{***}p < 0.001$.

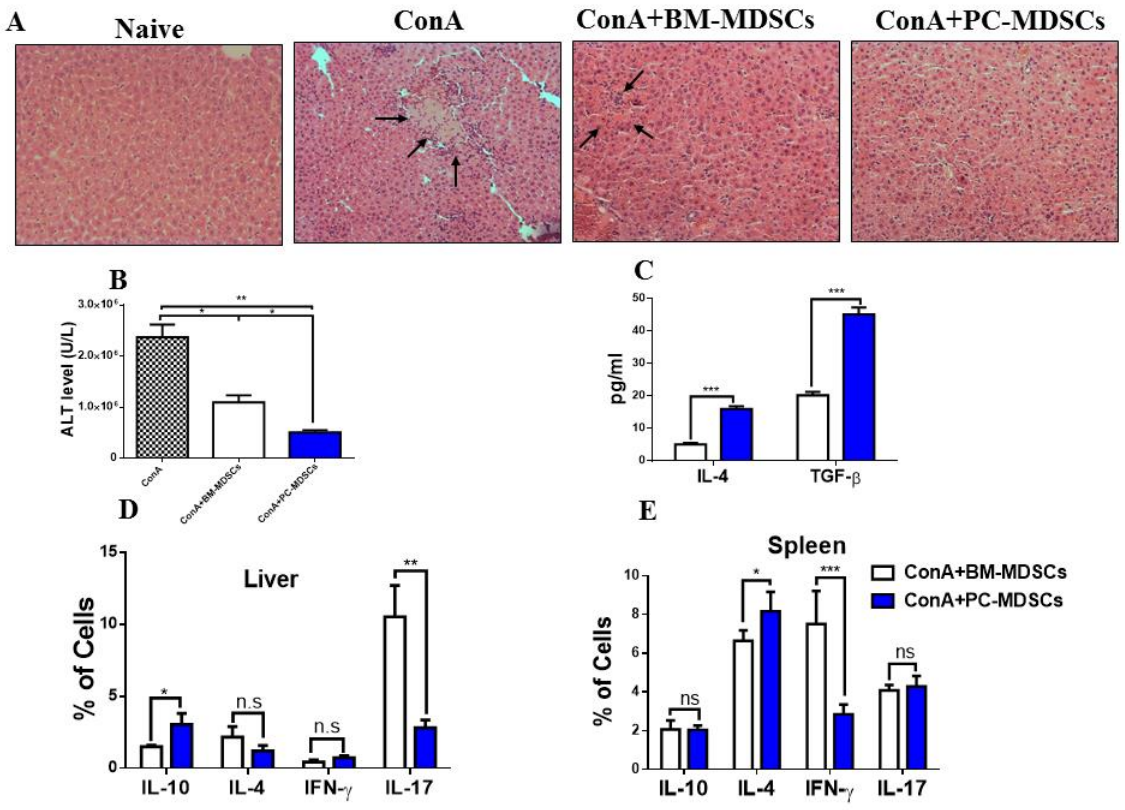

Figure 2.5: TCDD-induced MDSCs protect from ConA-induced liver damage and inflammation in vivo following adoptive transfer. C57BL/6 mice were injected intravenously with Con-A (12.5mg/kg) and these mice received 1 hr before, adoptive transfer of 5 million purified MDSCs from peritoneal cavity (PC-MDSCs) or bone marrow MDSCs (BM-MDSCs) from TCDD-treated mice. Mice were sacrificed after 48 hrs post treatment for further analysis. (A) H&E stain of liver tissue. (B) Measurement of ALT in sera. (C) Measurement of TGF-□ and IL-4 level in sera. Percentages of cells expressing various cytokines determined by flowcytometry in spleen(E), and liver (F). Vertical bars represent mean ± SEM. Student's t test *$p < 0.05$; **$p < 0.01$; ***$p < 0.001$.

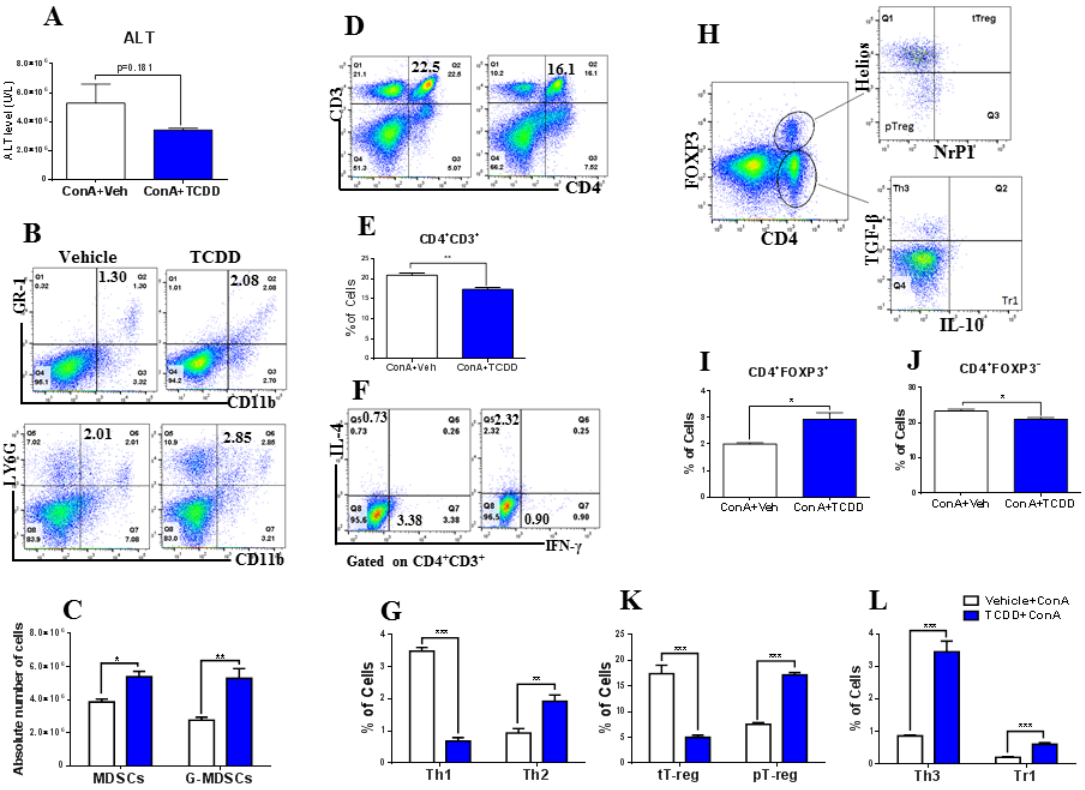

Figure 2.6: TCDD treatment attenuates ConA-induced hepatitis and associated inflammation. ConA was used to induce hepatitis as described in Fig 5 legend. These mice received TCDD (10 µg/kg) by i.p. route, 1 hr before ConA injection followed by analysis of spleens and liver for inflammation. (A) ALT level in serum of hepatitis-induced mice treated with vehicle or TCDD. (B, C) Percentage and total numbers of MDSCs and G-MDSCs in the spleens of two groups respectively. (D, E) Percentage of CD3+CD4+ cells in the spleens, respectively. (F,G) Percentages of Th1 and Th4 cells in splenocytes showing data from a representative and multiple experiments, respectively. (H-L) Elucidation of T-regs and their subsets in spleen cells showing both a representative experiment and data from multiple experiments in the form of vertical bars. Vertical bars represent mean ± SEM. Student's t test $^{**}p < 0.01$, $^{***}p < 0.001$.

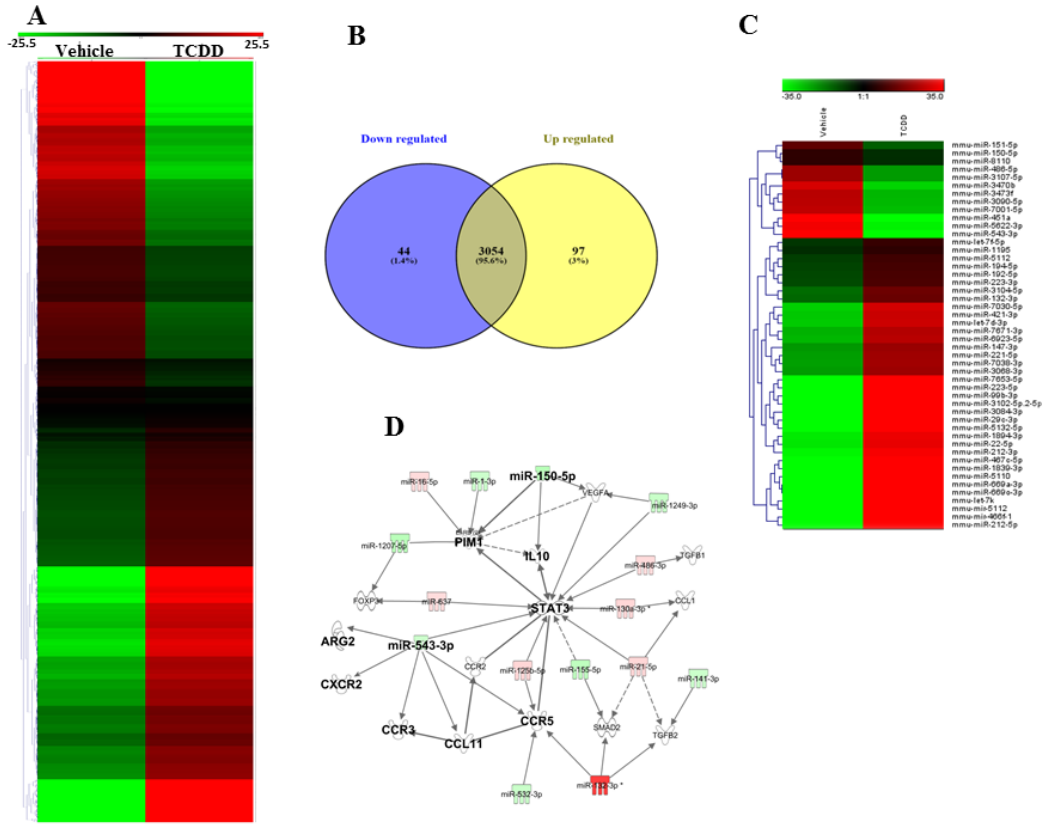

Figure 2.7: TCDD-mediated alterations in miRNA expression in MDSCs. Naïve mice were treated with TCDD as described in Fig 1 legend. The peritoneal MDSCs were analyzed for miRNA expression. (A) Heat map of miRNAs expression in MDSCs from vehicle and TCDD groups showing more than 3000 miRNAs. (B) Venn diagram showing miRNA that are up or down regulated in TCDD group when compared to vehicle controls. (C) Heat map of up and down regulated (greater than two-fold) of miRNAs in vehicle vs TCDD groups. (D) IPA ingenuity software analysis was used to determine interaction between up- and down-regulated miRNAs and targeted genes.

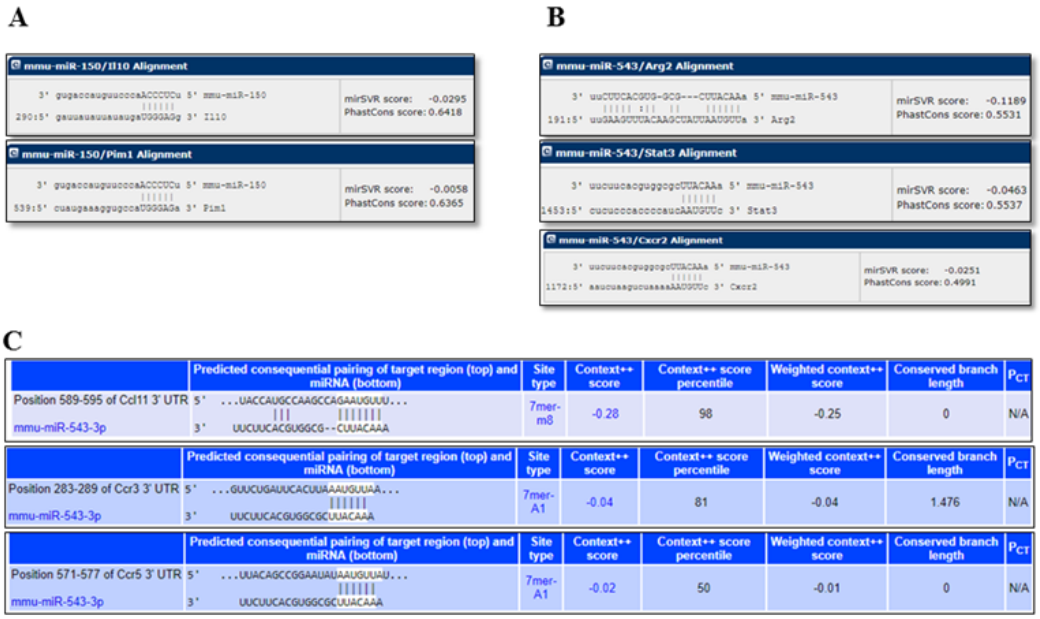

Figure 2.8: SVR and context alignment between miRNAs and targeted genes. (A,B) SVR score and alignment (miRNA.org) between mir-150-5p and targeted genes (IL-10 and PIM1) as well as between mir-543-3p and targeted genes (ARG2 and STAT3). (C) Context score and alignment (targetscan.org) between mir-543-3p and CCL11, CCR3, CCR5, and CXCR2.

.

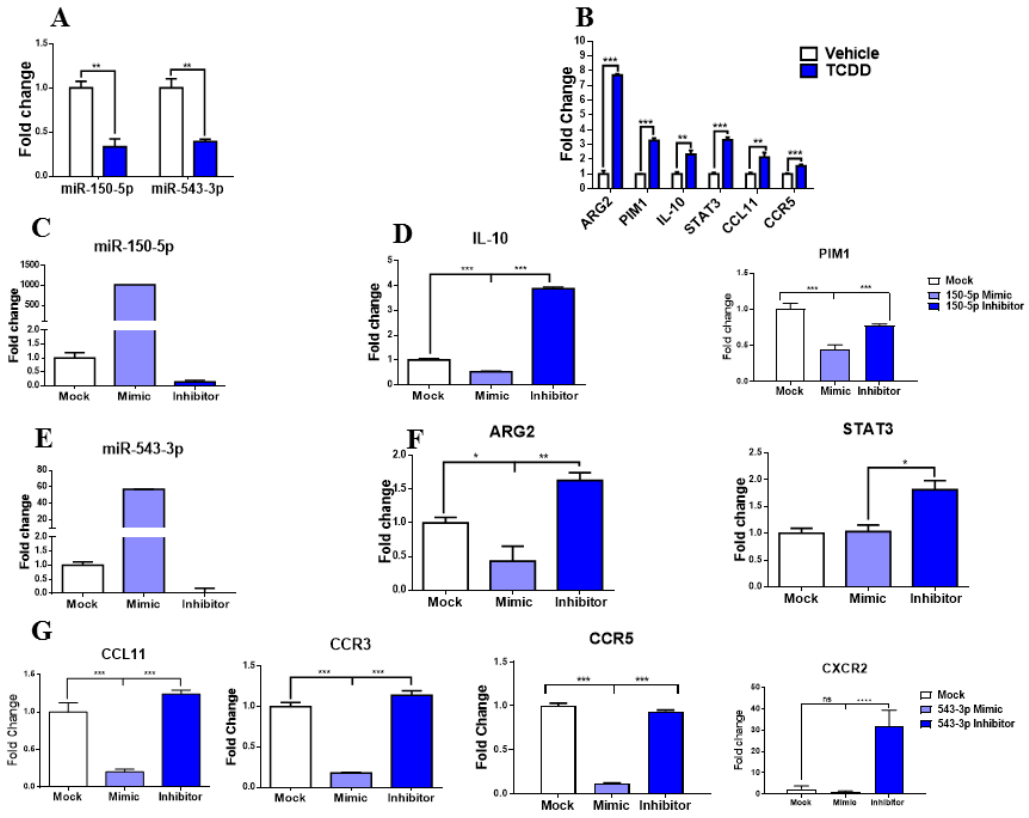

Figure 2.9: Q-PCR analysis of miRNA-150-5p and miRNA-543-3p and specific targeted genes. MDSCs were isolated as described in Fig 1 legend. (A) Expression of mir-150-5p and mir-543-3p in TCDD-induced MDSCs when compared to vehicle. (B). Expression of targeted genes IL-10, PIM1, ARG2, STAT3, CCL11, CCR3 and CCR5 in TCDD-induced MDSCs when compared to vehicle. MDSCs was transfected with mimic and inhibitor of both mir-150-5p and mir-543-3p (C) mir-150-5p expression with mimic compared to mock and inhibitor. (D) Expression of IL-10, PIM1 with inhibitor of mir-150-5p compared to mock and mimic of mir-150-5p. (E) Expression of mir-543-3p with mimic compared to mock and inhibitor. (F) Expression of ARG2, STAT3, CCL11, CCR3, and CCR5 in the presence of inhibitor of mir-543-3p compared to mock and to mimic of mir-543-3p. Vertical bars represent mean ± SEM. *$p < 0.05$; **$p < 0.01$; ***$p < 0.001$.

Table 2.1: The forward and reverse primers for listed genes:

Gene	Primer	Sequences (5'-3')
PIM1	Forward	TTCTGGACTGGTTCGAGAGG
	Reverse	TGTTCTCGTCCTTGATGTCG
Arg2	Forward	TGTCATCTGGGTTGATGCTC
	Reverse	CAGGAGGCTCCACATCTCTC
IL-10	Forward	CCCATTCCTCGTCACGATCTC
	Reverse	TCAGACTGGTTTGGGATAGGTTT
STAT3	Forward	CAATACCATTGACCTGCCGAT
	Reverse	GAGCGACTCAAACTGCCCT
CCL11	Forward	GAATCACCAACAACAGATGCAC
	Reverse	ATCCTGGACCCACTTCTTCTT
CCR1	Forward	CTCATGCAGCATAGGAGGCTT
	Reverse	ACATGGCATCACCAAAAATCCA
CCR3	Forward	TCAACTTGGCAATTTCTGACCT
	Reverse	CAGCATGGACGATAGCCAGG
CCR5	Forward	TTTTCAAGGGTCAGTTCCGAC

	Reverse	GGAAGACCATCATGTTACCCAC
CXCR2	Forward	ATGCCCTCTATTCTGCCAGAT
	Reverse	GTGCTCCGGTTGTATAAGATGAC

Table 2.2: Number of the sequences sites of the dioxin responsive element (DRE) on the promoter region of listed chemokines as well as accession and version for each chemokine.

Chemokine or miR	**Number of DRE Sequence Sites**		**Accession and Version**
	5'-CACGC-3'	5'-GCGTG-3'	
CCL2	1	2	AL626807.7
CCL3	1	2	AL596122.14
CCL4	1	2	AL596122.14
CCL11	2	2	AL645596.7
CXCL1	1	4	AC157938.9
CXCL2	2	5	AC157938.9
CXCL5	2	2	AC105995.9
CXCL9	3	4	AC109603.8
CXCR2	3	0	AC117757.23
miR-150-5p	19	11	AC126256.4
miR-543-3p	6	8	AC121784.2

CHAPTER 3

AHR ACTIVATION LEADS TO ALTERATIONS IN THE GUT MICROBIOME WITH CONSEQUENT EFFECT ON INDUCTION OF MYELOID DERIVED SUPPRESSER CELLS IN A CXCR2-DEPENDENT MANNER

3.1 ABSTRACT

Aryl hydrocarbon receptor (AhR) is a ligand activated transcription factor and 2,3,7,8-Tetrachlorodibenzo-p-dioxin (TCDD), a well-documented environmental halogenated aromatic hydrocarbon, is a potent ligand for AhR. Thus, AhR activation by TCDD leads to significant immunomodulation. Recent studies have shown that immune system homeostasis is also maintained by gut microbiota. Thus, whether TCDD-mediated regulation of immune response occurs through cross talk with gut microbiota is unclear. Previously, we observed that activation of AhR by TCDD in C57BL6 mice leads to massive mobilization of myeloid derived suppresser cells (MDSCs). In the current study, we observed that TCDD caused significant alterations in gut microbiome, specifically, increasing the abundance of several Prevotella and Lactobacillus at the genus level while decreasing Sutterella and Bacteroides. Fecal material transplantation (FMT) from TCDD-treated donor mice into antibiotic treated (ABX) mice induced MDSCs and MDSC subsets as well as increased Tregs. Injecting TCDD directly into ABX mice also induced MDSCs but to a much lesser degree than in naïve mice. These data suggested that TCDD-induced dysbiosis plays a critical role in MDSC induction. Interestingly, treatment with TCDD led to induction of MDSCs in the colon and

undetectable levels of cysteine. MDSCs suppressed T cell proliferation while reconstitution with cysteine restored this response. Lastly, blocking CXCR2 impeded TCDD-mediated MDSC induction. Our data demonstrate that AhR activation by TCDD triggers dysbiosis which in turn regulates, at least in part, induction of MDSCs.

3.2 INTRODUCTION

2,3,7,8-Tetrachlorodibenzo-p-dioxin (TCDD) is an environmental pollutant generated during the manufacture of herbicides or burning organic materials such as waste incarnation, fossil fuel, and wood combustion (146). Ingestion of contaminated food is one of the most common exposures of TCDD in humans (40). Following TCDD exposure, immune cells such as regulatory T cells (Tregs) are expanded and effector T-cells are suppressed (147), in addition to depletion of macrophages and dendritic cells in jejunum (148, 149). A single dose of oral TCDD administration decreased immunoglobulin (Ig) A secretion in the gut by impairing B-cell function (150). The gut is lined with a single layer of epithelia cells connected by tight junction proteins and is interspersed with mucus-secreting goblet cells and paneth cells which release antimicrobial peptides (151). Interestingly, mice treated orally with TCDD developed tolerance to ovalbumin (OVA) and showed suppression in the humoral immune response in the epithelial cells of lumen, as well as serum and fecal samples (152). However, in these same studies, alterations of other immune cells e.g. $CD4^+$, $CD8^+$, $CD19^+$, and $CD103^+MHCII^+CD11c^+$ by TCDD occurred only in the gut-specific draining lymph node (MLN).

The diversity of microbes within a given host can be defined by the number, abundance, and distribution of distinct types of organisms such as bacteria, archaea,

protists, fungi and viruses. The interaction and activity of these microbes has been linked to the homeostasis of immunologic, hormonal, and metabolic processes of the host. Microbial dysbiosis and alterations in the microbiome with negative effects on the host, occurs due to a wide range of causes such as diseases, environmental contamination, diet, and stress (52-54). The gastrointestinal tract is the largest habitat of the microbiota, and emerging studies have shown that TCDD exposure leads to its rapid absorption into the gastrointestinal tract which can cause shifts in gut microbiome commensals (55, 153). Nonetheless, whether there is a link between immunological changes induced by TCDD and the gut microbiota has not been previously studied.

Most of the activity of TCDD is mediated through the aryl hydrocarbon (AhR), a cytosolic-bound receptor expressed in a variety of immune cells including T-cells, monocytes, granulocytes, myeloid-derived suppressor cells (MDSCs), and mast cells. AhR activation by TCDD leads to alterations in the immune system involving several mechanisms such as disruption of the Treg/Th17 balance, suppression of the cytotoxic T-cells response, impairment of antibody production by B cells in a T cell dependent manner, and decrease in IL-6 and TNF production by macrophages, and induction of apoptosis in activated T cells (50, 87, 114, 154-156). TCDD is also well-characterized for its ability to induce Tregs (50, 157). Recently, we observed that TCDD administration leads to massive induction of MDSCs that are highly immunosuppressive (manuscript under review). Thus, in the current study, we investigated if the microbiota of the host plays any role in the induction of MDSCs by TCDD.

Using 16S rRNA sequencing of the gut microbiome, we noted that TCDD exposure resulted in alterations of the gut microbiome, and metabolome, such as

reduction in cysteine metabolism. Importantly, using fecal material transfer (FMT) experiments we found that MDSC induction by TCDD was dependent, at least in part, by the gut microbiota.

3.3 MATERIAL AND METHODS

Animals

Female C57BL/6 adult mice were purchased from Jackson laboratory (Bar Harbor, MA). All the animals were housed in the Animal Research Facility (ARF) located at the University of South Carolina (USC) under pathogen-free conditions. Mice were cared for in accordance with the NIH guideline for use of laboratory animals under protocols approved by the university Institutional Animal Care and Use Committee (IACUC) at USC.

Chemicals and reagents

TCDD was a kind gift from Dr. Steve Safe (Institute of Biosciences & Technology, Texas A&M Health Sciences Center, College Station, Texas). Culture medium reagents (RPMI 1640, Bacitracin, Gentamycin, Ciprofloxacin, Neomycin, Penicillin, Metronidazole, Ceftazidime, Streptomycin, and Vancomycin from Sigma-Aldrich (St. Louis, MO). HEPES, L-Glutamine, FBS, and PBS) were purchased from Invitrogen Life Technologies (Carlsbad, CA). The following antibodies were purchased from Biolegend (San Diego, CA) and used for surface markers, intra-cellular and/or intra-nuclear staining: Alexa Fluor 700-conjugated anti-CD11b, BV510-conjugated-GR-1, Alexa Fluor 488-conjugated anti-Ly6C, BV785-conjugated anti-Ly6G, BV785-conjugated anti-CD4, PE-conjugated anti-CD3, Alexa Fluor 488-conjugated anti-IL-17, BV605-conjugated anti-IL-10, BV650-conjugated anti-INF-γ, BV421-conjugated anti-

IL-4, BV510- conjugated anti-FOXP3 and, APC-conjugated anti-CD25. FC Block and monoclonal Mouse IgG anti-Arg1 were purchased from BD Biosciences (San Diego, USA). Monoclonal Rat IgG antibodies of CD11b and Ly6G/Ly6C (Gr-1) were purchased from Biolegend (San Diego, CA). Cytofix/CytopermTM Fixation/ Permeabilization kit was purchased from BD Biosciences. True-Nuclear™ Transcription Factor Buffer Set was purchased from BioLegend. EasySep™ PE Positive Selection Kits were purchased from Stem Cell Technologies (Vancouver, BC, Canada). N acetyl-cysteine (NAC) and CXCR2 antagonist Sch527123 were purchased from Sigma-Aldrich (St. Louis, MO). Cysteine Assay Kit was purchased from Abcam (Cambridge, United Kingdom).

TCDD Exposure and 16S rRNA amplicon sequencing

Female C57BL/6 between 6-8 weeks were injected i.p. with TCDD (10 µg/kg) or Vehicle (corn oil), as described previously (116, 158). Feces from individual mouse were collected from TCDD- or Vehicle-treated mice or from naïve mice, three days post treatments and kept in -80^{0}C for later use. 16S rRNA sequencing and analysis were performed as previously described (159). QIAamp DNA Stool Mini Kit (Qiagen) was used for DNA isolation from fecal pellets (100 mg) of the three groups following the protocol of the company (Qiagen). Genomic DNA samples were quantified by using nanodrop system (Thermo Scientific) and kept in -80^{0}C for further use. Amplification of the 16S rRNA V3–V4 hypervariable region was carried out using the 16S V3 314F forward (5′-TCGTCGGCAGCGTCAGATGTGTATAAGAGACAGCCTACGGGNGGC WGCAG-3′) and V4 805R reverse primers (5′-GTCTCGTGGGCTCGGAGATGTGTATAAGA,

GACAGGACTACHVGGGTATCTAATCC-3′). The Illumina overhang adapter sequences to be added to locus-specific sequences are:

Forward overhang: 5’ TCGTCGGCAGCGTCAGATGTGTATAAGAGACAG

Reverse overhang: 5’ GTCTCGTGGGCTCGGAGATGTGTATAAGAGACAG

The PCR program used were 3 min at 95°C, followed by 25 cycles of 30 s at 95°C, 30 s at 55°C, and 30 s at 72°C and a final extension at 72°C for 5 min. Each reaction mixture (25 µl) contained 50 ng of genomic DNA, 0.5 µl of amplicon PCR forward primer (0.2 µM), 0.5 µl of amplicon PCR reverse primer (0.2 µM), and 12.5 µl of 2× KAPA Hifi Hot Start Ready Mix. AMPure XP beads were used for each reaction to purify the 16S V3 and V4 amplicon away from free primers and primer dimer species. Attachment of dual indices and Illumina sequencing adapters was performed using the Nextera XTIndex Kit includes 5 µl of amplicon PCR product DNA, 5 µl of Illumina Nextera XT Index Primer 1 (N7xx), 5 µl of Nextera XT Index Primer 2 (S5xx), 25 µl of 2 × KAPA HiFi Hot Start Ready Mix, and 10 µl of PCR-grade water. Amplification was carried out under the following program: 3 min at 95°C, followed by 8 cycles of 30 s at 95°C, 30 s at 55°C, and 30 s at 72°C, and a final extension at 72°C for 5 min. Constructed 16S metagenomic libraries were purified with AM Pure XP beads and quantified with Quant-iTPicoGreen. Libraries were quantified using a fluorometric quantification method that uses dsDNA binding dyes. DNA concentration was calculated in nM based on the size of DNA amplicons as determined by an Agilent Technologies 2100 Bioanalyzer trace. Libraries were normalized and pooled to 40 nM based on quantified values. Pooled samples were denatured and diluted to a final concentration of 8 pM with a 30% PhiX (Illumina) control. Samples then were loaded, and results were provided by MiSeq Reporter

software (MSR). The Metagenomics workflow classifies organisms from V3 and V4 amplicon using a database of 16S rRNA data. The classification is based on the Greengenes database (http://greengenes.lbl.gov/). The output of this workflow is a classification of reads at several taxonomic levels: kingdom, phylum, class, order, family, genus, and species. The online 16S analysis software from the National Institutes of Health (Nephele) was used to analyze sequencing data collected on the Illumina MiSeq. The groups of related DNA sequences were assigned to operational taxonomic units (OTUs), and output files were analyzed to determine gut microbial composition. The Phylogenetic Investigation of Communities by Reconstruction of Unobserved States (PICRUSt) option during Nephele analysis was used to examine differences Level 2 (L2) and Level 3 (L3) KEGG pathways using collected 16S rRNA sequencing data. In order to differentiate significant alterations within the gut microbiome from experimental samples, linear discrimination analysis of effect size (LeFSe) was used as previously described (160).

Short chain fatty acid (SCFA) analysis

SCFAs were quantified as previously described by Mehrpouya-Bahrami et al (161). In brief, 100 mg cecal contents were acidified by metaphosphoric acid and allowed to sit on ice for 30 min. After centrifugation of acidified samples at 12,000xg for 15 min at 4^0C, supernatants were collected and filtered using MC filters at 12,000xg for 4 min in 4^0C. MTBE (400 µL) from Sigma (650560) was added to each sample after transferring samples in to glass vials. The samples were then centrifuged down at 1300 rpm for 5 min at RT and the top organic layer was transferred to a new vial. The standard mixtures with the internal standard were used to determine the response factors and linearity for each

SCFA standard acid. A HP 5890 gas chromatograph configured with the flame-ionization detector (GC-FID) for analysis of volatile organic compounds was used to detect the concentration of propionic, n-butyric, isovaleric, valeric, isobutyric, caproic, and n-heptanoic acid in the samples.

Depletion of the gut microbiota

Depletion of the gut microbiome was achieved using a cocktail of antibiotics (ABX) consisting of the following: Bacitracin 1 mg/ml, Gentamycin 170 µg/ml, Ciprofloxacin 125 µg/ml, Neomycin 100 µg/ml, Penicillin 100 U/ml, Metronidazole 100 µg/ml, Ceftazidime 100 µg/ml, Streptomycin 50 µg/ml, and Vancomycin 50 µg/ml, as previously described (96, 162, 163) ABX treatment lasted for 24 days and was supplied in the drinking water. Feces for transfer experiments were collected from individual mouse under sterile conditions. To validate microbiome reduction, DNA was isolated using QIAamp DNA Stool Mini Kit (Qiagen) and analyzed by performing agarose gel electrophoresis. DNA Fragments were visualized by Imaging Chemi-Blots on the Bio-Rad ChemiDoc XRS HQ. Band density of DNA from ABX-treated mice were compared to band density of DNA from WT control mice. In addition, swabs from ABX-treated mouse and control feces were cultured in aerobic and anaerobic conditions 2 days. ABX treatment was stopped on day 25, and mice to be inoculated with fecal material were co-housed with Vehicle and TCDD donors on day 26, followed by all subsequent treatments given to mice on day 27.

Fecal material transplantation (FMT)

FMTs were performed to determine the effects of TCDD on the gut microbiome after TCDD treatment. Donor mice were divided into two groups (n=8 per group). One

group was injected with 10 µg/kg i.p. injections of TCDD (T), and the second group was treated with corn oil as the vehicle (V). After 3 days, colon contents were collected under sterile and anaerobic conditions for dilution in sterile PBS. ABX-treated mice were divided into 5 groups (n=4-5 per group) and treated as follows: untreated, treated butyrate in their drinking water (1% sodium butyrate), with TCDD (10 µg/kg) (TCDD); with FMTs from vehicle treated mice (VFMT); FMT from TCDD-treated mice (TFMT). The mice were euthanized after three days using isoflurane overdose to collect cells from peritoneal exudates, spleens, and blood.

Flow cytometry to evaluate immune cell phenotypes

MDSCs and MDSCs subsets were stained and identified as described by us previously (103). Cells were harvested from peritoneal cavity of recipient and treated mice and stained with fluorescently-labeled antibodies (Biolegend and BD Biosciences) for phenotyping. Antibodies included Alexa Fluor 700-conjugated anti-CD11b, BV510-conjugated-Gr-1, Alexa Fluor 488-conjugated anti-Ly6C and BV785-conjugated anti-Ly6G BioLegend (San Diego, CA, USA) to determine MDSCs ($CD11b^{+}Gr\text{-}1^{+}$) and the following MDSC subsets: monocytic MDSCs ($CD11b^{+}Ly6G^{-}Ly6C^{hi}$) and granulocytic MDSCs ($CD11b^{+}Ly6G^{+}Ly6C^{lo}$). For T helper and transcription factor FOXP3 staining, antibodies used were BV785-conjugated anti-CD4, PE-conjugated anti-CD3, Alexa Fluor 488-conjugated anti-IL-17, BV605-conjugated anti-IL-10, BV650-conjugated anti-IFN-γ, BV421-conjugated anti-IL-4, and BV510-conjugated anti-FOXP3 to detect the following T helper (Th) subsets: Th1 ($CD3^{+}CD4^{+}IFN\text{-}\gamma^{+}$), Th2 ($CD3^{+}CD4^{+}IL\text{-}4^{+}$), Th17 ($CD3^{+}CD4^{+}IL\text{-}17^{+}$), and Tregs ($CD4^{+}FoxP3^{+}$). Flow cytometry analysis was performed using BD FACs Celeste and FlowJo software from ThermoFisher Scientific.

Real-Time (RT-PCR)

DNA was isolated from feces of experimental groups using QIAamp DNA Stool kit from Qiagen (Valencia, CA), and samples were diluted to 1ng/µl concentrations. MiScript primer assays kit and miScript SYBR Green PCR kit from Qiagen were used to perform PCRs following the protocols provided by the company. Sutterella and Lactobacillus PCR primers were purchased from IDT Technologies with primer sequences based on previous publications (164, 165). Cystathionase, XCT, 4F2 and ASC primers were designed based on a previous publication (120). The PCR products, generated from mouse gene-specific primer pairs or bacteria-specific primers pairs, were visualized with UV light performing electrophoresis (1.2% agarose gel). The band intensity of PCR products was determined using ChemiDoc image analysis system from Bio-Rad (Bio-Rad, Hercules, CA). The expression of the above genes were normalized against PCR products generated from mouse housekeeping gene GAPDH or against PCR product generated from Eubacteria gene (internal controls) as previously reported (67).

Purification of MDSCs

TCDD-induced MDSCs from the exudates of peritoneal cavities were purified as previously described using selection of Gr-1^{+} MDSCs (119). In brief, peritoneal exudates were collected from TCDD-exposed mice and after washing the cells two times with PBS, cells were labeled with a PE-conjugated Gr-1 antibody from Biolegend and magnetically sorted using a Positive Mouse PE Selection kit from Stem Cell Technologies (Cambridge, MA) following instructions from the manufacturer.

[3H] thymidine incorporation assay

To measure the proliferation of T-cells, splenocytes ($5x10^5$) from C57BL/6 naïve mice were cultured in the presence of Con A (2 µg/ml) in medium deficient in N-acetyl-cysteine (NAC) or with NAC (0.5 Mm) in a 96-well round bottom plate. The cells were cultured alone or cultured together with TCDD-induced peritoneal MDSCs in the ratio of 1:0.5 overnight. [3H] thymidine (1 µCi/well) was added to the cell cultures, and after 18 hrs radioactivity was measured using a MicroBeta Trilux liquid-scintillation counter (PerkinElmer Life and Analytical Sciences).

Detection of Cysteine level in peritoneal exudate, and colon exudate

Cysteine concentration was assessed in peritoneal and colon exudates collected from mice that received TCDD treatment using a fluorometric Cysteine Assay Kit (ab211099) from Abcam following the protocol from the manufacturer. Delta corresponding fluorescence values (Δ RFU) were calculated and applied to the cysteine standard curve to calculate reaction concentration.

Fluorescence staining of colon tissue sections

Colon tissue samples from three groups (Vehicle, TCDD, and TCDD+Sch527123) were fixed in 4% paraformaldehyde diluted in PBS overnight. Fixed colons were sectioned (5 µm thick) and placed on coated slides. Slides were incubated for 30 min in glycine 0.1% and 1x triton for tissue permeabilization for Arg1 staining or with glycine 0.1% only for CD11b and Gr-1 staining. Slides were then incubated with primary mouse anti-Arg1 antibodies or primary rat anti-CD11b and anti-Gr-1 antibodies purchased from Cell Signaling (Danvers, MA) at 4^0 C overnight, followed by a 2 hour incubation at room temperature with secondary Alexa Fluor 488 goat anti-mouse IgG

antibody for Arg1, Alexa Fluor 488 goat anti-rat IgG for CD11b, and Cy5 goat anti-rat IgG antibody for Gr-1. Fluorescent imaging of colon sections was taken using a Leica DM 2500 optical microscope from Leica Microsystems (Buffalo Grove, IL). Quantification of cell markers was calculated as corrected total cell fluorescence (CTCF) using Image J software (National Institutes of Health and the Laboratory for Optical and Computational Instrumentation).

Statistical analysis

GraphPad Prism software version 6.01 (San Diego, CA) was used for statistical analysis. Student's t-test was used for paired observations if data followed a normal distribution to compare between two groups while one-way analysis of variance (ANOVA) was used to compare between more than two groups. A P-value of ≤ 0.05 was considered statistically significant. For all experimental results, data was collected from at least two independent experiments with consistent results unless otherwise stated.

3.4 RESULTS

TCDD exposure alters the gut microbiome composition and SCFA production

TCDD is a well characterized high affinity ligand for AhR and therefore, we used TCDD to investigate how AhR activation alters the gut microbiota. 16S rRNA sequencing with the Illumina MiSeq platform was performed on feces from the following groups: wild-type mice (Naïve), mice treated with corn oil (Vehicle), and mice given 10µg/kg i.p. injections of TCDD (TCDD). Data collected from sequencing showed that Vehicle or TCDD treated mice had decreased alpha diversity when compared to naïve controls, which was assessed by Chao1 rarefaction measurement (Fig. 3.1A). Beta diversity from principle coordinate analysis (PCoA) also showed that Vehicle and TCDD

treated mice had gut microbial compositions dissimilar to Naïve mice, however, all groups clustered in their own respective treatment niches, suggesting TCDD-treated mice had a distinct composition when compared to Vehicle (Fig. 3.1B). However, sequencing data and OTU classification from the phylum to genus level showed that TCDD treatment had a marked effect on gut microbiome composition (Fig. 3.2-6).

In order to differentiate the significantly altered bacteria between all the experimental groups, LEfSe analysis was performed on the OTUs from phylum to genus. Results showed that there were several bacteria found to be distinctly expressed in the Naïve, Vehicle, and TCDD groups. These included the genus Bacteroides, Sutterella, Prevotella, and Lactobacillus (Fig. 3.1C-D). Among this LEfSe-identified bacteria, significantly altered OTUs between Vehicle and TCDD-treated mice included Prevotella, Sutterella, Lactobacillus, and Bacteroides (Fig. 3.1D). Specifically, after TCDD exposure, there was a significant increase in abundance of several Prevotella and Lactobacillus at the genus level however, Sutterella and Bacteroides were significantly decreased. To confirm the sequencing results, we quantified bacteria abundance from feces of experimental groups using bacteria-specific primers by PCR. These results confirmed that there was a significant increase (> 4 fold change) of Lactobacillus in TCDD-treated groups when compared to Naive and Vehicle groups (Fig. 3.1F). In addition, PCR validation experiments confirmed that there was a significant reduction in Sutterella (~50%) in TCDD-exposed mice (Fig. 3.1G). The phylogenetic sequencing and PCR validation data clearly demonstrated that TCDD exposure caused alterations in the microbiome, such as changing the abundance of Lactobacillus and Sutterella populations in the gut.

In addition to the phylogenetic data, bacterial metabolomic SCFA production was evaluated in the fecal samples from experimental mice exposed to TCDD. Of all the SCFAs studied, only two were found to be significantly altered after exposure to TCDD, which included acetic acid and butyric acid. Mice injected with TCDD showed significant increases in both acetic acid and butyric acid (Fig. 3.1H) when compared to Naïve control or Vehicle-treated mice. Taken altogether, these results showed that TCDD exposure leads to not only changes in the microbial phylogeny in the gut, but also alters some SCFA production as well.

TCDD-induced fecal microbiota when transferred into ABX mice can trigger MDSCs and Tregs.

TCDD exposure has been shown to regulate the immune response, particularly in suppressing the inflammatory T cell-mediated response (50, 166). Recently, we found that activation of AhR by TCDD induces large numbers of $CD11b^{+}Gr\text{-}1^{+}$ MDSCs in peritoneal cavity of mice (manuscript under consideration), as also shown (Fig 3.7A upper panels and 3.7B), which included both granulocytic-MDSCs and monocytic-MDSCs (Fig 3.7C upper panels and 3.7D). To further understand the role of microbiota in TCDD-mediated MDSC induction, FMT experiments were performed in ABX-treated mice. After confirming ABX treatment led to depletion of the gut microbiome (Fig. 3.8), various treatments and FMT experiments were performed to evaluate the contribution of the microbial changes to MDSC induction. This included fecal microbiota transfer (FMT) from Vehicle-treated mice into ABX mice (VFMT+ABX) or from TCDD-treated mice into ABX mice (TFMT+ABX). Interestingly, we observed that TFMT+ABX mice displayed higher proportion as well as increased numbers of MDSCs when compared to

VFMT+ABX mice (Fig. 3.7A lower panels, and 3.7B). Also, these MDSC induced in TFMT+ABX mice included both G-MDSCs and M-MDSCs (Fig 3.7C lower panels, and 3.7E). The FTM experiments were repeated with consistent results (Fig 3.9). These results strongly suggested that the gut microbiome plays a role in TCDD-mediated induction of MDSCs. Moreover, when we injected TCDD directly into ABX mice, we were able to induce MDSCs (Fig 3.9), although it was not as robust as injecting TCDD into naïve mice (Fig 3.7A upper panels) thereby showing that normal microbiota seen in naïve mice does play a role in MDSC induction by TCDD. We also injected butyrate into ABX mice to see if that would induce MDSCs and failed to detect any increase (Fig 3.9). The data that FMT from TCDD-treated mice into ABX mice could induce MDSCs and that TCDD could induce only a weak MDSC response in ABX mice, together demonstrated that induction of MDSCs by TCDD was dependent, at least in part, on gut microbiota.

AhR activation by TCDD, as well as MDSCs have been shown to induce Tregs (167, 168). To investigate if transplanted feces from TCDD-treated mice was able to induce Tregs, we harvested spleen cells from ABX-treated mice given TFMT or VFMT. We observed that TFMT mice did not exhibit any significant change in $CD3^{+}CD4^{+}$ cell numbers (Fig 3.10A-B) but interestingly, showed an increase in the numbers of $CD4^{+}FOXP3^{+}$ Tregs (Fig 3.10C-D). These data showed that induction of Tregs in naïve mice by TCDD may also depend, at least in part, on microbiota.

TCDD reduces cysteine level in colon and peritoneal exudates

In addition to phylogenetic data obtained from Nephele of the 16s rRNA sequencing data, theoretical analysis of the gut microbiome metabolomic profile was

determined using PICRUSt (Fig. 3.11A). Results from this in silico analysis assigning OTUs to KEGG pathways showed that TCDD caused a significant reduction in cysteine and methionine metabolism (Fig. 3.11B). To validate these findings, expression of cysteine-related genes were evaluated using PCR. Results showed that compared to Vehicle-induced peritoneal MDSCs, TCDD-induced peritoneal MDSCs express less cystathionase (CTH), the enzyme responsible for converting intracellular methionine to cysteine (Fig. 3.11C), as well as plasma membrane ASC (alanine-serine-cysteine transporter) neutral amino acid transporter and Xc^- and its light (XCT) and heavy chain (4F2) components, which are responsible for exporting cysteine and importing cystine from environment (Fig. 3.11C). Upon analysis of cysteine levels in the peritoneal and colon exudates of treated mice, it was found that cysteine levels were undetectable in mice exposed to TCDD, while Vehicle groups showed significant levels (Fig. 3.11D). In order to determine the role cysteine plays in MDSC function, proliferation assays were performed using ratios of MDSCs and T cells in the presence or absence of cysteine. As shown in Fig. 3.11E, upon activation with ConA adding cysteine in the media reduced the suppressive effect of MDSCs on the T-cells (Fig. 3.11E). These data demonstrated that TCDD exposure significantly impacted cysteine metabolism and this in turn has effects on the ability of MDSCs to suppress the activated T cell response.

TCDD-mediated effects on MDSCs and the gut microbiome are dependent on CXCR2

CXCR2 is a chemokine receptor important in the recruitment of MDSCs (169). Therefore, we investigated the effect of blocking CXCR2 on TCDD-mediated MDSC induction in the colon and peritoneal cavity. To test this notion, 50 mg/kg of CXCR2

antagonist, Sch527123, was injected in mice one day before treatment with TCDD. Colon sections from experimental mice were taken 3 days after TCDD exposure and stained with MDSC-specific markers (CD11b, Gr-1 and Arg1). Results showed that CD11b, Gr-1, and Arg1 expression increased in the colon after injection with TCDD when compared to colons from Vehicle-treated mice but this increase was lost in mice treated with the CXCR2 antagonist (Fig. 3.12A-D). Results also showed that blocking CXCR2 prevented the accumulation of MDSCs in the peritoneal cavity after injecting with TCDD (Fig. 3.12E-F). Taken together with the FMT results, these data suggested that TCDD-mediated effect on MSDCs is dependent on CXCR2.

3.5 DISCUSSION

In the last past several decades, numerous studies have shown that exposure of laboratory animals to TCDD leads to profound immunosuppression (109-112). More recent studies have shown that AhR activation by TCDD can suppress the immune system in mice by way of induction of Tregs (9, 49). Previous studies from our lab have also shown that TCDD was able to attenuate the clinical and inflammatory markers of colitis (50). The gut microbiome consists of trillions of bacteria which are sensitive to many endogenous and exogenous factors including diet, age, health condition, life style, and environmental exposures (170). A fundamental role of microbiome in the induction, education, and function of the host immune system is therefore understandable. In a mutually reciprocal relationship, microbial colonization in the host gut affects the development of the immune system, but also subtle changes in the immune system has effects on the gut microbiome composition (171). There are few studies on how AhR activation or exposure to TCDD can directly or indirectly cause changes in gut

microbiota, bile acids, and short chain fatty acid (SCFA) metabolism (172, 173). Previous studies have shown that TCDD, when given orally to mice, caused a shift in mouse gut commensals (56, 174). TCDD was even shown to play a role in influencing a shift favoring bacteria that expressed antimicrobial resistance genes (ARGs) (153).

In the current study, we observed significant alterations in the gut microbiome 3 days after exposure to TCDD. These alterations were characterized by reductions in certain bacteria, such as Sutterella, while significant increases in the abundance of other bacteria were observed, such as Lactobacillus. Some studies have reported that a decrease in Sutteralla and an increase in Lactobacillus are related to immune tolerance. Tang et al. observed that a reduction in Alcaligenaceae and Sutterella levels in normal mice after feeding with purple sweet potato polysaccharides caused an increase in anti-inflammatory cytokines IL-2 and IL-6 (175). Similarly, Pena et al. found significant reductions in pro-inflammatory IFN-γ and TNF-α in the spleen of probiotic-treated mice using a mixture of *Lactobacillus paracasei* and *Lactobacillus reuteri*, which resulted in lessening the severity of colitis in IL-10-deficient mice infected with Helicobacter hepaticus (176).

Alterations in gut microbiome, also leads to changes in bacterial metabolome, such as the production of SCFAs. SCFA, like acetic acid, butyric acid, and propionic acid, are metabolic end products of undigested complex carbohydrates for bacterial fermentation in the colon (177). We observed that the level of two SCFAs, butyric acid and acetic acid, were significantly higher in mice exposed to TCDD. Butyrate is known to exhibit tolerance-inducing activities such as induction of Treg cells, as well as other anti-inflammatory activities to include increased production of IL-22 (178). Several

studies, both in vivo and in vitro, have demonstrated that SCFA inhibit of histone deacetylases (HDACs), which results in many cases in the inactivation of nuclear factor-κB (NF-κB) and downregulation of a number of pro-inflammatory cytokines, like tumor necrosis factor (TNF) (179, 180). In addition, increased SCFA could enhance the differentiation of peripheral Treg populations through HDAC9 inhibition, and consequently attenuation of colitis in mice (181). Gallausiaux et al. also show butyrate produced by gut commensal bacteria influence the proportion and activation of anti-inflammatory regulatory T cells (Treg) (182). Given this information, the increase in SCFAs like butyrate after TCDD exposure could explain some of the mechanisms which drive the immune suppression of this environmental pollutant. However, we found that direct administration of butyrate into ABX mice failed to induce MDSCs.

Mammalian cells, including immune cells, require the essential amino acid cysteine for protein synthesis and proliferation (183, 184). Cysteine is generated by cells through two distinct pathways. One involves reducing intracellular disulfide-bonded cystine which is imported through plasma membrane transporter Xc- to form cysteine, which is eventually exported through the plasma membrane ASC transporter. Another pathway involves converting intracellular methionine to cysteine if the cells synthesize cystathionase enzyme. T cells does not express Xc- and ASC however, and thus, they depend on antigen presenting cells (APCs) such as macrophage and dendritic cells to obtain cysteine (185-189). MDSCs sequester cystine and do not export cysteine because they express only Xc-. Therefore, a large number of MDSCs in the microenvironment creates competition for cysteine between MDSCs and other immune cells, which can lead to reduction in cysteine levels, causing the suppression of T cell proliferation (120). In

the current report, TCDD reduced cysteine and methionine metabolism as evidenced through examination by PICRUSt, and these results were validated showing cysteine levels in the peritoneal cavity and colon exudates were decreased after TCDD exposure. The reason behind cysteine reduction after TCDD exposure could be attributed to sequestering by MDSCs, or it could also be attributed to an increase in bacteria, such as Lactobacillus, which use cysteine as a sulfur source to grow (190). It was thus interesting that when cysteine was provided in culture, it reversed the suppression of T cell proliferation mediated by MDSCs.

CXCR2 was shown to play a critical role in the induction of MDSCs. CXCR2 has been shown to play a critical role in MDSC migration to endometrial lesions through interactions with CXCL1, 2, and 5 (123). The fact that blocking CXCR2 reduced MDSCs significantly both in the colon and peritoneal cavity of TCDD-treated mice, confirmed the important role played by CXCR2 in inducing MDSCs in the colon. In an earlier study, we noted that TCDD can induce CXCR2 in naïve mice because it expresses several DREs on its promoter . Thus, AhR activation by TCDD involving DREs on CXCR2 gene promoter may help induce CXCR2 which in turn triggers MDSCs.

In summary, the current report provides evidence that TCDD causes a shift in the resident gut microbiome, particularly through increasing Lactobacillus and decreasing Sutterella abundances. FMT experiments confirmed that TCDD-mediated changes in the gut microbiome altered the immune system, specifically by increasing the MDSCs in a CXCR2-dependent manner, which resulted in decreased cysteine levels. Such events may promote an immunosuppressive response, thus providing evidence that AhR activation by

TCDD alters the microbiome in such a way that it influences the immune system of the host.

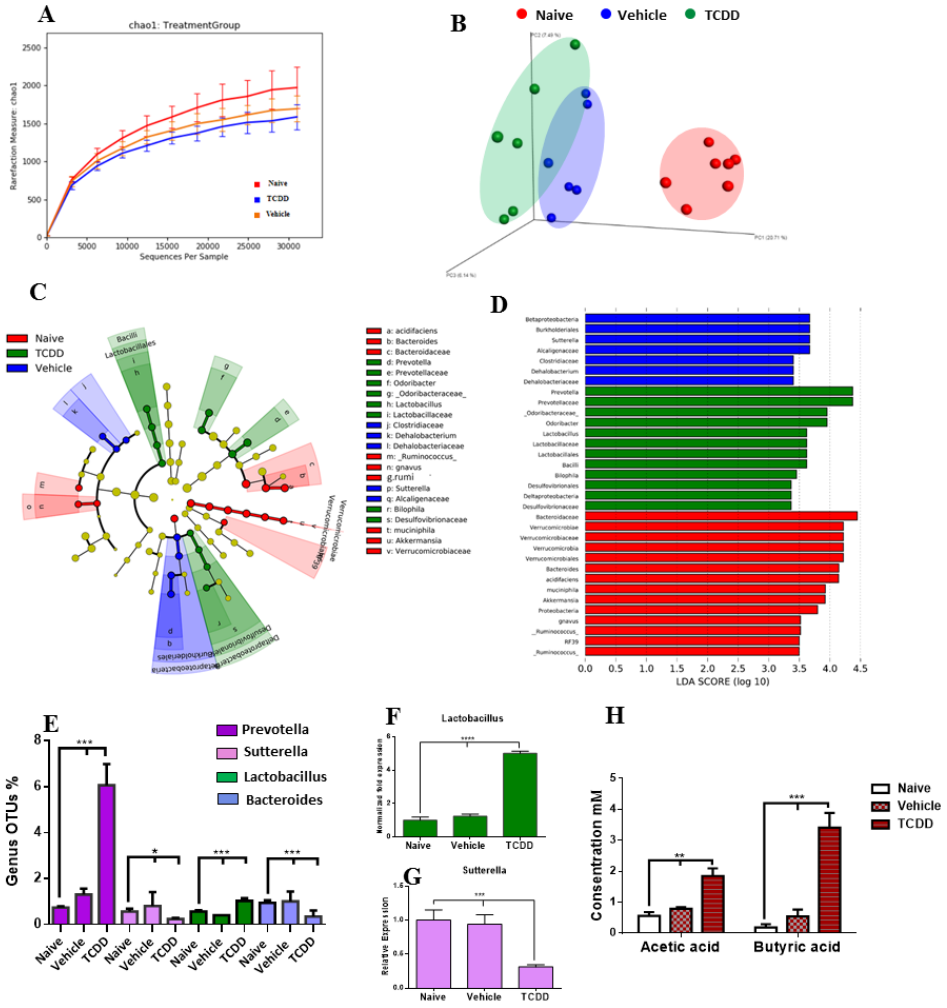

Figure 3.1: TCDD treatment alters microbiome composition. C57BL/6 mice were treated with TCDD (10 µg/kg) or vehicle and 3 days later, feces were collected for 16S rRNA sequencing. (A) Rarefaction curves depicting alpha diversity within groups (Chao1 index) of naïve (n=7), vehicle (n=6) and TCDD-treatment groups (n=6) are shown. (B) Three-dimensional principle coordinate analysis (PCoA) based on the unweighted UniFrac distance of all samples for three groups, naïve, vehicle and TCDD. (C) LeFSE-generated cladogram for OTUs showing the phylum, class, order, family, genus and species from the outer to inner swirl, respectively. Red indicates enrichment in taxa in samples from naïve group, blue from vehicle group, and green from TCDD group. (D) LeFSE-generated LDA scores for differentially expressed taxa. The threshold of LDA score was set to 3.5. (E) Percentage of OTUs of significantly-altered bacteria at the genus level. (F-G) q-PCR validation with primers for Lactobacillus (F) Sutterella and bacteria. (H) Concentration of butyric acid and acetic acid produced by the microbiota in the fecal contents. Bar graphs consists of vertical bars representing mean ± SEM. One-way analysis of variance (ANOVA) with Tukey's multiple comparisons test was used to determine significance; *$p < 0.05$; **$p < 0.01$; ***$p < 0.001$.

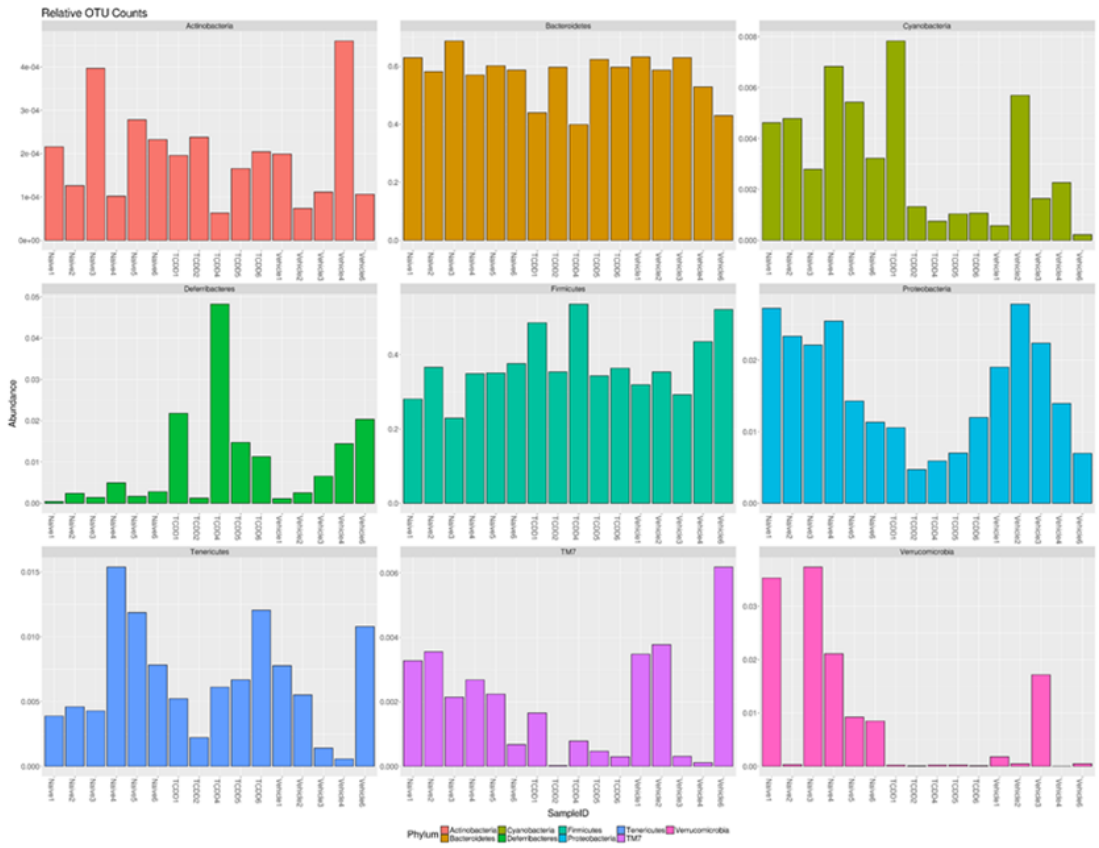

Figure 3.2: Mini blot bar from Nephele analysis showing 16s rRNA sequencing data depicting relative OTU abundance at the phylum level.

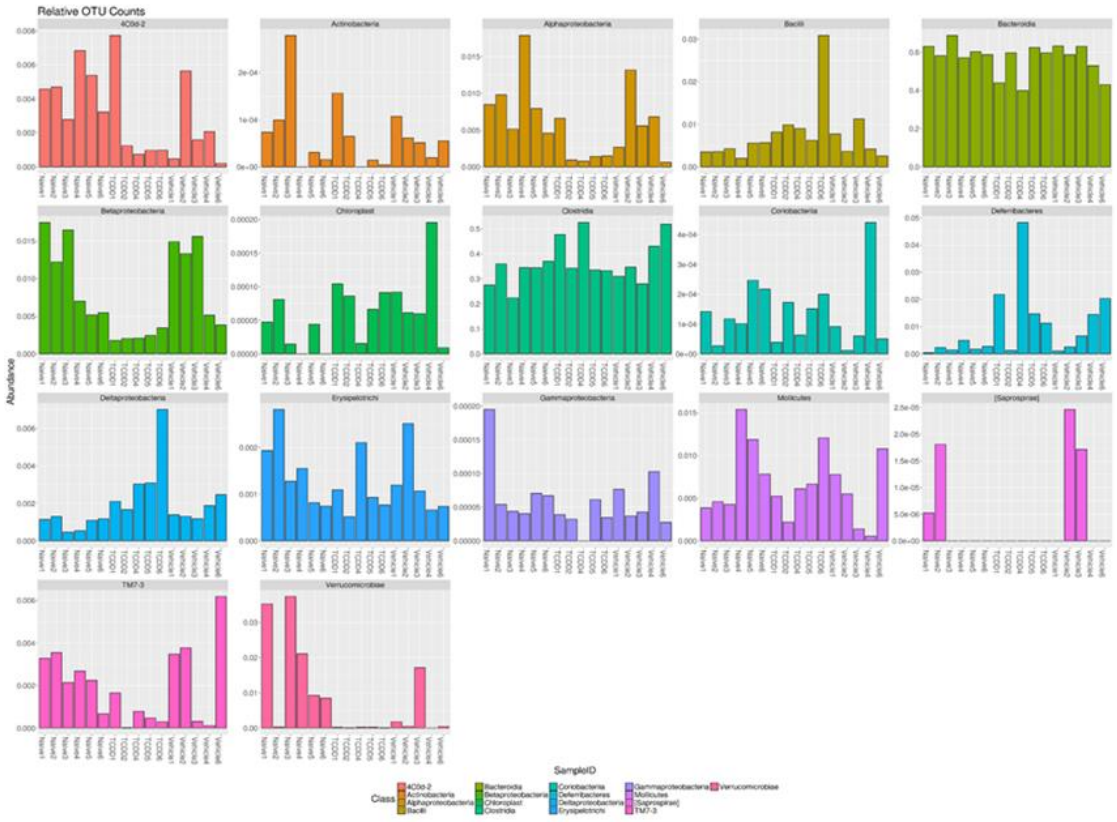

Figure 3.3: Mini blot bar from Nephele analysis showing 16s rRNA sequencing data depicting relative OTU abundance at the class level.

.

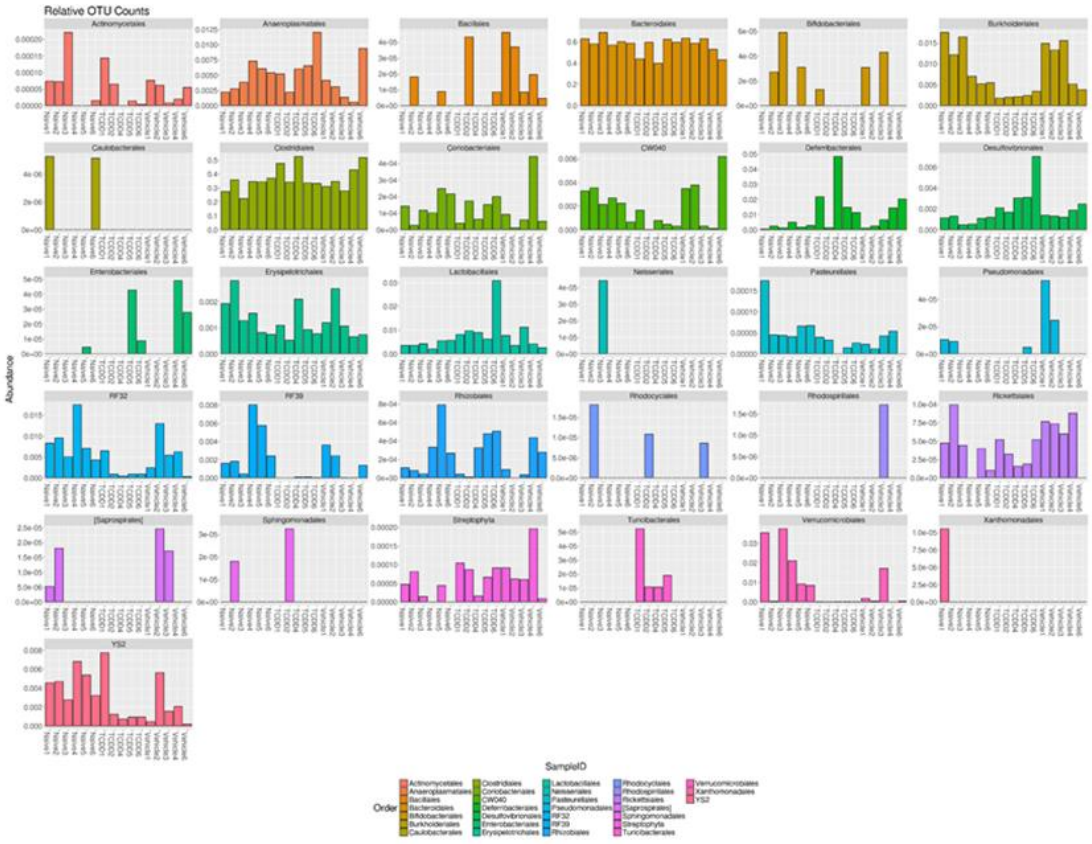

Figure 3.4: Mini blot bar from Nephele analysis showing 16s rRNA sequencing data depicting relative OTU abundance at the order level.

Figure 3.5: Mini blot bar from Nephele analysis showing 16s rRNA sequencing data depicting relative OTU abundance at the family level.

Figure 3.6: Mini blot bar from Nephele analysis showing 16s rRNA sequencing data depicting relative OTU abundance at the genus level.

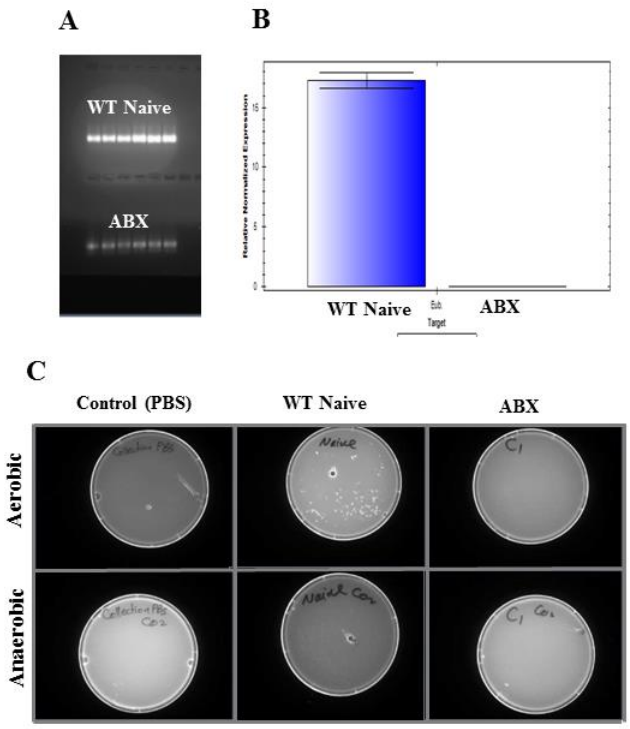

Figure 3.7: Bacterial depletion in ABX mice. Naïve mice were treated with a cocktail of antibiotics for 3 weeks prior to FMT experiments. (A) UV agarose gel electrophoresis image of genomic DNA in naïve WT and ABX mice showing PCR expression of Eubacteria. (B) Relative normalized expression of Eubacteria in WT Naïve or ABX mice using qRT-PCR (C) UV images of culture plates with swabs from fecal samples from control, WT Naïve, and ABX mice in aerobic (top) and anaerobic conditions (bottom).

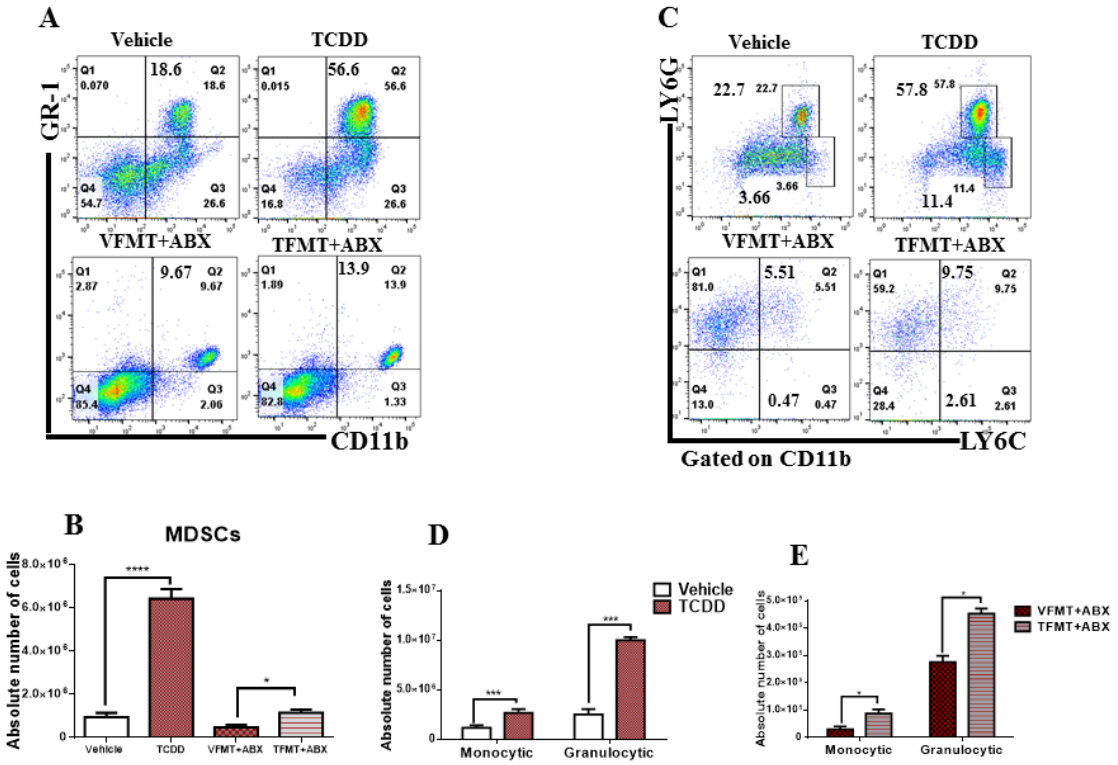

Figure 3.8: Effect of fecal microbiota transplantation on MDSCs and MDSC subset induction. Normal mice received Vehicle or TCDD and were analyzed for MDSCs or MDSC subsets in the peritoneal cavity (upper panels A, C, and panels B,D). Expression of CD11b and Gr-1 was used for MDSCs and CD11b and LY6C or LY6G for monocytic and granulocytic MDSCS, respectively. Also, ABX mice received feces from colon from vehicle (VFMT+ABX) or TCDD-treated mice (TFMT+ABX). And peritoneal cells were stained for MDSCs or subsets (lower panels A,C and panels B, E). Panels A and C show percentages of MDSCs while panels B, D, E show absolute number of MDSCs. Vertical bars represent mean ± SEM. Student's t test *$p < 0.05$; **$p < 0.01$; ***$p < 0.001$; ****$p < 0.0001$.

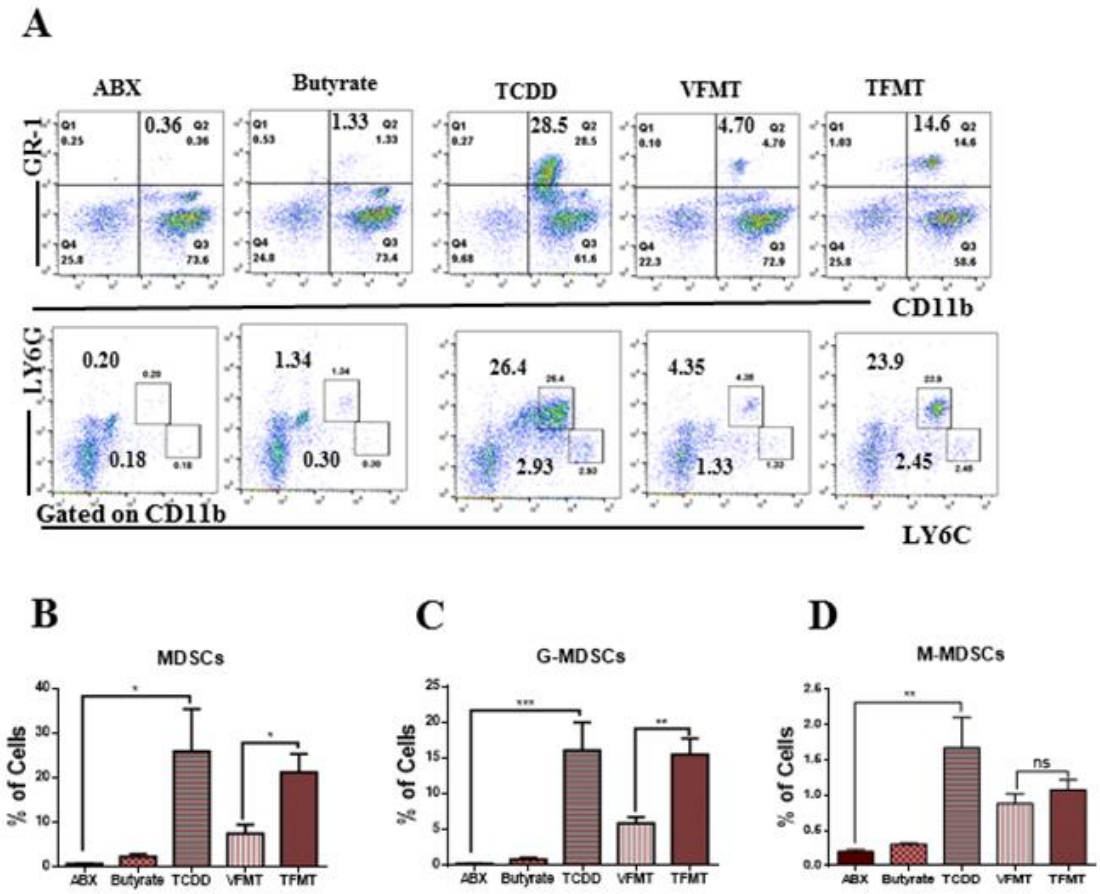

Figure 3.9: Effect of TCDD or FMT transfer into ABX mice on MDSC induction in ABX mice. These experiments were carried out as described in Fig 2 legend. ABX mice were administered TCDD alone, sodium butyrate alone, FMT from vehicle-treated (VFMT) or TCDD-treated (TFMT) donor mice. Peritoneal cavity fluid was collected and stained for CD11b Gr-1 for MDSCs and CD11b LY6C or LY6G for monocytic and granulocytic, respectively. (A) Representative flow plots of MDSCs (top) and MDSC subsets (bottom) in the ABX-treated mice given Butyrate, TCDD, VFMTs, and TFMT. (B-D) Total percentage of MDSCs and MDSC subsets in the ABX-treated mice given Butyrate, TCDD, and FMTs. Bar graphs consists of vertical bars representing mean ± SEM. One-way analysis of variance (ANOVA) with Tukey's multiple comparisons test was used to determine significance; *$p < 0.05$; **$p < 0.01$; ***$p < 0.001$.

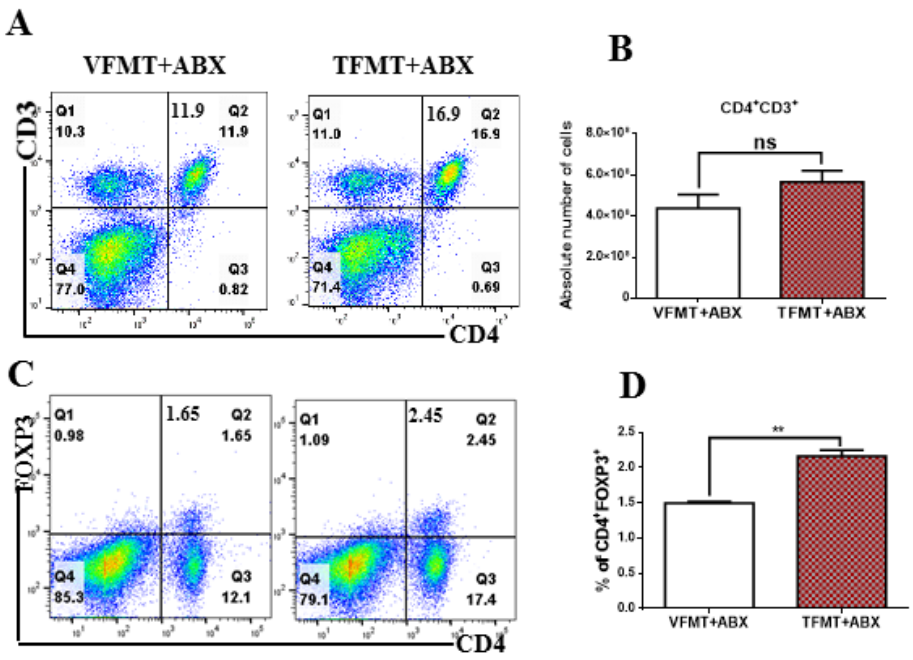

Figure 3.10: Fecal transplantation from TCDD-treated mice to ABX mice leads to induction of Tregs. FMT was performed as described in Fig 2 legend. Cells from spleens of VFMT or TFMT recipient mice were processed to stain stained for T cell markers. (A) Representative flow plot (CD4+CD3+) in spleen cells of ABX recipient mice following FMT from vehicle (VFMT) or TCDD (TFMT) donors. (B) Total cell number (CD4+CD3+) in spleen cells of ABX recipient mice following FMT from vehicle (VFMT) or TCDD (TFMT) donors. (C) Representative flow plot of Tregs (CD4+FoxP3+). (D) Percentage of Tregs from multiple experiments. Vertical bars represent mean ± SEM. Student's t test was used for compression between the two groups (VFMT vs. TFMT). *$p < 0.05$; **$p < 0.01$.

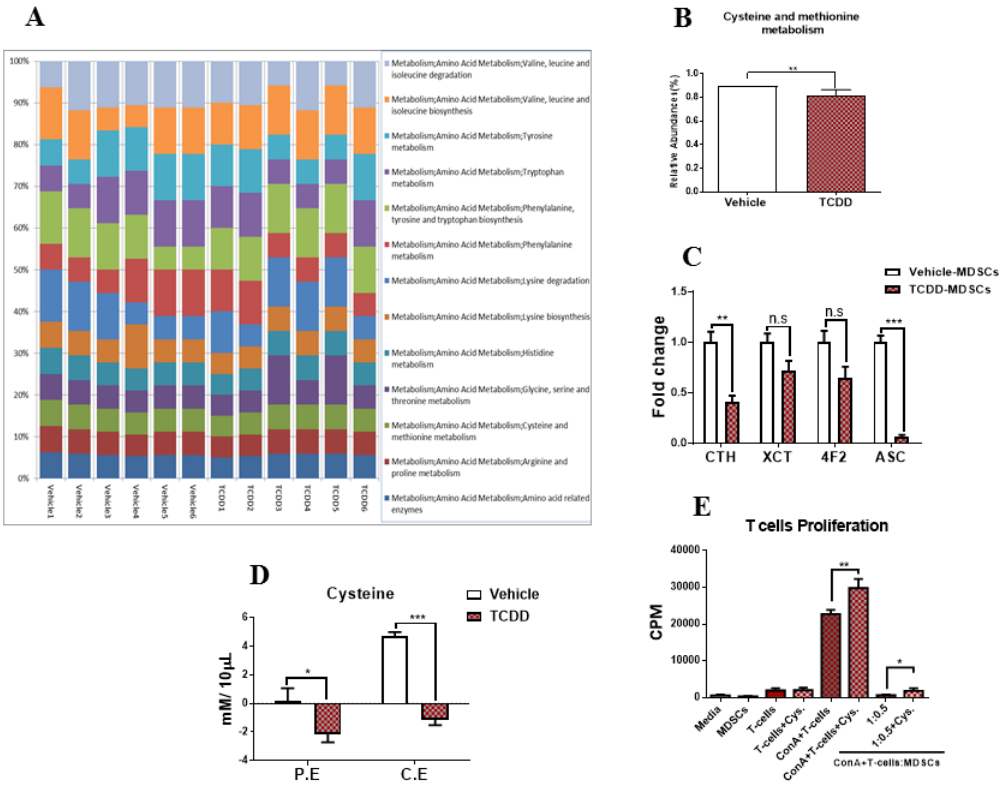

Figure 3.11: Role of cysteine in TCDD-mediated immunomodulation. C57BL/6 mice were treated with TCDD (10 µg/kg) or vehicle and feces were collected for 16S rRNA sequencing. (A) PICRUSt data from Nephele depicting KEGG pathways altered in vehicle (n=6), and TCDD (n=6) gut microbiome. (B) Percent OTUs attributed to cysteine and methionine metabolism. (C) qPCR quantification of ASC (alanine-serine-cysteine transporter) neutral amino acid transporter, XCT (light chain of antiporter Xc-) and 4F2 (heavy chain of antiporter Xc-) chains; CTH (cystathionase) . MDSCs were selected by PE selection kit from peritoneal fluid of vehicle or TCDD-treated groups. (D) Cysteine level quantification in peritoneal and colon exudate in vehicle or TCDD mice. (E) Representative 3H-thymidine incorporation assay for T-cell proliferation in media deficient in cysteine or with cysteine. Student's t test and one-way analysis of variance (ANOVA) were used to compare between the groups in panels *$p < 0.05$; **$p < 0.01$; ***$p < 0.001$.

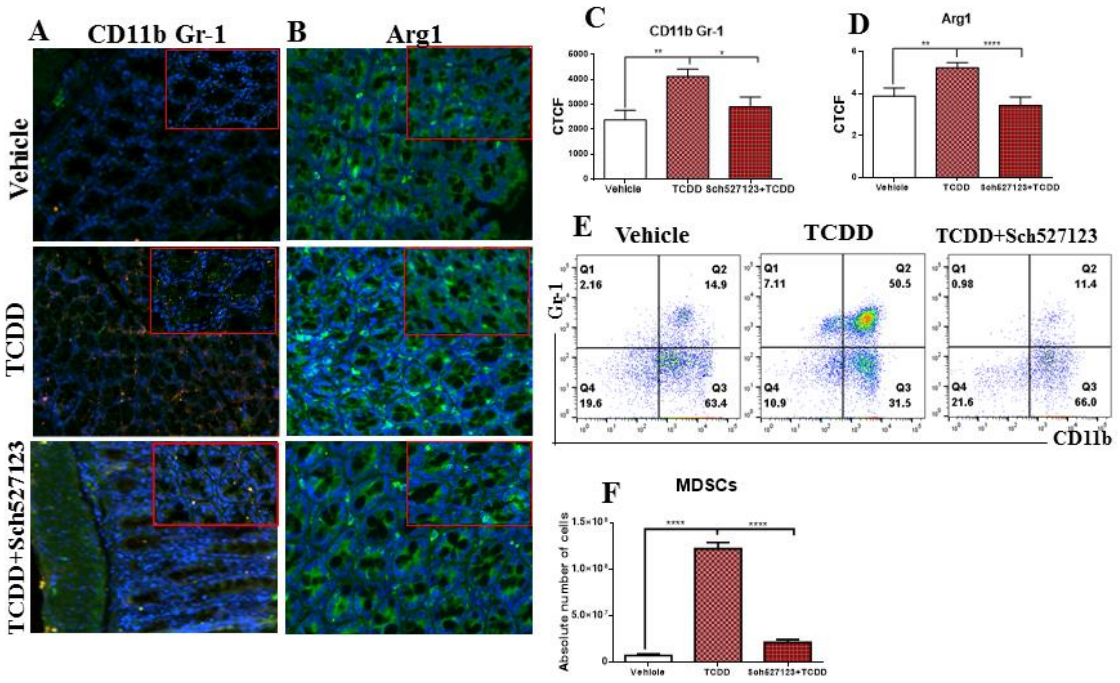

Figure 3.12: Role of CXCR2 in TCDD-mediated induction of MDSCs. Colon samples from three groups: Vehicle, TCDD, and TCDD with CXCR2 antagonist Sch527123 were fixed with 4% paraformaldehyde in PBS overnight and then sectioned to 5 µm thickness on coated slides. Slides were incubated with antibody detection of Gr-1, CD11b, and Arg1 (A) CD11b Gr-1 fluorescence staining in colon. Colon section from three groups were stained with CD11b (green) and Gr-1(red) to detect MDSCs. (B) Arg1 fluorescence staining (green) to quantify Arg1 expression in colon of three groups. (C-D) Statistical analysis of CD11b Gr-1 and Arg1 expression in colon sections of three groups as measured in CTCF using image J software. (E) Representative flow plots of MDSCs in peritoneal fluid in vehicle, TCDD and TCDD with CXCR2 antagonist Sch527123. (F) Absolute numbers of MDSCs in peritoneal fluid in vehicle, TCDD and TCDD with CXCR2 antagonist Sch527123. One-way analysis of variance (ANOVA) and Tukey's multiple comparisons test were used to compare between the groups. *$p < 0.05$; **$p < 0.01$; ***$p < 0.001$. ****$p < 0.0001$.

CHAPTER 4

RESVERATROL-MEDIATED ATTENUATION OF TCDD-INDUCED MDSCS MOBILIZATION, DIFFERENTIATION AND SUPPRESSIVE FUNCTION

4.1 ABSTRACT

Myeloid-derived suppressor cells (MDSCs) are a heterogeneous population of cells that are defined by their myeloid origin, immature state, and ability to potently suppress immune response. Murine MDSCs are characterized by the expression of CD11b and G-r1 cell markers and can be subdivided into two groups, monocytic and polymorphonuclear MDSCs based on the expression of Ly6C and Ly6G molecules. Previously, we found that 2,3,7,8-Tetrachlorodibenzo-p-dioxin (TCDD), an Ahr high affinity binding ligand induces MDSCs and MDSC subset migration from bone marrow to peritoneal cavity. In the current study, we demonstrate that oral administration of 3,5,4′-trihydroxy-trans-stilbene (Resveratrol, RSV) reduced the number of MDSCs in the peritoneal cavity and immobilized these cells in the bone marrow. Cell bioenergetic profile and suppressive function of MDSCs were evaluated in TCDD group with and without RSV treatment. MDSCs with RSV treatment exhibited low glycolytic proton efflux rate (PER) which negatively affected their suppressive functions against T-cell proliferation. Furthermore, we found by flow cytometry strategy that both TCDD and RSV play a significant role in monocyte and dendritic cell differentiation and Class II-MHC expression. In summary, our data revealed that RSV can prevent MDSCs mobilization, differentiation and suppressive function that was induced by TCDD.

4.2 INTRODUCTION

Myeloid cells have a significant role in the innate immune response via several functions including the phagocytosis of pathogens (by macrophages), processing and presentation of antigens (by dendritic cells (DCs), stimulation of an inflammatory response (by neutrophils), and promotion of wound healing (by platelets) (191). Monocytes that derive from bone marrow, migrate to tissue and differentiate into macrophage and DC. Immature myeloid cells that do not have immunosuppressive activity are present constantly in health individuals (192). However, the accumulation of undifferentiated myeloid derived suppresser cells (MDSCs) which have high suppressive activity against T cells is one of the reasons that contribute to development of cancers, chronic infections, and autoimmune diseases (193-195). MDSCs consist of two large group of cells: granulocytic or polymorphonuclear MDSCs (PMN-MDSCs) can be defined as $CD11b^{+}Ly6G^{+}Ly6C^{low}$ cells with high side scatter and monocytic MDSCs (M-MDSCs) that are defined as $CD11b^{+}Ly6G^{-}Ly6C^{hi}$ cells with low side scatter (22). Both groups have different phenotypes and suppressive functions (196).

Macrophage in the peritoneal cavity (PerC) have been divided according to their morphology into two distinct subsets: large peritoneal macrophages (LPMs) are defined as $CD11b^{hi}F4/80^{hi}$ and express low levels of MHC class II (MHCII) and small peritoneal macrophage which can be defined as $CD11b^{in}F4/80^{in}$ and express high levels of MHCII (197).

Aryl hydrocarbon receptor (AhR) is a ligand-activated transcription factor that cross talks with environmental, dietary, microbial and metabolic signals to control complex transcriptional programs in a ligand-specific, cell-type-specific and context-

specific manner (198). AhR has important role in regulation of innate and adaptive immunity because it is expressed by numerous of immune cells (199). Previous studies from our lab showed that AhR activation caused thymus atrophy by upregulation of genes including Fas, LIGHT, and CD30 that enhance negative selection and lead to thymic atrophy (85), or by regulation of FasL and NF-kappaB in stromal cells, which in turn plays a critical role in initiating apoptosis in thymic T cells (86). AhR activation also reversed Th17/Treg differentiation for Treg favor in colitis animals model (50). Expression of hypersensitivity to LPS-induced septic shock with increasing mortality rate in AhR deficient mice is an indicator of the critical role of AhR in immune system homeostasis (200). There are also studies that showed how Ahr activation can impair the differentiation of human monocytes to macrophages or dendritic cells (201, 202). Also, sustained exposure for over 6 days of bone marrow-derived myeloid precursors from $AhR^{+/+}$ or $AhR^{-/-}$ mice to subtoxic doses of BaP showed that AhR-induced gene regulation is crucial for homeostasis of pro- and anti-inflammatory cytokines during macrophage activation (203).

A broad range of ligands with agonistic and antagonistic properties and with various affinity binding sites to AhR have been investigated for their role in immunomodulation. These ligands could be exogenous such as indole-3-carbinol and resveratrol or toxic environmental pollutants such as 2,3,7,8-tetrachlorodibenzo-p-dioxin (TCDD), or could be endogenous ligands such as kynurenine and 6 Formylindolo[3,2-b]carbazole (5). Interestingly, AhR activation influences many and different aspects of immunological function, for example, TCDD and FICZ are high affinity AhR ligands, however TCDD induce anti-inflammatory molecules/cytokines such as FOXP3 and IL-10

that suppressed experimental autoimmune encephalomyelitis while FICZ induces pro-inflammatory cytokine IL-17 and increases the severity of experimental autoimmune encephalomyelitis in mice (89).

From previous work, we found TCDD (10µg/kg) induced rapid and massive mobilization of MDSCs and MDSCs subsets such as monocytic and polymorphonuclear MDSCs from bone marrow to peritoneal cavity. In the present study, we observed that resveratrol ameliorated immunotoxicity effect of TCDD and attenuated the proportion of MDSCs and MDSCs subset in the peritoneal cavity. Also, we found both AhR agonist and antagonists had significant influence on monocyte differentiation in the peritoneal cavity post treatment.

4.3 MATERIALS AND METHODS

Experimental Animals:

Female mice C57BL/6 mice (6-8) weeks old were purchased from Jackson laboratory, USA. All mice were housed in specific pathogen-free condition at the AAALAC-accredited University of South Carolina, School of Medicine, Animal Resource Facility. All experiments performed using mice in this manuscript were approved by the Institutional Animal Care and Use Committee (IACUC), University of South Carolina.

Chemicals and reagents:

TCDD was a kind gift from Dr. Steve Safe (Institute of Biosciences & Technology, Texas A&M Health Sciences Center, College Station, Texas). Resveratrol (RSV) was from Sigma-Aldrich (St. Louis, MO). Culture medium reagents (RPMI 1640, Penicillin-Streptomycin, HEPES, L-Glutamine, FBS, and PBS) were purchased from

Invitrogen Life Technologies (Carlsbad, CA). The following antibodies were used for surface markers staining were purchased from BioLegend (San Diego, CA-USA): Alexa Fluor 700-conjugated anti-CD11b, BV510-conjugated-Gr-1, Alexa Fluor 488-conjugated anti-Ly6C, BV785-conjugated anti-Ly6G, BV421-conjugated anti-MHCII, and BV605 or PE-conjugated anti-CD11c. Fc Blocker reagent was procured from BD Biosciences (San Diego, USA). PE Positive Selection Kits were purchased from Stem cells Technologies (Vancouver, BC, Canada). XFp glycolytic rate assay kit and XFP cell mito stress test kit were purchased from Agilent Technologies.

Animals treatment and flow cytometry staining

C57BL6 mice (n=5) were given 50 mg/kg orally RSV and the following day, they were injected with 10 µg/kg TCDD and 90 min later they given a second dose of RSV. Next day, they sacrificed and peritoneal exudates harvested and stained for flow cytometry. Flow cytometry analysis was performed using BD FACs Celeste and FlowJo software from ThermoFisher Scientific.

Flow cytometry to evaluate immune cell phenotypes

Cells were harvested from peritoneal cavity of naïve, RSV, TCDD, and RSV+TCDD mice and stained with CD11b and Gr-1 to identify MDSCs ($CD11b^{+}Gr\text{-}1^{+}$) and LY6C and LY6G to identify Monocytic ($CD11b^{+}Ly6G^{-}Ly6C^{hi}$) and Polymorphonuclear ($CD11b^{+}Ly6G^{+}Ly6C^{lo}$) MDSCs as described by us previously (103). According to flow cytometer strategy of gating (204), we stained with CD11b and F4/80 to define monocytes ($CD11b^{+}F4/80^{-}$), LPM ($CD11b^{+}F4/80^{+}$), and SPM ($CD11b^{in}F4/80^{in}$). CD11c and Gr-1 markers used after gating on CD11b to determine Neutrophils ($CD11c^{-}Gr\text{-}1^{+}$), Dendritic ($CD11c^{+}Gr\text{-}1^{-}$), and nonNCorDC ($CD11c^{-}Gr\text{-}1^{-}$). Also, MHCII

expression detected in LPM, SPM, MDSCs, and nonNCorDC. Flow cytometry analysis was performed using BD FACs Celeste and FlowJo software from ThermoFisher Scientific.

Purification of MDSCs

MDSCs were purified from peritoneal exudates of RSV, TCDD, and RSV+TCDD mice, as described previously (31). In brief, peritoneal exudates were collected and labeled with PE-conjugated Gr-1 antibody. PE-selection kit from Stem Cells Technologies was used for selection by following the protocol from company. After purification, flow cytometry (BD FACScelesta) was used to assess the purity of MDSCs.

Effect of MDSCs from TCDD or RSV+TCDD on T-cell proliferation in vitro.

To examine the suppressive effect of MDSCs on T-cell proliferation, splenocytes ($5x10^5$) from C57BL/6 naïve mice were cultured in the presence of Con-A (2µg/ml) together with 1:0.5 ratios of MDSCs from TCDD or RSV+TCDD for 24 hrs, as described (104). [3H]thymidine (1µCi/well) was added to the cell cultures and after 18 hrs, radioactivity was measured using a liquid-scintillation counter (MicroBeta Trilux; PerkinElmer Life and Analytical Sciences).

Measuring Glycolytic Rate

Proton efflux rate (PER) was measured in 2×10^5 purified MDSCs from peritoneal cavity of RSV, TCDD, and RSV+TCDD-treated mice using XF Extracellular Flux Analyzer (Seahorse Bioscience). MDSCs were plated in XF cell culture plate coated with 15 µg CellTak in phenol red-free Base Medium enriched with 2 mM glutamine, 10 mM glucose, 1 mM pyruvate, and 5 mM HEPES as initial conditions. Cells monitored under stressed conditions and in response to 0.5 µM Rotenone plus Antimycin A (Rot/AA) and

50 mM 2-Deoxy-D-glucose (2-DG). PER quantified by Seahorse Bioscience XFp Extracellular Flux Analyzer (Agilent Technologies).

4.4 RESULTS

RSV attenuated MDSCs mobilization from bone marrow to peritoneal cavity.

From previous work, we found that TCDD caused massive mobilization of MDSCs to the peritoneal exudate. While TCDD and RSV both are AhR ligands, TCDD has high binding affinity towards AhR (205) while RSV binds to AhR with low affinity (92) Moreover studies from our lab have previously shown that based on the dose of RSV, it can also act as an antagonist for AhR (205). Thus, in the current study, we investigated if RSV would reverse the ability of TCDD to induce MDSCs. We observed that the proportion and absolute numbers of MDSCs in bone marrow of TCDD-treated mice decreased significantly within 16 hours of exposure while we noted significant increase in MDSCs in the peritoneal cavity (Fig 4.1A-D). Interestingly, RSV+TCDD treated groups showed reversal of TCDD effects inasmuch as there were more numbers of MDSCs in the bone marrow while there was less MDSCs induced in the peritoneal cavity (Fig 4.1A-D). A similar trend was seen at 24 hours in the peritoneal cavity (Fig 4.1E-F).

RSV impaired glycolytic rate and suppressive function of TCDD-induced MDSCs.

Next, we tested the Proton Efflux Rate (PER) in MDSCs that were induced by TCDD with or without RSV. Interstitially, we found that RSV impaired PER in MDSCs cells compared to MDSCs treated with TCDD (Fig 4.2A). Also, all PER parameters including basal glycolysis, percentage of PER, and compensatory glycolysis were reduced in RSV+TCDD group when compared to TCDD (Fig 4.2B). When we tested the

suppressive function of MDSCs, we found that MDSCs from TCDD treated mice were highly immunosuppressive while MDSCs from RSV+TCDD mice were less immunosuppressive when compared to TCDD-treated mice (Fig 4.2C). Together, these data demonstrated that RSV is capable to reducing the migration, and function of TCDD-induced MDSCs.

RSV and TCDD, AhR ligands influence in peritoneal cavity monocytes differentiation

We also examined if Ahr activation by TCDD influences in the differentiation of monocytes in murine peritoneal cavity. According to flow cytometer strategy of gating (204), we found that the proportion of $CD11b^{+}$ monocytes reduced significantly in TCDD group when compared to other groups. Small peritoneal macrophages (SPM) $CD11b^{in}F4/80^{in}$, were seen in all experimental groups at low levels. However, there was a significant difference between naïve and RSV and between TCDD and RSV+TCDD groups. Peritoneal cells from RSV expressed higher percentages of large peritoneal macrophage (LPM) that were $CD11b^{+}F4/80^{+}$ when compared to cells in TCDD and RSV+TCDD (Fig 4.3B,K). MDSCs as well as PMN-MDSCs and M-MDSCs increased markedly in TCDD group and RSV attenuated this effect (Fig 4.3C,D,L). Dendritic cells ($CD11c^{+}Gr\text{-}1^{-}$) increased in peritoneal of RSV+TCDD compared to TCDD, and neutrophils ($CD11c^{-}Gr\text{-}1^{+}$) exhibited high level expression in TCDD, while showing decreased presence in RSV+TCDD groups. Non-DC or NC $CD11b^{-}CD11c^{-}$ were in high proportion in naïve mice and decreased dramatically in TCDD while RSV+TCDD showed an increase when compared to TCDD (Fig 4.3E,M). MHCII was expressed at higher levels in SPM, while it's expression in LPM was lower and increased gradually with TCDD and RSV+TCDD. Like SPM, nonDCorNC expressed high MHCII (Fig

4.3F,I,M), while in contrast, the expression of MHCII was lacking in MDSCs. However, MDSCs in RSV treated group exhibited higher levels of MHCII expression (Fig 4.3G,N), demonstrating a virous effect of Ahr ligand on differentiation of the peritoneal cavity monocytes.

4.5 DISSUCSION

TCDD and other aryl hydrocarbon receptor (AhR) xenobiotic ligands, such as polycyclic aromatic hydrocarbons (PAHs), are environmental toxicants generated by the chemical industry. They are present in air pollution from industrial furnace gas and burning processes. Many AhR ligands, especially the halogenated have long biological half-life in body fat which keep increasing with time (206). Resveratrol a polyphenolic natural compound has been extensively studied for its therapeutic benefits against a wide array of diseases including cancer, cardiovascular, neurological and inflammatory diseases (62, 66, 81, 82, 122). In the current study, we investigated other protective role of RSV against immunotoxicity effect of TCDD. We found that RSV attenuated the massive mobilization of MDSCs from bone marrow to peritoneal cavity in TCDD treatment (Fig 4.1). Both TCDD and RSV are AhR agonists and binding to different residues binding domain (AhRLBD) in AhR. However, some of the residues in AhR LBD contribute significantly to binding with the ligands (92) that lead to create a kind of competition between the ligands on binding site. Also, our previous studies have shown that RSV can both act as an agonist and antagonist based on the dose (207) .

Tumor-infiltrating MDSC (T-MDSC) increase fatty acid uptake and activated fatty acid oxidation (FAO) that is accompanied by an increase in oxygen consumption rate (208). Thus, FAO inhibition alone significantly delayed tumor growth in a T-cell-

dependent manner and enhanced the antitumor effect of adoptive T-cell therapy (26). In the present study, we observed that RSV impaired protein efflux rate during glycolysis that was seen at high levels with TCDD treatment (Fig 4.2A-B). Inhibition glycolysis by RSV potentially had a reduced effect on suppressive function of MDSCs in T-cells proliferation (Fig 4.2C).

AhR is expressed at high levels in monocytes, macrophage, Th17, ILC3 and DC, inducible in B cells and NK, and low levels in Th1, Th2, ILC1and2, and granulocytes (209). Because AhR is expressed highly in monocytes, activation AhR by their agonists perhaps control monocyte differentiation. A couple studies addressed this question and found that activation of AhR impeded the differentiation of myeloid cells to macrophage (202, 203). In the present study, we found that TCDD impaired the proportion of peritoneal macrophage subset, LPM and SPM. However, LPM with RSV treatment exhibited higher percentages demonstrating that both ligands have differential effects on LPM differentiation. Induction of LMP and SMP by RSV can be one of reasons behand reduced MDSCs population in TCDD with RSV (Fig 4.3B,K). Also, increase of DC expression with RSV+TCDD may be because DC express highly level of AhR that lead to increase the proportion of these cells with two ligands. NonDCorNC show a high proportion in naïve mice when compared to treatments, giving evidence for critical roles of both TCDD and RSV in monocytes differentiation (Fig 4.3E,M). RSV also caused a decrease in MDSC subsets, PMN-MDSCs and M-MDSCs when compared to TCDD (Fig 4.3C,L) which correlated with a decrease in MDSC induction as well. SPM expresses high levels of MHCII, which is not expressed on LPM (204). Similarly, we found SPM in all experimental groups expressed MHCII, however the expression of MHCII in LPM

increased with RSV+TCDD, which may explains why RSV treatment reduces the suppressive activity of MDSCs (Fig 4.3F,I,M). MDSCs normally lack MHCII expression and it can be distinguished from monocytes by this feature (196). We observed that MHCII expression in MDSCs in TCDD was negligible, however MDSCs with RSV showed slight increase in MHCII (Fig 4.3G,N) that may have also caused reversal of suppressive functions (Fig 2).

In summary, the current study demonstrates that RSV can neutralize the immunotoxicity of TCDD. Specifically, RSV decreased the induction of MDSCs by TCDD. Also, RSV reversed the immunosuppressive functions of TCDD -induced MDSCs against T cell proliferation. Lastly, TCDD also altered the differentiation of dendritic cells and monocytes and RSV also interfered in this process. Clearly additional studies are necessary to understand if the effect of TCDD on monocytes and DCs results from maturation of MDSCs or if this is an independent effect directly on these cells.

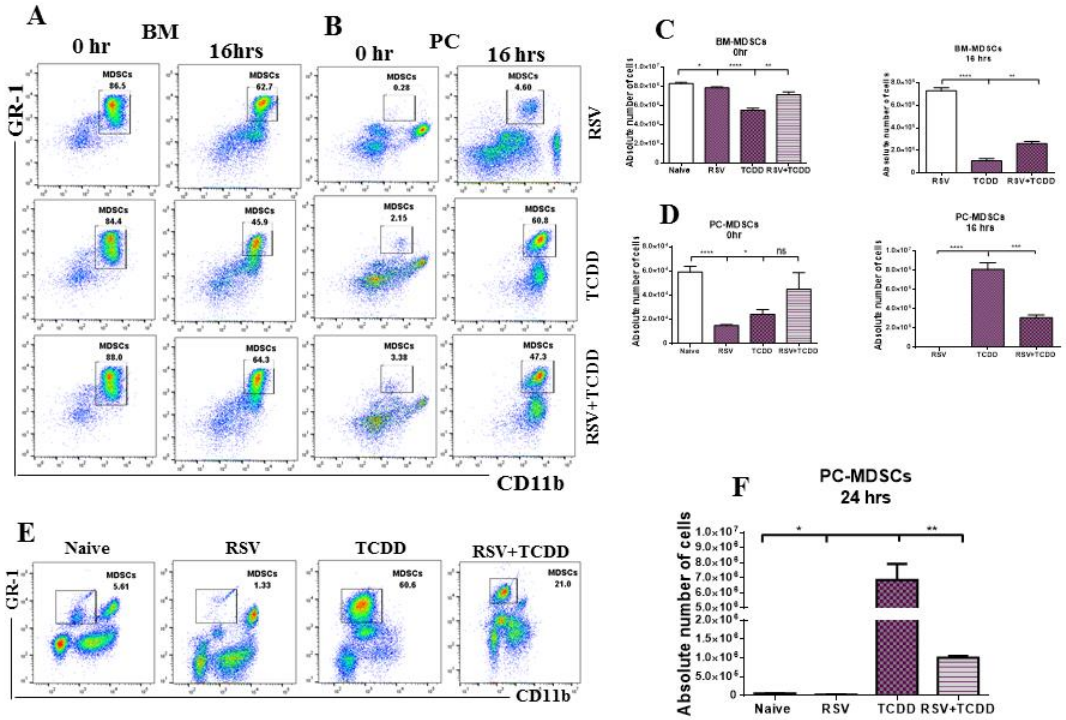

Figure 4.1: Resveratrol (RSV) attenuated MDSCs mobilization from bone marrow to the peritoneal cavity. Mice were given prior 50 mg/kg orally RSV, next day they injected with 10 µg/kg TCDD and 90 min later they given a second dose of RSV. Next day they sacrificed and peritoneal exudates harvested to stain with CD11b Gr-1 to identify MDSCs and LY6C and LY6G to identify monocytic M-MDSCs and polymorphonuclear PMN-MDSCs respectively. (A) Representative plots from flowjo software analysis of flow cytometry data showing MDSCs proportion in BM in 0 hr and after 16 hrs. (B) Representative pseudocolor plots showing MDSCs proportion in peritoneal exudate in 0 hr and 16 hrs later. (C) Absolute number of bon marrow-MDSCs (BM-MDSCs) in 0 hr and after 16 hrs. (D) Absolute number of peritoneal cavity-MDSCs (PC-MDSCs) in 0 hr and 16 hrs later. (E,F) Percentage and absolute number of MDSCs in peritoneal cavity in 24 hrs later. Vertical bars represent mean ± SEM. Student's t test and one way ANOA *$p < 0.05$; **$p < 0.01$; ***$p < 0.001$.

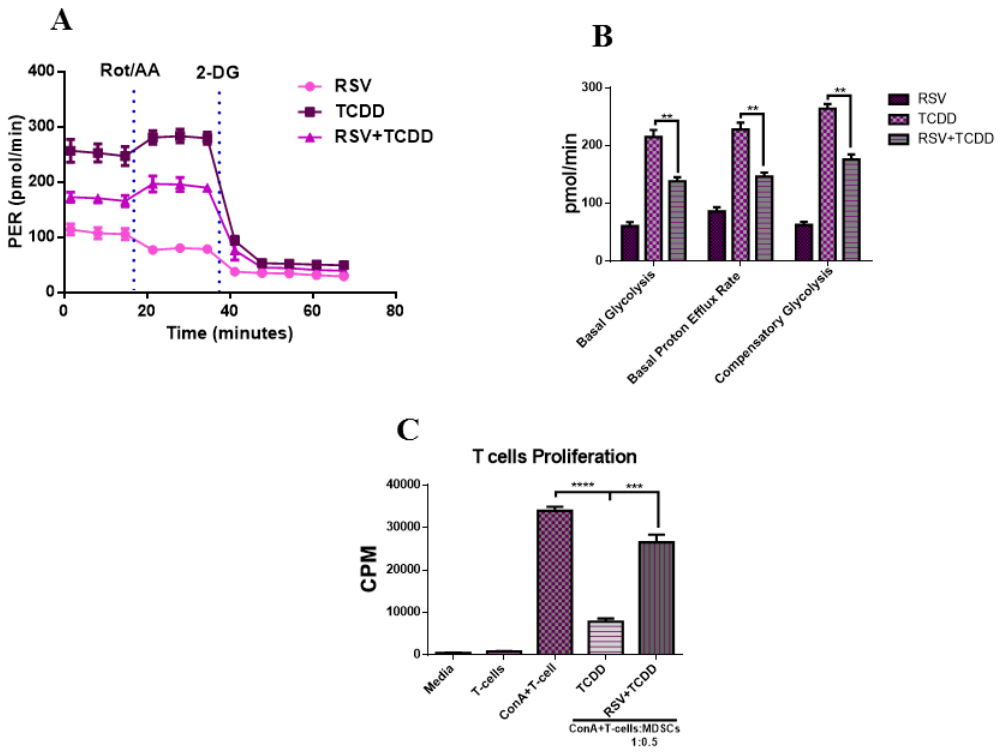

Figure 4.2: RSV impaired protein efflux rate (PER) and immunosuppressive function in MDSCs. MDSCs were purified from the peritoneal cavity of RSV, TCDD, and RSV+TCDD mice as described in material and methods and utilized for PER and 3H-thymidine assays. (A) Proton efflux rate in peritoneal MDSCs in three experimental groups. (B) Glycolysis parameters quantification including glycolysis, percentage of PER, and compensatory glycolysis in RSV, TCDD, and RSV+TCDD. (C) Purified peritoneal MDSCs from TCDD and RSV+TCDD were incubated with spleen cells activated with ConA at 1:0.5. T cell proliferation was assessed by 3H-thymidine incorporation assay. in Vertical bars represent mean ± SEM. Student's t test *$p < 0.05$; **$p < 0.01$; ***$p < 0.001$.

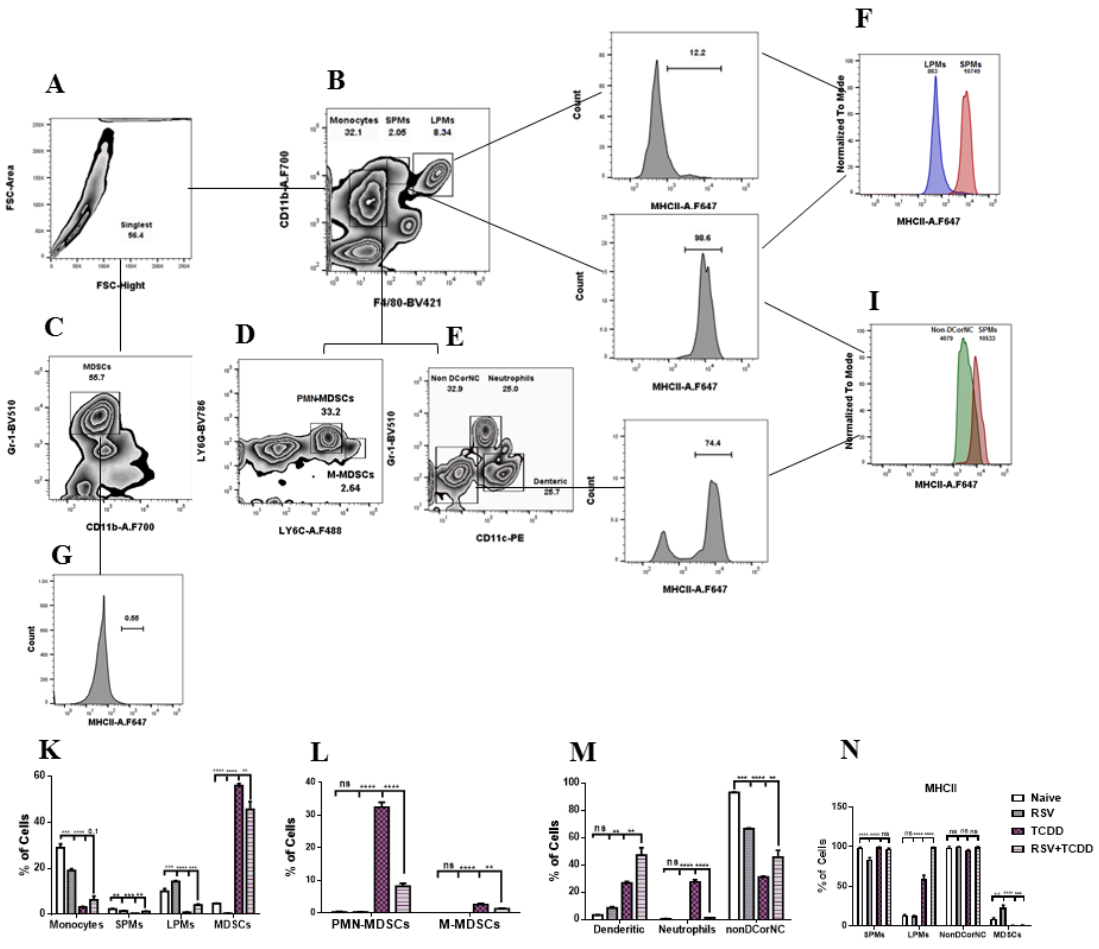

Figure 4.3: Flow gating strategy to identify immune cells in the peritoneal cavity. Based on surface molecules, peritoneal fluid cells in naïve, RSV, TCDD, and RSV+TCDD stained for. (A) Single cells selection by gating on FSC-H and FSC-A. (B) Single cells gated on CD11b and F4/80 to identify monocytes $CD11b^{+}F4/80^{-}$, large peritoneal macrophage (LPM) can be defined as $CD11b^{+}F4/80^{+}$ cells with high side scatter, small peritoneal macrophage (SPM) can be defined as CD11binF4/80in with intermediate side scatter. (C) MDSCs $CD11b^{+}Gr\text{-}1^{+}$ gated on single cells. (D) Polymorphonuclear (PMN) and Monocytic (M) MDSCs gated on CD11b. (E) Gr-1 and CD11c gated on CD11b to identify Neutrophils $Gr\text{-}1^{+}CD11c^{-}$, Dendritic cells $CD11c^{+}Gr\text{-}1^{-}$ as well as $CD11c^{-}$ $Gr\text{-}1^{-}$ NonNCorDC. (F,I) MHCII expression on LPM, SPM, and NonNCorDC. (G) MHCII expression on MDSCs. (K) Percentage of Monocytes, LPM, SPM, and MDSCs. (L) Percentage of MDSCs subset population. (M) DC, NC and NonNCorDC proportion. (N) MHCII expression in LPM, SPM, NonNCorDC and MDSCs. Vertical bars represent mean ± SEM. One way ANOVA test $*p < 0.05$; $**p < 0.01$; $***p < 0.001$.

CHAPTER 5

SUMMARY AND CONCLUSION

The aryl hydrocarbon receptor (AhR) is a ligand-activated transcription factor that acts as biological sensor by initiating gene expression programs in response to endogenous and exogenous signals. One of the contaminant exogenous ligands that has high affinity binding to AhR with immunotoxic and carcinogenic properties is TCDD (2,3,7,8-Tetrachlorodibenzo-p-dioxin). The data presented in this dissertation showed that TCDD caused significant immunomodulation and alterations in gut microbiota. On the other hand, resveratrol, a natural polyphenolic compound with known agonistic and antagonistic activity attenuated immunomodulatory effects of TCDD.

TCDD induced immunomodulation included massive mobilization of MDSCs from bone marrow to peritoneal cavity that was associated with increases in several chemokines and their receptors. TCDD-induced MDSCs were highly immunosuppressive as demonstrated using in vitro and adoptive transfer experiments which correlated with increase in bioenergetic profile of these cells. TCDD also caused epigenetic modification in MDSCs that was accompanied with down-regulation in the expression of miR-150-5p and miR-543-3p which led to increase in the expression of target genes including IL-10, PIM1, ARG2, STAT3, and CCL11 and chemokines receptors CCR3, CCR5, and CXCR2. Upregulation of these anti-inflammatory genes, chemokines, and their receptors played a major role in the migration, expansion and function of MDSCs.

The influence of TCDD was not limited only to the immune system, TCDD also caused shift in the resident gut microbiome, particularly through increasing Lactobacillus and decreasing Sutterella abundances. FMT experiments confirmed that TCDD-mediated changes in the gut microbiome altered the immune system, specifically by increasing the MDSCs in a CXCR2-dependent manner, which resulted in decreased cysteine levels.

Data presented in the current work also provide evidence for neutralizing the immunotoxicity of TCDD. Resveratrol, a natural compound, was found to reduce significantly the massive MDSC mobilization to the peritoneal cavity and reversed their suppressive function.

Together, these studies demonstrate for the first time how AhR activation by ligands can serve as a double-edged sword on one hand inducing MDSCs that may be beneficial to treat inflammatory and autoimmune diseases while on the other hand promoting cancer. This may explain how some dietary AhR ligands may help suppress inflammation in the colon and systemically, while some environmental toxicants such as TCDD and methyl cholanthrene may induce cancer. Our studies form the basis for further investigations into such mechanisms which may help develop novel therapies to treat inflammatory and autoimmune diseases as well as prevent cancers induced by environmental contaminants.

REFERENCES

1. Bersten DC, Sullivan AE, Peet DJ, Whitelaw ML. bHLH-PAS proteins in cancer. Nature reviews Cancer. 2013;13(12):827-41. doi: 10.1038/nrc3621. PubMed PMID: 24263188.

2. Conney AH, Miller EC, Miller JA. Substrate-induced synthesis and other properties of benzpyrene hydroxylase in rat liver. The Journal of biological chemistry. 1957;228(2):753-66. PubMed PMID: 13475357.

3. Conney AH, Gillette JR, Inscoe JK, Trams ER, Posner HS. Induced synthesis of liver microsomal enzymes which metabolize foreign compounds. Science. 1959;130(3387):1478-9. PubMed PMID: 13811550.

4. Nebert DW. Aryl hydrocarbon receptor (AHR): "pioneer member" of the basic-helix/loop/helix per-Arnt-sim (bHLH/PAS) family of "sensors" of foreign and endogenous signals. Progress in lipid research. 2017;67:38-57. doi: 10.1016/j.plipres.2017.06.001. PubMed PMID: 28606467; PubMed Central PMCID: PMC5568781.

5. Denison MS, Nagy SR. Activation of the aryl hydrocarbon receptor by structurally diverse exogenous and endogenous chemicals. Annual review of pharmacology and toxicology. 2003;43:309-34. doi: 10.1146/annurev.pharmtox.43.100901.135828. PubMed PMID: 12540743.

6. Wilson SR, Joshi AD, Elferink CJ. The tumor suppressor Kruppel-like factor 6 is a novel aryl hydrocarbon receptor DNA binding partner. The Journal of pharmacology

and experimental therapeutics. 2013;345(3):419-29. doi: 10.1124/jpet.113.203786. PubMed PMID: 23512538; PubMed Central PMCID: PMC3657114.

7. Lawrence BP, Denison MS, Novak H, Vorderstrasse BA, Harrer N, Neruda W, Reichel C, Woisetschlager M. Activation of the aryl hydrocarbon receptor is essential for mediating the anti-inflammatory effects of a novel low-molecular-weight compound. Blood. 2008;112(4):1158-65. doi: 10.1182/blood-2007-08-109645. PubMed PMID: 18270326; PubMed Central PMCID: PMC2515129.

8. Hauben E, Gregori S, Draghici E, Migliavacca B, Olivieri S, Woisetschlager M, Roncarolo MG. Activation of the aryl hydrocarbon receptor promotes allograft-specific tolerance through direct and dendritic cell-mediated effects on regulatory T cells. Blood. 2008;112(4):1214-22. doi: 10.1182/blood-2007-08-109843. PubMed PMID: 18550851.

9. Kerkvliet NI, Steppan LB, Vorachek W, Oda S, Farrer D, Wong CP, Pham D, Mourich DV. Activation of aryl hydrocarbon receptor by TCDD prevents diabetes in NOD mice and increases Foxp3+ T cells in pancreatic lymph nodes. Immunotherapy. 2009;1(4):539-47. doi: 10.2217/imt.09.24. PubMed PMID: 20174617; PubMed Central PMCID: PMC2823486.

10. Stockinger B, Di Meglio P, Gialitakis M, Duarte JH. The aryl hydrocarbon receptor: multitasking in the immune system. Annual review of immunology. 2014;32:403-32. doi: 10.1146/annurev-immunol-032713-120245. PubMed PMID: 24655296.

11. Veldhoen M, Hirota K, Christensen J, O'Garra A, Stockinger B. Natural agonists for aryl hydrocarbon receptor in culture medium are essential for optimal differentiation of Th17 T cells. The Journal of experimental medicine. 2009;206(1):43-9. doi:

10.1084/jem.20081438. PubMed PMID: 19114668; PubMed Central PMCID: PMC2626686.

12. Mezrich JD, Fechner JH, Zhang X, Johnson BP, Burlingham WJ, Bradfield CA. An interaction between kynurenine and the aryl hydrocarbon receptor can generate regulatory T cells. Journal of immunology. 2010;185(6):3190-8. doi: 10.4049/jimmunol.0903670. PubMed PMID: 20720200; PubMed Central PMCID: PMC2952546.

13. Benson JM, Shepherd DM. Aryl hydrocarbon receptor activation by TCDD reduces inflammation associated with Crohn's disease. Toxicological sciences : an official journal of the Society of Toxicology. 2011;120(1):68-78. doi: 10.1093/toxsci/kfq360. PubMed PMID: 21131560; PubMed Central PMCID: PMC3044199.

14. Metidji A, Omenetti S, Crotta S, Li Y, Nye E, Ross E, Li V, Maradana MR, Schiering C, Stockinger B. The Environmental Sensor AHR Protects from Inflammatory Damage by Maintaining Intestinal Stem Cell Homeostasis and Barrier Integrity. Immunity. 2018;49(2):353-62 e5. doi: 10.1016/j.immuni.2018.07.010. PubMed PMID: 30119997; PubMed Central PMCID: PMC6104739.

15. Fang L, Pang Z, Shu W, Wu W, Sun M, Cong Y, Liu Z. Anti-TNF Therapy Induces CD4+ T-Cell Production of IL-22 and Promotes Epithelial Repairs in Patients With Crohn's Disease. Inflammatory bowel diseases. 2018;24(8):1733-44. doi: 10.1093/ibd/izy126. PubMed PMID: 29718341.

16. Nikoopour E, Bellemore SM, Singh B. IL-22, cell regeneration and autoimmunity. Cytokine. 2015;74(1):35-42. doi: 10.1016/j.cyto.2014.09.007. PubMed PMID: 25467639.

17. Fukumoto S, Toshimitsu T, Matsuoka S, Maruyama A, Oh-Oka K, Takamura T, Nakamura Y, Ishimaru K, Fujii-Kuriyama Y, Ikegami S, Itou H, Nakao A. Identification of a probiotic bacteria-derived activator of the aryl hydrocarbon receptor that inhibits colitis. Immunology and cell biology. 2014;92(5):460-5. doi: 10.1038/icb.2014.2. PubMed PMID: 24518984.

18. Kumar V, Patel S, Tcyganov E, Gabrilovich DI. The Nature of Myeloid-Derived Suppressor Cells in the Tumor Microenvironment. Trends in immunology. 2016;37(3):208-20. doi: 10.1016/j.it.2016.01.004. PubMed PMID: 26858199; PubMed Central PMCID: PMC4775398.

19. Geissmann F, Manz MG, Jung S, Sieweke MH, Merad M, Ley K. Development of monocytes, macrophages, and dendritic cells. Science. 2010;327(5966):656-61. doi: 10.1126/science.1178331. PubMed PMID: 20133564; PubMed Central PMCID: PMC2887389.

20. Barreda DR, Hanington PC, Belosevic M. Regulation of myeloid development and function by colony stimulating factors. Developmental and comparative immunology. 2004;28(5):509-54. doi: 10.1016/j.dci.2003.09.010. PubMed PMID: 15062647.

21. Marvel D, Gabrilovich DI. Myeloid-derived suppressor cells in the tumor microenvironment: expect the unexpected. The Journal of clinical investigation.

2015;125(9):3356-64. doi: 10.1172/JCI80005. PubMed PMID: 26168215; PubMed Central PMCID: PMC4588239.

22. Damuzzo V, Pinton L, Desantis G, Solito S, Marigo I, Bronte V, Mandruzzato S. Complexity and challenges in defining myeloid-derived suppressor cells. Cytometry Part B, Clinical cytometry. 2015;88(2):77-91. doi: 10.1002/cyto.b.21206. PubMed PMID: 25504825; PubMed Central PMCID: PMC4405078.

23. Dolcetti L, Peranzoni E, Ugel S, Marigo I, Fernandez Gomez A, Mesa C, Geilich M, Winkels G, Traggiai E, Casati A, Grassi F, Bronte V. Hierarchy of immunosuppressive strength among myeloid-derived suppressor cell subsets is determined by GM-CSF. European journal of immunology. 2010;40(1):22-35. doi: 10.1002/eji.200939903. PubMed PMID: 19941314.

24. Faulconer L, Camacho I, Nagarkatti M, Nagarkatti PS. Superantigen-primed T cells exposed to 2,3,7,8-tetrachlorodibenzo-p-dioxin (TCDD) replicate poorly following recall encounter. Archives of toxicology. 2006;80(3):134-45. doi: 10.1007/s00204-005-0024-6. PubMed PMID: 16189661.

25. Donkor MK, Lahue E, Hoke TA, Shafer LR, Coskun U, Solheim JC, Gulen D, Bishay J, Talmadge JE. Mammary tumor heterogeneity in the expansion of myeloid-derived suppressor cells. International immunopharmacology. 2009;9(7-8):937-48. doi: 10.1016/j.intimp.2009.03.021. PubMed PMID: 19362167.

26. Hossain F, Al-Khami AA, Wyczechowska D, Hernandez C, Zheng L, Reiss K, Valle LD, Trillo-Tinoco J, Maj T, Zou W, Rodriguez PC, Ochoa AC. Inhibition of Fatty Acid Oxidation Modulates Immunosuppressive Functions of Myeloid-Derived Suppressor Cells and Enhances Cancer Therapies. Cancer immunology research.

2015;3(11):1236-47. doi: 10.1158/2326-6066.CIR-15-0036. PubMed PMID: 26025381; PubMed Central PMCID: PMC4636942.

27. Condamine T, Gabrilovich DI. Molecular mechanisms regulating myeloid-derived suppressor cell differentiation and function. Trends in immunology. 2011;32(1):19-25. doi: 10.1016/j.it.2010.10.002. PubMed PMID: 21067974; PubMed Central PMCID: PMC3053028.

28. Yan D, Yang Q, Shi M, Zhong L, Wu C, Meng T, Yin H, Zhou J. Polyunsaturated fatty acids promote the expansion of myeloid-derived suppressor cells by activating the JAK/STAT3 pathway. European journal of immunology. 2013;43(11):2943-55. doi: 10.1002/eji.201343472. PubMed PMID: 23897117.

29. Condamine T, Mastio J, Gabrilovich DI. Transcriptional regulation of myeloid-derived suppressor cells. Journal of leukocyte biology. 2015;98(6):913-22. doi: 10.1189/jlb.4RI0515-204R. PubMed PMID: 26337512; PubMed Central PMCID: PMC4661041.

30. Jackson AR, Hegde VL, Nagarkatti PS, Nagarkatti M. Characterization of endocannabinoid-mediated induction of myeloid-derived suppressor cells involving mast cells and MCP-1. Journal of leukocyte biology. 2014;95(4):609-19. doi: 10.1189/jlb.0613350. PubMed PMID: 24319288; PubMed Central PMCID: PMC3958741.

31. Sido JM, Nagarkatti PS, Nagarkatti M. Delta(9)-Tetrahydrocannabinol attenuates allogeneic host-versus-graft response and delays skin graft rejection through activation of cannabinoid receptor 1 and induction of myeloid-derived suppressor cells. Journal of

leukocyte biology. 2015;98(3):435-47. doi: 10.1189/jlb.3A0115-030RR. PubMed PMID: 26034207; PubMed Central PMCID: PMC4541500.

32. Youn JI, Kumar V, Collazo M, Nefedova Y, Condamine T, Cheng P, Villagra A, Antonia S, McCaffrey JC, Fishman M, Sarnaik A, Horna P, Sotomayor E, Gabrilovich DI. Epigenetic silencing of retinoblastoma gene regulates pathologic differentiation of myeloid cells in cancer. Nature immunology. 2013;14(3):211-20. doi: 10.1038/ni.2526. PubMed PMID: 23354483; PubMed Central PMCID: PMC3578019.

33. Sahakian E, Powers JJ, Chen J, Deng SL, Cheng F, Distler A, Woods DM, Rock-Klotz J, Sodre AL, Youn JI, Woan KV, Villagra A, Gabrilovich D, Sotomayor EM, Pinilla-Ibarz J. Histone deacetylase 11: A novel epigenetic regulator of myeloid derived suppressor cell expansion and function. Molecular immunology. 2015;63(2):579-85. doi: 10.1016/j.molimm.2014.08.002. PubMed PMID: 25155994; PubMed Central PMCID: PMC4252813.

34. Noman MZ, Janji B, Hu S, Wu JC, Martelli F, Bronte V, Chouaib S. Tumor-Promoting Effects of Myeloid-Derived Suppressor Cells Are Potentiated by Hypoxia-Induced Expression of miR-210. Cancer research. 2015;75(18):3771-87. doi: 10.1158/0008-5472.CAN-15-0405. PubMed PMID: 26206559.

35. Liu Y, Lai L, Chen Q, Song Y, Xu S, Ma F, Wang X, Wang J, Yu H, Cao X, Wang Q. MicroRNA-494 is required for the accumulation and functions of tumor-expanded myeloid-derived suppressor cells via targeting of PTEN. Journal of immunology. 2012;188(11):5500-10. doi: 10.4049/jimmunol.1103505. PubMed PMID: 22544933.

36. Li L, Zhang J, Diao W, Wang D, Wei Y, Zhang CY, Zen K. MicroRNA-155 and MicroRNA-21 promote the expansion of functional myeloid-derived suppressor cells. Journal of immunology. 2014;192(3):1034-43. doi: 10.4049/jimmunol.1301309. PubMed PMID: 24391219.

37. Chen S, Huang A, Chen H, Yang Y, Xia F, Jin L, Zhang J. miR-34a inhibits the apoptosis of MDSCs by suppressing the expression of N-myc. Immunology and cell biology. 2016;94(6):563-72. doi: 10.1038/icb.2016.11. PubMed PMID: 26833183.

38. Deziel NC, Nuckols JR, Colt JS, De Roos AJ, Pronk A, Gourley C, Severson RK, Cozen W, Cerhan JR, Hartge P, Ward MH. Determinants of polychlorinated dibenzo-p-dioxins and polychlorinated dibenzofurans in house dust samples from four areas of the United States. The Science of the total environment. 2012;433:516-22. doi: 10.1016/j.scitotenv.2012.06.098. PubMed PMID: 22832089; PubMed Central PMCID: PMC3431600.

39. Apostoli P, Bergonzi R, Catalani S. [Classification as carcinogenic for 2,3,7,8-tetrachlorodibenzo-para-dioxin: an eventful journey]. Giornale italiano di medicina del lavoro ed ergonomia. 2011;33(1):84-99. PubMed PMID: 21425634.

40. Schecter A, Birnbaum L, Ryan JJ, Constable JD. Dioxins: an overview. Environmental research. 2006;101(3):419-28. doi: 10.1016/j.envres.2005.12.003. PubMed PMID: 16445906.

41. Fine JS, Silverstone AE, Gasiewicz TA. Impairment of prothymocyte activity by 2,3,7,8-tetrachlorodibenzo-p-dioxin. Journal of immunology. 1990;144(4):1169-76. PubMed PMID: 2303704.

42. Kamath AB, Xu H, Nagarkatti PS, Nagarkatti M. Evidence for the induction of apoptosis in thymocytes by 2,3,7,8-tetrachlorodibenzo-p-dioxin in vivo. Toxicology and applied pharmacology. 1997;142(2):367-77. doi: 10.1006/taap.1996.8049. PubMed PMID: 9070360.

43. Kamath AB, Nagarkatti PS, Nagarkatti M. Characterization of phenotypic alterations induced by 2,3,7,8-tetrachlorodibenzo-p-dioxin on thymocytes in vivo and its effect on apoptosis. Toxicology and applied pharmacology. 1998;150(1):117-24. doi: 10.1006/taap.1998.8390. PubMed PMID: 9630460.

44. Lundberg K, Gronvik KO, Goldschmidt TJ, Klareskog L, Dencker L. 2,3,7,8-Tetrachlorodibenzo-p-dioxin (TCDD) alters intrathymic T-cell development in mice. Chemico-biological interactions. 1990;74(1-2):179-93. PubMed PMID: 2108807.

45. Beamer CA, Kreitinger JM, Cole SL, Shepherd DM. Targeted deletion of the aryl hydrocarbon receptor in dendritic cells prevents thymic atrophy in response to dioxin. Archives of toxicology. 2019;93(2):355-68. doi: 10.1007/s00204-018-2366-x. PubMed PMID: 30499018; PubMed Central PMCID: PMC6367717.

46. Phadnis-Moghe AS, Crawford RB, Kaminski NE. Suppression of human B cell activation by 2,3,7,8-tetrachlorodibenzo-p-dioxin involves altered regulation of B cell lymphoma-6. Toxicological sciences : an official journal of the Society of Toxicology. 2015;144(1):39-50. doi: 10.1093/toxsci/kfu257. PubMed PMID: 25543051; PubMed Central PMCID: PMC4349138.

47. Lu H, Crawford RB, Suarez-Martinez JE, Kaplan BL, Kaminski NE. Induction of the aryl hydrocarbon receptor-responsive genes and modulation of the immunoglobulin M response by 2,3,7,8-tetrachlorodibenzo-p-dioxin in primary human B cells.

Toxicological sciences : an official journal of the Society of Toxicology. 2010;118(1):86-97. doi: 10.1093/toxsci/kfq234. PubMed PMID: 20702590; PubMed Central PMCID: PMC2955211.

48. Apetoh L, Quintana FJ, Pot C, Joller N, Xiao S, Kumar D, Burns EJ, Sherr DH, Weiner HL, Kuchroo VK. The aryl hydrocarbon receptor interacts with c-Maf to promote the differentiation of type 1 regulatory T cells induced by IL-27. Nature immunology. 2010;11(9):854-61. doi: 10.1038/ni.1912. PubMed PMID: 20676095; PubMed Central PMCID: PMC2940320.

49. Funatake CJ, Marshall NB, Steppan LB, Mourich DV, Kerkvliet NI. Cutting edge: activation of the aryl hydrocarbon receptor by 2,3,7,8-tetrachlorodibenzo-p-dioxin generates a population of CD4+ CD25+ cells with characteristics of regulatory T cells. Journal of immunology. 2005;175(7):4184-8. PubMed PMID: 16177056.

50. Singh NP, Singh UP, Singh B, Price RL, Nagarkatti M, Nagarkatti PS. Activation of aryl hydrocarbon receptor (AhR) leads to reciprocal epigenetic regulation of FoxP3 and IL-17 expression and amelioration of experimental colitis. PloS one. 2011;6(8):e23522. doi: 10.1371/journal.pone.0023522. PubMed PMID: 21858153; PubMed Central PMCID: PMC3156147.

51. Zhang L, Ma J, Takeuchi M, Usui Y, Hattori T, Okunuki Y, Yamakawa N, Kezuka T, Kuroda M, Goto H. Suppression of experimental autoimmune uveoretinitis by inducing differentiation of regulatory T cells via activation of aryl hydrocarbon receptor. Investigative ophthalmology & visual science. 2010;51(4):2109-17. doi: 10.1167/iovs.09-3993. PubMed PMID: 20007828.

52. Jin Y, Wu S, Zeng Z, Fu Z. Effects of environmental pollutants on gut microbiota. Environmental pollution. 2017;222:1-9. doi: 10.1016/j.envpol.2016.11.045. PubMed PMID: 28086130.

53. Herstad KMV, Gajardo K, Bakke AM, Moe L, Ludvigsen J, Rudi K, Rud I, Sekelja M, Skancke E. A diet change from dry food to beef induces reversible changes on the faecal microbiota in healthy, adult client-owned dogs. BMC veterinary research. 2017;13(1):147. doi: 10.1186/s12917-017-1073-9. PubMed PMID: 28558792; PubMed Central PMCID: PMC5450340.

54. Bailey MT, Lubach GR, Coe CL. Prenatal stress alters bacterial colonization of the gut in infant monkeys. Journal of pediatric gastroenterology and nutrition. 2004;38(4):414-21. PubMed PMID: 15085020.

55. Lefever DE, Xu J, Chen Y, Huang G, Tamas N, Guo TL. TCDD modulation of gut microbiome correlated with liver and immune toxicity in streptozotocin (STZ)-induced hyperglycemic mice. Toxicology and applied pharmacology. 2016;304:48-58. doi: 10.1016/j.taap.2016.05.016. PubMed PMID: 27221631.

56. Stedtfeld RD, Brett Sallach J, Crawford RB, Stedtfeld TM, Williams MR, Waseem H, Johnston CT, Li H, Teppen BJ, Kaminski NE, Boyd SA, Tiedje JM, Hashsham SA. TCDD administered on activated carbon eliminates bioavailability and subsequent shifts to a key murine gut commensal. Applied microbiology and biotechnology. 2017;101(19):7409-15. doi: 10.1007/s00253-017-8460-9. PubMed PMID: 28812142; PubMed Central PMCID: PMC5909190.

57. Antus C, Radnai B, Dombovari P, Fonai F, Avar P, Matyus P, Racz B, Sumegi B, Veres B. Anti-inflammatory effects of a triple-bond resveratrol analog: structure and

function relationship. European journal of pharmacology. 2015;748:61-7. doi: 10.1016/j.ejphar.2014.12.009. PubMed PMID: 25528327.

58. Anisimova NY, Kiselevsky MV, Sosnov AV, Sadovnikov SV, Stankov IN, Gakh AA. Trans-, cis-, and dihydro-resveratrol: a comparative study. Chemistry Central journal. 2011;5:88. doi: 10.1186/1752-153X-5-88. PubMed PMID: 22185600; PubMed Central PMCID: PMC3313904.

59. Lozano-Perez AA, Rodriguez-Nogales A, Ortiz-Cullera V, Algieri F, Garrido-Mesa J, Zorrilla P, Rodriguez-Cabezas ME, Garrido-Mesa N, Utrilla MP, De Matteis L, de la Fuente JM, Cenis JL, Galvez J. Silk fibroin nanoparticles constitute a vector for controlled release of resveratrol in an experimental model of inflammatory bowel disease in rats. International journal of nanomedicine. 2014;9:4507-20. doi: 10.2147/IJN.S68526. PubMed PMID: 25285004; PubMed Central PMCID: PMC4181735.

60. Martin AR, Villegas I, La Casa C, de la Lastra CA. Resveratrol, a polyphenol found in grapes, suppresses oxidative damage and stimulates apoptosis during early colonic inflammation in rats. Biochemical pharmacology. 2004;67(7):1399-410. doi: 10.1016/j.bcp.2003.12.024. PubMed PMID: 15013856.

61. Jackson LJ, Pheneger JA, Pheneger TJ, Davis G, Wright AD, Robinson JE, Allen S, Munson MC, Carter LL. The role of PIM kinases in human and mouse CD4+ T cell activation and inflammatory bowel disease. Cellular immunology. 2012;272(2):200-13. doi: 10.1016/j.cellimm.2011.10.011. PubMed PMID: 22078270.

62. Rieder SA, Nagarkatti P, Nagarkatti M. Multiple anti-inflammatory pathways triggered by resveratrol lead to amelioration of staphylococcal enterotoxin B-induced

lung injury. British journal of pharmacology. 2012;167(6):1244-58. doi: 10.1111/j.1476-5381.2012.02063.x. PubMed PMID: 22646800; PubMed Central PMCID: PMC3504991.

63. Alghetaa H, Mohammed A, Sultan M, Busbee P, Murphy A, Chatterjee S, Nagarkatti M, Nagarkatti P. Resveratrol protects mice against SEB-induced acute lung injury and mortality by miR-193a modulation that targets TGF-beta signalling. Journal of cellular and molecular medicine. 2018;22(5):2644-55. doi: 10.1111/jcmm.13542. PubMed PMID: 29512867; PubMed Central PMCID: PMC5908132.

64. Chen L, Yang S, Zumbrun EE, Guan H, Nagarkatti PS, Nagarkatti M. Resveratrol attenuates lipopolysaccharide-induced acute kidney injury by suppressing inflammation driven by macrophages. Molecular nutrition & food research. 2015;59(5):853-64. doi: 10.1002/mnfr.201400819. PubMed PMID: 25643926; PubMed Central PMCID: PMC4420731.

65. Kadhim S, Singh NP, Zumbrun EE, Cui T, Chatterjee S, Hofseth L, Abood A, Nagarkatti P, Nagarkatti M. Resveratrol-Mediated Attenuation of Staphylococcus aureus Enterotoxin B-Induced Acute Liver Injury Is Associated With Regulation of microRNA and Induction of Myeloid-Derived Suppressor Cells. Frontiers in microbiology. 2018;9:2910. doi: 10.3389/fmicb.2018.02910. PubMed PMID: 30619104; PubMed Central PMCID: PMC6304356.

66. Altamemi I, Murphy EA, Catroppo JF, Zumbrun EE, Zhang J, McClellan JL, Singh UP, Nagarkatti PS, Nagarkatti M. Role of microRNAs in resveratrol-mediated mitigation of colitis-associated tumorigenesis in Apc(Min/+) mice. The Journal of pharmacology and experimental therapeutics. 2014;350(1):99-109. doi:

10.1124/jpet.114.213306. PubMed PMID: 24817032; PubMed Central PMCID: PMC4056272.

67. Alrafas HR, Busbee PB, Nagarkatti M, Nagarkatti PS. Resveratrol modulates the gut microbiota to prevent murine colitis development through induction of Tregs and suppression of Th17 cells. Journal of leukocyte biology. 2019. doi: 10.1002/JLB.3A1218-476RR. PubMed PMID: 30897248.

68. Alharris E, Alghetaa H, Seth R, Chatterjee S, Singh NP, Nagarkatti M, Nagarkatti P. Resveratrol Attenuates Allergic Asthma and Associated Inflammation in the Lungs Through Regulation of miRNA-34a That Targets FoxP3 in Mice. Frontiers in immunology. 2018;9:2992. doi: 10.3389/fimmu.2018.02992. PubMed PMID: 30619345; PubMed Central PMCID: PMC6306424.

69. Gandy KAO, Zhang J, Nagarkatti P, Nagarkatti M. Resveratrol (3, 5, 4'-Trihydroxy-trans-Stilbene) Attenuates a Mouse Model of Multiple Sclerosis by Altering the miR-124/Sphingosine Kinase 1 Axis in Encephalitogenic T Cells in the Brain. Journal of neuroimmune pharmacology : the official journal of the Society on NeuroImmune Pharmacology. 2019. doi: 10.1007/s11481-019-09842-5. PubMed PMID: 30941623.

70. Belguendouz L, Fremont L, Linard A. Resveratrol inhibits metal ion-dependent and independent peroxidation of porcine low-density lipoproteins. Biochemical pharmacology. 1997;53(9):1347-55. PubMed PMID: 9214696.

71. Bastianetto S, Zheng WH, Quirion R. Neuroprotective abilities of resveratrol and other red wine constituents against nitric oxide-related toxicity in cultured hippocampal neurons. British journal of pharmacology. 2000;131(4):711-20. doi:

10.1038/sj.bjp.0703626. PubMed PMID: 11030720; PubMed Central PMCID: PMC1572384.

72. Benoit CE, Bastianetto S, Brouillette J, Tse Y, Boutin JA, Delagrange P, Wong T, Sarret P, Quirion R. Loss of quinone reductase 2 function selectively facilitates learning behaviors. The Journal of neuroscience : the official journal of the Society for Neuroscience. 2010;30(38):12690-700. doi: 10.1523/JNEUROSCI.2808-10.2010. PubMed PMID: 20861374.

73. Britton RG, Kovoor C, Brown K. Direct molecular targets of resveratrol: identifying key interactions to unlock complex mechanisms. Annals of the New York Academy of Sciences. 2015;1348(1):124-33. doi: 10.1111/nyas.12796. PubMed PMID: 26099829.

74. Dadi PK, Ahmad M, Ahmad Z. Inhibition of ATPase activity of Escherichia coli ATP synthase by polyphenols. International journal of biological macromolecules. 2009;45(1):72-9. doi: 10.1016/j.ijbiomac.2009.04.004. PubMed PMID: 19375450.

75. Hotra A, Suter M, Biukovic G, Ragunathan P, Kundu S, Dick T, Gruber G. Deletion of a unique loop in the mycobacterial F-ATP synthase gamma subunit sheds light on its inhibitory role in ATP hydrolysis-driven H(+) pumping. The FEBS journal. 2016;283(10):1947-61. doi: 10.1111/febs.13715. PubMed PMID: 26996828.

76. Kim TH, Park JH, Woo JS. Resveratrol induces cell death through ROSdependent downregulation of Notch1/PTEN/Akt signaling in ovarian cancer cells. Molecular medicine reports. 2019. doi: 10.3892/mmr.2019.9962. PubMed PMID: 30816513.

77. Yang Z, Xie Q, Chen Z, Ni H, Xia L, Zhao Q, Chen Z, Chen P. Resveratrol suppresses the invasion and migration of human gastric cancer cells via inhibition of

MALAT1-mediated epithelial-to-mesenchymal transition. Experimental and therapeutic medicine. 2019;17(3):1569-78. doi: 10.3892/etm.2018.7142. PubMed PMID: 30783423; PubMed Central PMCID: PMC6364244.

78. Yang T, Zhang J, Zhou J, Zhu M, Wang L, Yan L. Resveratrol inhibits Interleukin-6 induced invasion of human gastric cancer cells. Biomedicine & pharmacotherapy = Biomedecine & pharmacotherapie. 2018;99:766-73. doi: 10.1016/j.biopha.2018.01.153. PubMed PMID: 29710474.

79. Sun L, Chen B, Jiang R, Li J, Wang B. Resveratrol inhibits lung cancer growth by suppressing M2-like polarization of tumor associated macrophages. Cellular immunology. 2017;311:86-93. doi: 10.1016/j.cellimm.2016.11.002. PubMed PMID: 27825563.

80. Hofseth LJ, Singh UP, Singh NP, Nagarkatti M, Nagarkatti PS. Taming the beast within: resveratrol suppresses colitis and prevents colon cancer. Aging. 2010;2(4):183-4. doi: 10.18632/aging.100143. PubMed PMID: 20436227; PubMed Central PMCID: PMC2881508.

81. Cui X, Jin Y, Hofseth AB, Pena E, Habiger J, Chumanevich A, Poudyal D, Nagarkatti M, Nagarkatti PS, Singh UP, Hofseth LJ. Resveratrol suppresses colitis and colon cancer associated with colitis. Cancer prevention research. 2010;3(4):549-59. doi: 10.1158/1940-6207.CAPR-09-0117. PubMed PMID: 20332304; PubMed Central PMCID: PMC2853724.

82. Singh NP, Hegde VL, Hofseth LJ, Nagarkatti M, Nagarkatti P. Resveratrol (trans-3,5,4'-trihydroxystilbene) ameliorates experimental allergic encephalomyelitis, primarily via induction of apoptosis in T cells involving activation of aryl hydrocarbon receptor

and estrogen receptor. Molecular pharmacology. 2007;72(6):1508-21. doi: 10.1124/mol.107.038984. PubMed PMID: 17872969; PubMed Central PMCID: PMC4796949.

83. Fernandez-Salguero PM, Hilbert DM, Rudikoff S, Ward JM, Gonzalez FJ. Aryl-hydrocarbon receptor-deficient mice are resistant to 2,3,7,8-tetrachlorodibenzo-p-dioxin-induced toxicity. Toxicology and applied pharmacology. 1996;140(1):173-9. doi: 10.1006/taap.1996.0210. PubMed PMID: 8806883.

84. McIntosh BE, Hogenesch JB, Bradfield CA. Mammalian Per-Arnt-Sim proteins in environmental adaptation. Annual review of physiology. 2010;72:625-45. doi: 10.1146/annurev-physiol-021909-135922. PubMed PMID: 20148691.

85. Fisher MT, Nagarkatti M, Nagarkatti PS. Combined screening of thymocytes using apoptosis-specific cDNA array and promoter analysis yields novel gene targets mediating TCDD-induced toxicity. Toxicological sciences : an official journal of the Society of Toxicology. 2004;78(1):116-24. doi: 10.1093/toxsci/kfh058. PubMed PMID: 14718646.

86. Camacho IA, Singh N, Hegde VL, Nagarkatti M, Nagarkatti PS. Treatment of mice with 2,3,7,8-tetrachlorodibenzo-p-dioxin leads to aryl hydrocarbon receptor-dependent nuclear translocation of NF-kappaB and expression of Fas ligand in thymic stromal cells and consequent apoptosis in T cells. Journal of immunology. 2005;175(1):90-103. PubMed PMID: 15972635.

87. Camacho IA, Nagarkatti M, Nagarkatti PS. 2,3,7,8-Tetrachlorodibenzo-p-dioxin (TCDD) induces Fas-dependent activation-induced cell death in superantigen-primed T

cells. Archives of toxicology. 2002;76(10):570-80. doi: 10.1007/s00204-002-0390-2. PubMed PMID: 12373453.

88. Schmidt JV, Bradfield CA. Ah receptor signaling pathways. Annual review of cell and developmental biology. 1996;12:55-89. doi: 10.1146/annurev.cellbio.12.1.55. PubMed PMID: 8970722.

89. Quintana FJ, Basso AS, Iglesias AH, Korn T, Farez MF, Bettelli E, Caccamo M, Oukka M, Weiner HL. Control of T(reg) and T(H)17 cell differentiation by the aryl hydrocarbon receptor. Nature. 2008;453(7191):65-71. doi: 10.1038/nature06880. PubMed PMID: 18362915.

90. Singh NP, Singh UP, Rouse M, Zhang J, Chatterjee S, Nagarkatti PS, Nagarkatti M. Dietary Indoles Suppress Delayed-Type Hypersensitivity by Inducing a Switch from Proinflammatory Th17 Cells to Anti-Inflammatory Regulatory T Cells through Regulation of MicroRNA. Journal of immunology. 2016;196(3):1108-22. doi: 10.4049/jimmunol.1501727. PubMed PMID: 26712945; PubMed Central PMCID: PMC4724476.

91. Loub WD, Wattenberg LW, Davis DW. Aryl hydrocarbon hydroxylase induction in rat tissues by naturally occurring indoles of cruciferous plants. Journal of the National Cancer Institute. 1975;54(4):985-8. PubMed PMID: 1127728.

92. Chitrala KN, Yang X, Nagarkatti P, Nagarkatti M. Comparative analysis of interactions between aryl hydrocarbon receptor ligand binding domain with its ligands: a computational study. BMC structural biology. 2018;18(1):15. doi: 10.1186/s12900-018-0095-2. PubMed PMID: 30522477; PubMed Central PMCID: PMC6282305.

93. Rouse M, Singh NP, Nagarkatti PS, Nagarkatti M. Indoles mitigate the development of experimental autoimmune encephalomyelitis by induction of reciprocal differentiation of regulatory T cells and Th17 cells. British journal of pharmacology. 2013;169(6):1305-21. doi: 10.1111/bph.12205. PubMed PMID: 23586923; PubMed Central PMCID: PMC3831710.

94. Hubbard TD, Murray IA, Perdew GH. Indole and Tryptophan Metabolism: Endogenous and Dietary Routes to Ah Receptor Activation. Drug metabolism and disposition: the biological fate of chemicals. 2015;43(10):1522-35. doi: 10.1124/dmd.115.064246. PubMed PMID: 26041783; PubMed Central PMCID: PMC4576673.

95. Gabrilovich DI, Nagaraj S. Myeloid-derived suppressor cells as regulators of the immune system. Nature reviews Immunology. 2009;9(3):162-74. doi: 10.1038/nri2506. PubMed PMID: 19197294; PubMed Central PMCID: PMC2828349.

96. Grivennikov SI, Wang K, Mucida D, Stewart CA, Schnabl B, Jauch D, Taniguchi K, Yu GY, Osterreicher CH, Hung KE, Datz C, Feng Y, Fearon ER, Oukka M, Tessarollo L, Coppola V, Yarovinsky F, Cheroutre H, Eckmann L, Trinchieri G, Karin M. Adenoma-linked barrier defects and microbial products drive IL-23/IL-17-mediated tumour growth. Nature. 2012;491(7423):254-8. doi: 10.1038/nature11465. PubMed PMID: 23034650; PubMed Central PMCID: PMC3601659.

97. Young MR, Endicott RA, Duffie GP, Wepsic HT. Suppressor alveolar macrophages in mice bearing metastatic Lewis lung carcinoma tumors. Journal of leukocyte biology. 1987;42(6):682-8. PubMed PMID: 3500255.

98. Seung LP, Rowley DA, Dubey P, Schreiber H. Synergy between T-cell immunity and inhibition of paracrine stimulation causes tumor rejection. Proceedings of the National Academy of Sciences of the United States of America. 1995;92(14):6254-8. PubMed PMID: 7603979; PubMed Central PMCID: PMC41496.

99. Dai J, El Gazzar M, Li GY, Moorman JP, Yao ZQ. Myeloid-derived suppressor cells: paradoxical roles in infection and immunity. Journal of innate immunity. 2015;7(2):116-26. doi: 10.1159/000368233. PubMed PMID: 25401944; PubMed Central PMCID: PMC4348209.

100. Goh C, Narayanan S, Hahn YS. Myeloid-derived suppressor cells: the dark knight or the joker in viral infections? Immunological reviews. 2013;255(1):210-21. doi: 10.1111/imr.12084. PubMed PMID: 23947357; PubMed Central PMCID: PMC3748397.

101. Park MJ, Lee SH, Kim EK, Lee EJ, Baek JA, Park SH, Kwok SK, Cho ML. Interleukin-10 produced by myeloid-derived suppressor cells is critical for the induction of Tregs and attenuation of rheumatoid inflammation in mice. Scientific reports. 2018;8(1):3753. doi: 10.1038/s41598-018-21856-2. PubMed PMID: 29491381; PubMed Central PMCID: PMC5830490.

102. Maeda A, Eguchi H, Nakahata K, Lo PC, Yamanaka K, Kawamura T, Matsuura R, Sakai R, Asada M, Okuyama H, Miyagawa S. Monocytic MDSCs regulate macrophage-mediated xenogenic cytotoxicity. Transplant immunology. 2015;33(2):140-5. doi: 10.1016/j.trim.2015.07.002. PubMed PMID: 26209355.

103. Hegde VL, Nagarkatti M, Nagarkatti PS. Cannabinoid receptor activation leads to massive mobilization of myeloid-derived suppressor cells with potent immunosuppressive properties. European journal of immunology. 2010;40(12):3358-71.

doi: 10.1002/eji.201040667. PubMed PMID: 21110319; PubMed Central PMCID: PMC3076065.

104. Hegde VL, Tomar S, Jackson A, Rao R, Yang X, Singh UP, Singh NP, Nagarkatti PS, Nagarkatti M. Distinct microRNA expression profile and targeted biological pathways in functional myeloid-derived suppressor cells induced by Delta9-tetrahydrocannabinol in vivo: regulation of CCAAT/enhancer-binding protein alpha by microRNA-690. The Journal of biological chemistry. 2013;288(52):36810-26. doi: 10.1074/jbc.M113.503037. PubMed PMID: 24202177; PubMed Central PMCID: PMC3873541.

105. Yang X, Hegde VL, Rao R, Zhang J, Nagarkatti PS, Nagarkatti M. Histone modifications are associated with Delta9-tetrahydrocannabinol-mediated alterations in antigen-specific T cell responses. The Journal of biological chemistry. 2014;289(27):18707-18. doi: 10.1074/jbc.M113.545210. PubMed PMID: 24841204; PubMed Central PMCID: PMC4081916.

106. Singh UP, Singh NP, Singh B, Price RL, Nagarkatti M, Nagarkatti PS. Cannabinoid receptor-2 (CB2) agonist ameliorates colitis in IL-10(-/-) mice by attenuating the activation of T cells and promoting their apoptosis. Toxicology and applied pharmacology. 2012;258(2):256-67. doi: 10.1016/j.taap.2011.11.005. PubMed PMID: 22119709; PubMed Central PMCID: PMC4117838.

107. Busbee PB, Nagarkatti M, Nagarkatti PS. Natural indoles, indole-3-carbinol (I3C) and 3,3'-diindolylmethane (DIM), attenuate staphylococcal enterotoxin B-mediated liver injury by downregulating miR-31 expression and promoting caspase-2-mediated

apoptosis. PloS one. 2015;10(2):e0118506. doi: 10.1371/journal.pone.0118506. PubMed PMID: 25706292; PubMed Central PMCID: PMC4338211.

108. Hegde VL, Nagarkatti PS, Nagarkatti M. Role of myeloid-derived suppressor cells in amelioration of experimental autoimmune hepatitis following activation of TRPV1 receptors by cannabidiol. PloS one. 2011;6(4):e18281. doi: 10.1371/journal.pone.0018281. PubMed PMID: 21483776; PubMed Central PMCID: PMC3069975.

109. Greenlee WF, Dold KM, Irons RD, Osborne R. Evidence for direct action of 2,3,7,8-tetrachlorodibenzo-p-dioxin (TCDD) on thymic epithelium. Toxicology and applied pharmacology. 1985;79(1):112-20. PubMed PMID: 2996175.

110. Holladay SD, Lindstrom P, Blaylock BL, Comment CE, Germolec DR, Heindell JJ, Luster MI. Perinatal thymocyte antigen expression and postnatal immune development altered by gestational exposure to tetrachlorodibenzo-p-dioxin (TCDD). Teratology. 1991;44(4):385-93. doi: 10.1002/tera.1420440405. PubMed PMID: 1683717.

111. Esser C. Dioxins and the immune system: mechanisms of interference. A meeting report. International archives of allergy and immunology. 1994;104(2):126-30. PubMed PMID: 8199455.

112. Kerkvliet NI, Shepherd DM, Baecher-Steppan L. T lymphocytes are direct, aryl hydrocarbon receptor (AhR)-dependent targets of 2,3,7,8-tetrachlorodibenzo-p-dioxin (TCDD): AhR expression in both CD4+ and CD8+ T cells is necessary for full suppression of a cytotoxic T lymphocyte response by TCDD. Toxicology and applied pharmacology. 2002;185(2):146-52. PubMed PMID: 12490139.

113. Mimura J, Fujii-Kuriyama Y. Functional role of AhR in the expression of toxic effects by TCDD. Biochimica et biophysica acta. 2003;1619(3):263-8. PubMed PMID: 12573486.

114. Kerkvliet NI. Recent advances in understanding the mechanisms of TCDD immunotoxicity. International immunopharmacology. 2002;2(2-3):277-91. PubMed PMID: 11811931.

115. Sulentic CE, Holsapple MP, Kaminski NE. Aryl hydrocarbon receptor-dependent suppression by 2,3,7, 8-tetrachlorodibenzo-p-dioxin of IgM secretion in activated B cells. Molecular pharmacology. 1998;53(4):623-9. PubMed PMID: 9547351.

116. Singh NP, Singh UP, Guan H, Nagarkatti P, Nagarkatti M. Prenatal exposure to TCDD triggers significant modulation of microRNA expression profile in the thymus that affects consequent gene expression. PloS one. 2012;7(9):e45054. doi: 10.1371/journal.pone.0045054. PubMed PMID: 23024791; PubMed Central PMCID: PMC3443208.

117. Camacho IA, Nagarkatti M, Nagarkatti PS. Evidence for induction of apoptosis in T cells from murine fetal thymus following perinatal exposure to 2,3,7,8-tetrachlorodibenzo-p-dioxin (TCDD). Toxicological sciences : an official journal of the Society of Toxicology. 2004;78(1):96-106. doi: 10.1093/toxsci/kfh048. PubMed PMID: 14718643.

118. Elliott DM, Singh N, Nagarkatti M, Nagarkatti PS. Cannabidiol Attenuates Experimental Autoimmune Encephalomyelitis Model of Multiple Sclerosis Through Induction of Myeloid-Derived Suppressor Cells. Frontiers in immunology. 2018;9:1782.

doi: 10.3389/fimmu.2018.01782. PubMed PMID: 30123217; PubMed Central PMCID: PMC6085417.

119. Sido JM, Yang X, Nagarkatti PS, Nagarkatti M. Delta9-Tetrahydrocannabinol-mediated epigenetic modifications elicit myeloid-derived suppressor cell activation via STAT3/S100A8. Journal of leukocyte biology. 2015;97(4):677-88. doi: 10.1189/jlb.1A1014-479R. PubMed PMID: 25713087; PubMed Central PMCID: PMC4370051.

120. Ostrand-Rosenberg S. Myeloid-derived suppressor cells: more mechanisms for inhibiting antitumor immunity. Cancer immunology, immunotherapy : CII. 2010;59(10):1593-600. doi: 10.1007/s00262-010-0855-8. PubMed PMID: 20414655; PubMed Central PMCID: PMC3706261.

121. Bronte V, Apolloni E, Cabrelle A, Ronca R, Serafini P, Zamboni P, Restifo NP, Zanovello P. Identification of a CD11b(+)/Gr-1(+)/CD31(+) myeloid progenitor capable of activating or suppressing CD8(+) T cells. Blood. 2000;96(12):3838-46. PubMed PMID: 11090068; PubMed Central PMCID: PMC2734459.

122. Singh UP, Singh NP, Singh B, Hofseth LJ, Taub DD, Price RL, Nagarkatti M, Nagarkatti PS. Role of resveratrol-induced CD11b(+) Gr-1(+) myeloid derived suppressor cells (MDSCs) in the reduction of CXCR3(+) T cells and amelioration of chronic colitis in IL-10(-/-) mice. Brain, behavior, and immunity. 2012;26(1):72-82. doi: 10.1016/j.bbi.2011.07.236. PubMed PMID: 21807089; PubMed Central PMCID: PMC3506001.

123. Zhang T, Zhou J, Man GCW, Leung KT, Liang B, Xiao B, Ma X, Huang S, Huang H, Hegde VL, Zhong Y, Li Y, Kong GWS, Yiu AKW, Kwong J, Ng PC, Lessey

BA, Nagarkatti PS, Nagarkatti M, Wang CC. MDSCs drive the process of endometriosis by enhancing angiogenesis and are a new potential therapeutic target. European journal of immunology. 2018;48(6):1059-73. doi: 10.1002/eji.201747417. PubMed PMID: 29460338; PubMed Central PMCID: PMC6273458.

124. Umansky V, Sevko A. Tumor microenvironment and myeloid-derived suppressor cells. Cancer microenvironment : official journal of the International Cancer Microenvironment Society. 2013;6(2):169-77. doi: 10.1007/s12307-012-0126-7. PubMed PMID: 23242672; PubMed Central PMCID: PMC3717060.

125. Veglia F, Perego M, Gabrilovich D. Myeloid-derived suppressor cells coming of age. Nature immunology. 2018;19(2):108-19. doi: 10.1038/s41590-017-0022-x. PubMed PMID: 29348500; PubMed Central PMCID: PMC5854158.

126. Dolcetti L, Marigo I, Mantelli B, Peranzoni E, Zanovello P, Bronte V. Myeloid-derived suppressor cell role in tumor-related inflammation. Cancer letters. 2008;267(2):216-25. doi: 10.1016/j.canlet.2008.03.012. PubMed PMID: 18433992.

127. Guan H, Singh NP, Singh UP, Nagarkatti PS, Nagarkatti M. Resveratrol prevents endothelial cells injury in high-dose interleukin-2 therapy against melanoma. PloS one. 2012;7(4):e35650. doi: 10.1371/journal.pone.0035650. PubMed PMID: 22532866; PubMed Central PMCID: PMC3331985.

128. Hoechst B, Gamrekelashvili J, Manns MP, Greten TF, Korangy F. Plasticity of human Th17 cells and iTregs is orchestrated by different subsets of myeloid cells. Blood. 2011;117(24):6532-41. doi: 10.1182/blood-2010-11-317321. PubMed PMID: 21493801.

129. Lebrun A, Lo Re S, Chantry M, Izquierdo Carerra X, Uwambayinema F, Ricci D, Devosse R, Ibouraadaten S, Brombin L, Palmai-Pallag M, Yakoub Y, Pasparakis M,

Lison D, Huaux F. CCR2(+) monocytic myeloid-derived suppressor cells (M-MDSCs) inhibit collagen degradation and promote lung fibrosis by producing transforming growth factor-beta1. The Journal of pathology. 2017;243(3):320-30. doi: 10.1002/path.4956. PubMed PMID: 28799208.

130. Moffat ID, Boutros PC, Celius T, Linden J, Pohjanvirta R, Okey AB. microRNAs in adult rodent liver are refractory to dioxin treatment. Toxicological sciences : an official journal of the Society of Toxicology. 2007;99(2):470-87. doi: 10.1093/toxsci/kfm189. PubMed PMID: 17698510.

131. Yoshioka W, Higashiyama W, Tohyama C. Involvement of microRNAs in dioxin-induced liver damage in the mouse. Toxicological sciences : an official journal of the Society of Toxicology. 2011;122(2):457-65. doi: 10.1093/toxsci/kfr130. PubMed PMID: 21602190.

132. Hanieh H. Aryl hydrocarbon receptor-microRNA-212/132 axis in human breast cancer suppresses metastasis by targeting SOX4. Molecular cancer. 2015;14:172. doi: 10.1186/s12943-015-0443-9. PubMed PMID: 26377202; PubMed Central PMCID: PMC4573482.

133. Sofo V, Gotte M, Lagana AS, Salmeri FM, Triolo O, Sturlese E, Retto G, Alfa M, Granese R, Abrao MS. Correlation between dioxin and endometriosis: an epigenetic route to unravel the pathogenesis of the disease. Archives of gynecology and obstetrics. 2015;292(5):973-86. doi: 10.1007/s00404-015-3739-5. PubMed PMID: 25920525.

134. Reithmair M, Buschmann D, Marte M, Kirchner B, Hagl D, Kaufmann I, Pfob M, Chouker A, Steinlein OK, Pfaffl MW, Schelling G. Cellular and extracellular miRNAs are blood-compartment-specific diagnostic targets in sepsis. Journal of cellular and

molecular medicine. 2017;21(10):2403-11. doi: 10.1111/jcmm.13162. PubMed PMID: 28382754; PubMed Central PMCID: PMC5618677.

135. Zhang R, Liu C, Niu Y, Jing Y, Zhang H, Wang J, Yang J, Zen K, Zhang J, Zhang CY, Li D. MicroRNA-128-3p regulates mitomycin C-induced DNA damage response in lung cancer cells through repressing SPTAN1. Oncotarget. 2017;8(35):58098-107. doi: 10.18632/oncotarget.12300. PubMed PMID: 28938540; PubMed Central PMCID: PMC5601636.

136. Lacedonia D, Palladino GP, Foschino-Barbaro MP, Scioscia G, Carpagnano GE. Expression profiling of miRNA-145 and miRNA-338 in serum and sputum of patients with COPD, asthma, and asthma-COPD overlap syndrome phenotype. International journal of chronic obstructive pulmonary disease. 2017;12:1811-7. doi: 10.2147/COPD.S130616. PubMed PMID: 28694694; PubMed Central PMCID: PMC5491577.

137. Tian J, Rui K, Tang X, Ma J, Wang Y, Tian X, Zhang Y, Xu H, Lu L, Wang S. MicroRNA-9 Regulates the Differentiation and Function of Myeloid-Derived Suppressor Cells via Targeting Runx1. Journal of immunology. 2015;195(3):1301-11. doi: 10.4049/jimmunol.1500209. PubMed PMID: 26091714.

138. Chen S, Zhang Y, Kuzel TM, Zhang B. Regulating Tumor Myeloid-Derived Suppressor Cells by MicroRNAs. Cancer cell & microenvironment. 2015;2(1). doi: 10.14800/ccm.637. PubMed PMID: 26005707; PubMed Central PMCID: PMC4440580.

139. Rebe C, Vegran F, Berger H, Ghiringhelli F. STAT3 activation: A key factor in tumor immunoescape. Jak-Stat. 2013;2(1):e23010. doi: 10.4161/jkst.23010. PubMed PMID: 24058791; PubMed Central PMCID: PMC3670267.

140. Munder M, Schneider H, Luckner C, Giese T, Langhans CD, Fuentes JM, Kropf P, Mueller I, Kolb A, Modolell M, Ho AD. Suppression of T-cell functions by human granulocyte arginase. Blood. 2006;108(5):1627-34. doi: 10.1182/blood-2006-11-010389. PubMed PMID: 16709924.

141. Sinha P, Clements VK, Bunt SK, Albelda SM, Ostrand-Rosenberg S. Cross-talk between myeloid-derived suppressor cells and macrophages subverts tumor immunity toward a type 2 response. Journal of immunology. 2007;179(2):977-83. PubMed PMID: 17617589.

142. Narlik-Grassow M, Blanco-Aparicio C, Carnero A. The PIM family of serine/threonine kinases in cancer. Medicinal research reviews. 2014;34(1):136-59. doi: 10.1002/med.21284. PubMed PMID: 23576269.

143. Lamas B, Richard ML, Leducq V, Pham HP, Michel ML, Da Costa G, Bridonneau C, Jegou S, Hoffmann TW, Natividad JM, Brot L, Taleb S, Couturier-Maillard A, Nion-Larmurier I, Merabtene F, Seksik P, Bourrier A, Cosnes J, Ryffel B, Beaugerie L, Launay JM, Langella P, Xavier RJ, Sokol H. CARD9 impacts colitis by altering gut microbiota metabolism of tryptophan into aryl hydrocarbon receptor ligands. Nature medicine. 2016;22(6):598-605. doi: 10.1038/nm.4102. PubMed PMID: 27158904; PubMed Central PMCID: PMC5087285.

144. Wheeler MA, Rothhammer V, Quintana FJ. Control of immune-mediated pathology via the aryl hydrocarbon receptor. The Journal of biological chemistry. 2017;292(30):12383-9. doi: 10.1074/jbc.R116.767723. PubMed PMID: 28615443; PubMed Central PMCID: PMC5535014.

145. Kumahara T. [Measurement of radiation energy and its application. II. 2. Electronics for energy measurement]. Radioisotopes. 1989;38(12):537-44. PubMed PMID: 2616821.

146. Carcinogens Report Adds Seven Agents. Cancer discovery. 2017;7(1):5. doi: 10.1158/2159-8290.CD-NB2016-150. PubMed PMID: 27872129.

147. Marshall NB, Vorachek WR, Steppan LB, Mourich DV, Kerkvliet NI. Functional characterization and gene expression analysis of CD4+ CD25+ regulatory T cells generated in mice treated with 2,3,7,8-tetrachlorodibenzo-p-dioxin. Journal of immunology. 2008;181(4):2382-91. PubMed PMID: 18684927; PubMed Central PMCID: PMC4118493.

148. Fader KA, Nault R, Ammendolia DA, Harkema JR, Williams KJ, Crawford RB, Kaminski NE, Potter D, Sharratt B, Zacharewski TR. 2,3,7,8-Tetrachlorodibenzo-p-Dioxin Alters Lipid Metabolism and Depletes Immune Cell Populations in the Jejunum of C57BL/6 Mice. Toxicological sciences : an official journal of the Society of Toxicology. 2015;148(2):567-80. doi: 10.1093/toxsci/kfv206. PubMed PMID: 26377647; PubMed Central PMCID: PMC5009443.

149. Faria AM, Weiner HL. Oral tolerance. Immunological reviews. 2005;206:232-59. doi: 10.1111/j.0105-2896.2005.00280.x. PubMed PMID: 16048553; PubMed Central PMCID: PMC3076704.

150. Kinoshita H, Abe J, Akadegawa K, Yurino H, Uchida T, Ikeda S, Matsushima K, Ishikawa S. Breakdown of mucosal immunity in gut by 2,3,7,8-tetraclorodibenzo-p-dioxin (TCDD). Environmental health and preventive medicine. 2006;11(5):256-63. doi:

10.1007/BF02898015. PubMed PMID: 21432354; PubMed Central PMCID: PMC2723348.

151. Artis D. Epithelial-cell recognition of commensal bacteria and maintenance of immune homeostasis in the gut. Nature reviews Immunology. 2008;8(6):411-20. doi: 10.1038/nri2316. PubMed PMID: 18469830.

152. Chmill S, Kadow S, Winter M, Weighardt H, Esser C. 2,3,7,8-Tetrachlorodibenzo-p-dioxin impairs stable establishment of oral tolerance in mice. Toxicological sciences : an official journal of the Society of Toxicology. 2010;118(1):98-107. doi: 10.1093/toxsci/kfq232. PubMed PMID: 20729464.

153. Stedtfeld RD, Stedtfeld TM, Fader KA, Williams MR, Bhaduri P, Quensen J, Zacharewski TR, Tiedje JM, Hashsham SA. TCDD influences reservoir of antibiotic resistance genes in murine gut microbiome. FEMS microbiology ecology. 2017;93(5). doi: 10.1093/femsec/fix058. PubMed PMID: 28475713; PubMed Central PMCID: PMC5458050.

154. Rhile MJ, Nagarkatti M, Nagarkatti PS. Role of Fas apoptosis and MHC genes in 2,3,7,8-tetrachlorodibenzo-p-dioxin (TCDD)-induced immunotoxicity of T cells. Toxicology. 1996;110(1-3):153-67. PubMed PMID: 8658555.

155. Nagarkatti PS, Sweeney GD, Gauldie J, Clark DA. Sensitivity to suppression of cytotoxic T cell generation by 2,3,7,8-tetrachlorodibenzo-p-dioxin (TCDD) is dependent on the Ah genotype of the murine host. Toxicology and applied pharmacology. 1984;72(1):169-76. PubMed PMID: 6608808.

156. Zeytun A, McKallip RJ, Fisher M, Camacho I, Nagarkatti M, Nagarkatti PS. Analysis of 2,3,7,8-tetrachlorodibenzo-p-dioxin-induced gene expression profile in vivo

using pathway-specific cDNA arrays. Toxicology. 2002;178(3):241-60. PubMed PMID: 12167310.

157. Ehrlich AK, Pennington JM, Bisson WH, Kolluri SK, Kerkvliet NI. TCDD, FICZ, and Other High Affinity AhR Ligands Dose-Dependently Determine the Fate of CD4+ T Cell Differentiation. Toxicological sciences : an official journal of the Society of Toxicology. 2018;161(2):310-20. doi: 10.1093/toxsci/kfx215. PubMed PMID: 29040756; PubMed Central PMCID: PMC5837604.

158. Camacho IA, Nagarkatti M, Nagarkatti PS. Effect of 2,3,7,8-tetrachlorodibenzo-p-dioxin (TCDD) on maternal immune response during pregnancy. Archives of toxicology. 2004;78(5):290-300. doi: 10.1007/s00204-003-0538-8. PubMed PMID: 15146310.

159. Gandy KAO, Zhang J, Nagarkatti P, Nagarkatti M. The role of gut microbiota in shaping the relapse-remitting and chronic-progressive forms of multiple sclerosis in mouse models. Scientific reports. 2019;9(1):6923. doi: 10.1038/s41598-019-43356-7. PubMed PMID: 31061496; PubMed Central PMCID: PMC6502871.

160. Segata N, Izard J, Waldron L, Gevers D, Miropolsky L, Garrett WS, Huttenhower C. Metagenomic biomarker discovery and explanation. Genome biology. 2011;12(6):R60. doi: 10.1186/gb-2011-12-6-r60. PubMed PMID: 21702898; PubMed Central PMCID: PMC3218848.

161. Mehrpouya-Bahrami P, Chitrala KN, Ganewatta MS, Tang C, Murphy EA, Enos RT, Velazquez KT, McCellan J, Nagarkatti M, Nagarkatti P. Blockade of CB1 cannabinoid receptor alters gut microbiota and attenuates inflammation and diet-induced

obesity. Scientific reports. 2017;7(1):15645. doi: 10.1038/s41598-017-15154-6. PubMed PMID: 29142285; PubMed Central PMCID: PMC5688117.

162. Li G, Xie C, Lu S, Nichols RG, Tian Y, Li L, Patel D, Ma Y, Brocker CN, Yan T, Krausz KW, Xiang R, Gavrilova O, Patterson AD, Gonzalez FJ. Intermittent Fasting Promotes White Adipose Browning and Decreases Obesity by Shaping the Gut Microbiota. Cell metabolism. 2017;26(5):801. doi: 10.1016/j.cmet.2017.10.007. PubMed PMID: 29117546; PubMed Central PMCID: PMC5695033.

163. Chevalier C, Stojanovic O, Colin DJ, Suarez-Zamorano N, Tarallo V, Veyrat-Durebex C, Rigo D, Fabbiano S, Stevanovic A, Hagemann S, Montet X, Seimbille Y, Zamboni N, Hapfelmeier S, Trajkovski M. Gut Microbiota Orchestrates Energy Homeostasis during Cold. Cell. 2015;163(6):1360-74. doi: 10.1016/j.cell.2015.11.004. PubMed PMID: 26638070.

164. Williams BL, Hornig M, Parekh T, Lipkin WI. Application of novel PCR-based methods for detection, quantitation, and phylogenetic characterization of Sutterella species in intestinal biopsy samples from children with autism and gastrointestinal disturbances. mBio. 2012;3(1). doi: 10.1128/mBio.00261-11. PubMed PMID: 22233678; PubMed Central PMCID: PMC3252763.

165. Kang B-H, Yang E-H, Kwon H-S, Yeon S-W, Kim T-Y. Rapid identification of probiotic Lactobacillus species by multiplex PCR using species-specific primers based on the region extending from 16S rRNA through 23S rRNA. FEMS Microbiology Letters. 2004;239(2):267-75. doi: 10.1016/j.femsle.2004.08.049.

166. Busbee PB, Rouse M, Nagarkatti M, Nagarkatti PS. Use of natural AhR ligands as potential therapeutic modalities against inflammatory disorders. Nutrition reviews.

2013;71(6):353-69. doi: 10.1111/nure.12024. PubMed PMID: 23731446; PubMed Central PMCID: PMC4076843.

167. Nakamura T, Nakao T, Ashihara E, Yoshimura N. Myeloid-derived Suppressor Cells Recruit CD4(+)/Foxp3(+) Regulatory T Cells in a Murine Cardiac Allograft. Transplantation proceedings. 2016;48(4):1275-8. doi: 10.1016/j.transproceed.2015.10.060. PubMed PMID: 27320602.

168. Pal S, Nandi M, Dey D, Chakraborty BC, Shil A, Ghosh S, Banerjee S, Santra A, Ahammed SKM, Chowdhury A, Datta S. Myeloid-derived suppressor cells induce regulatory T cells in chronically HBV infected patients with high levels of hepatitis B surface antigen and persist after antiviral therapy. Alimentary pharmacology & therapeutics. 2019;49(10):1346-59. doi: 10.1111/apt.15226. PubMed PMID: 30982998.

169. Zhang H, Ye YL, Li MX, Ye SB, Huang WR, Cai TT, He J, Peng JY, Duan TH, Cui J, Zhang XS, Zhou FJ, Wang RF, Li J. CXCL2/MIF-CXCR2 signaling promotes the recruitment of myeloid-derived suppressor cells and is correlated with prognosis in bladder cancer. Oncogene. 2017;36(15):2095-104. doi: 10.1038/onc.2016.367. PubMed PMID: 27721403.

170. Rooks MG, Garrett WS. Gut microbiota, metabolites and host immunity. Nature reviews Immunology. 2016;16(6):341-52. doi: 10.1038/nri.2016.42. PubMed PMID: 27231050; PubMed Central PMCID: PMC5541232.

171. Alam MM, O'Neill LA. MicroRNAs and the resolution phase of inflammation in macrophages. European journal of immunology. 2011;41(9):2482-5. doi: 10.1002/eji.201141740. PubMed PMID: 21952801.

172. Jin UH, Cheng Y, Park H, Davidson LA, Callaway ES, Chapkin RS, Jayaraman A, Asante A, Allred C, Weaver EA, Safe S. Short Chain Fatty Acids Enhance Aryl Hydrocarbon (Ah) Responsiveness in Mouse Colonocytes and Caco-2 Human Colon Cancer Cells. Scientific reports. 2017;7(1):10163. doi: 10.1038/s41598-017-10824-x. PubMed PMID: 28860561; PubMed Central PMCID: PMC5579248.

173. Fader KA, Nault R, Zhang C, Kumagai K, Harkema JR, Zacharewski TR. 2,3,7,8-Tetrachlorodibenzo-p-dioxin (TCDD)-elicited effects on bile acid homeostasis: Alterations in biosynthesis, enterohepatic circulation, and microbial metabolism. Scientific reports. 2017;7(1):5921. doi: 10.1038/s41598-017-05656-8. PubMed PMID: 28725001; PubMed Central PMCID: PMC5517430.

174. Jin C, Zeng Z, Fu Z, Jin Y. Oral imazalil exposure induces gut microbiota dysbiosis and colonic inflammation in mice. Chemosphere. 2016;160:349-58. doi: 10.1016/j.chemosphere.2016.06.105. PubMed PMID: 27393971.

175. Tang C, Sun J, Zhou B, Jin C, Liu J, Kan J, Qian C, Zhang N. Effects of polysaccharides from purple sweet potatoes on immune response and gut microbiota composition in normal and cyclophosphamide treated mice. Food & function. 2018;9(2):937-50. doi: 10.1039/c7fo01302g. PubMed PMID: 29322139.

176. Pena JA, Rogers AB, Ge Z, Ng V, Li SY, Fox JG, Versalovic J. Probiotic Lactobacillus spp. diminish Helicobacter hepaticus-induced inflammatory bowel disease in interleukin-10-deficient mice. Infection and immunity. 2005;73(2):912-20. doi: 10.1128/IAI.73.2.912-920.2005. PubMed PMID: 15664933; PubMed Central PMCID: PMC547020.

177. Cummings JH, Pomare EW, Branch WJ, Naylor CP, Macfarlane GT. Short chain fatty acids in human large intestine, portal, hepatic and venous blood. Gut. 1987;28(10):1221-7. PubMed PMID: 3678950; PubMed Central PMCID: PMC1433442.

178. Arpaia N, Campbell C, Fan X, Dikiy S, van der Veeken J, deRoos P, Liu H, Cross JR, Pfeffer K, Coffer PJ, Rudensky AY. Metabolites produced by commensal bacteria promote peripheral regulatory T-cell generation. Nature. 2013;504(7480):451-5. doi: 10.1038/nature12726. PubMed PMID: 24226773; PubMed Central PMCID: PMC3869884.

179. Chang PV, Hao L, Offermanns S, Medzhitov R. The microbial metabolite butyrate regulates intestinal macrophage function via histone deacetylase inhibition. Proceedings of the National Academy of Sciences of the United States of America. 2014;111(6):2247-52. doi: 10.1073/pnas.1322269111. PubMed PMID: 24390544; PubMed Central PMCID: PMC3926023.

180. Trompette A, Gollwitzer ES, Yadava K, Sichelstiel AK, Sprenger N, Ngom-Bru C, Blanchard C, Junt T, Nicod LP, Harris NL, Marsland BJ. Gut microbiota metabolism of dietary fiber influences allergic airway disease and hematopoiesis. Nature medicine. 2014;20(2):159-66. doi: 10.1038/nm.3444. PubMed PMID: 24390308.

181. Tao R, de Zoeten EF, Ozkaynak E, Chen C, Wang L, Porrett PM, Li B, Turka LA, Olson EN, Greene MI, Wells AD, Hancock WW. Deacetylase inhibition promotes the generation and function of regulatory T cells. Nature medicine. 2007;13(11):1299-307. doi: 10.1038/nm1652. PubMed PMID: 17922010.

182. Martin-Gallausiaux C, Beguet-Crespel F, Marinelli L, Jamet A, Ledue F, Blottiere HM, Lapaque N. Butyrate produced by gut commensal bacteria activates TGF-beta1

expression through the transcription factor SP1 in human intestinal epithelial cells. Scientific reports. 2018;8(1):9742. doi: 10.1038/s41598-018-28048-y. PubMed PMID: 29950699; PubMed Central PMCID: PMC6021401.

183. Iglehart JK, York RM, Modest AP, Lazarus H, Livingston DM. Cystine requirement of continuous human lymphoid cell lines of normal and leukemic origin. The Journal of biological chemistry. 1977;252(20):7184-91. PubMed PMID: 903356.

184. Yamauchi A, Bloom ET. Requirement of thiol compounds as reducing agents for IL-2-mediated induction of LAK activity and proliferation of human NK cells. Journal of immunology. 1993;151(10):5535-44. PubMed PMID: 8228244.

185. Gmunder H, Eck HP, Droge W. Low membrane transport activity for cystine in resting and mitogenically stimulated human lymphocyte preparations and human T cell clones. European journal of biochemistry. 1991;201(1):113-7. PubMed PMID: 1680678.

186. Eagle H, Washington C, Friedman SM. The synthesis of homocystine, cystathionine, and cystine by cultured diploid and heteroploid human cells. Proceedings of the National Academy of Sciences of the United States of America. 1966;56(1):156-63. PubMed PMID: 5229844; PubMed Central PMCID: PMC285689.

187. Bannai S. Transport of cystine and cysteine in mammalian cells. Biochimica et biophysica acta. 1984;779(3):289-306. PubMed PMID: 6383474.

188. Gmunder H, Eck HP, Benninghoff B, Roth S, Droge W. Macrophages regulate intracellular glutathione levels of lymphocytes. Evidence for an immunoregulatory role of cysteine. Cellular immunology. 1990;129(1):32-46. PubMed PMID: 2364441.

189. Sato H, Watanabe H, Ishii T, Bannai S. Neutral amino acid transport in mouse peritoneal macrophages. The Journal of biological chemistry. 1987;262(27):13015-9. PubMed PMID: 3115975.

190. Wuthrich D, Wenzel C, Bavan T, Bruggmann R, Berthoud H, Irmler S. Transcriptional Regulation of Cysteine and Methionine Metabolism in Lactobacillus paracasei FAM18149. Frontiers in microbiology. 2018;9:1261. doi: 10.3389/fmicb.2018.01261. PubMed PMID: 29942297; PubMed Central PMCID: PMCPMC6004538.

191. Weiskopf K, Schnorr PJ, Pang WW, Chao MP, Chhabra A, Seita J, Feng M, Weissman IL. Myeloid Cell Origins, Differentiation, and Clinical Implications. Microbiology spectrum. 2016;4(5). doi: 10.1128/microbiolspec.MCHD-0031-2016. PubMed PMID: 27763252; PubMed Central PMCID: PMC5119546.

192. Velten L, Haas SF, Raffel S, Blaszkiewicz S, Islam S, Hennig BP, Hirche C, Lutz C, Buss EC, Nowak D, Boch T, Hofmann WK, Ho AD, Huber W, Trumpp A, Essers MA, Steinmetz LM. Human haematopoietic stem cell lineage commitment is a continuous process. Nature cell biology. 2017;19(4):271-81. doi: 10.1038/ncb3493. PubMed PMID: 28319093; PubMed Central PMCID: PMC5496982.

193. Ioannou M, Alissafi T, Lazaridis I, Deraos G, Matsoukas J, Gravanis A, Mastorodemos V, Plaitakis A, Sharpe A, Boumpas D, Verginis P. Crucial role of granulocytic myeloid-derived suppressor cells in the regulation of central nervous system autoimmune disease. Journal of immunology. 2012;188(3):1136-46. doi: 10.4049/jimmunol.1101816. PubMed PMID: 22210912.

194. Dorhoi A, Du Plessis N. Monocytic Myeloid-Derived Suppressor Cells in Chronic Infections. Frontiers in immunology. 2017;8:1895. doi: 10.3389/fimmu.2017.01895. PubMed PMID: 29354120; PubMed Central PMCID: PMC5758551.

195. Meyer C, Sevko A, Ramacher M, Bazhin AV, Falk CS, Osen W, Borrello I, Kato M, Schadendorf D, Baniyash M, Umansky V. Chronic inflammation promotes myeloid-derived suppressor cell activation blocking antitumor immunity in transgenic mouse melanoma model. Proceedings of the National Academy of Sciences of the United States of America. 2011;108(41):17111-6. doi: 10.1073/pnas.1108121108. PubMed PMID: 21969559; PubMed Central PMCID: PMC3193202.

196. Movahedi K, Guilliams M, Van den Bossche J, Van den Bergh R, Gysemans C, Beschin A, De Baetselier P, Van Ginderachter JA. Identification of discrete tumor-induced myeloid-derived suppressor cell subpopulations with distinct T cell-suppressive activity. Blood. 2008;111(8):4233-44. doi: 10.1182/blood-2007-07-099226. PubMed PMID: 18272812.

197. Cassado Ados A, D'Imperio Lima MR, Bortoluci KR. Revisiting mouse peritoneal macrophages: heterogeneity, development, and function. Frontiers in immunology. 2015;6:225. doi: 10.3389/fimmu.2015.00225. PubMed PMID: 26042120; PubMed Central PMCID: PMC4437037.

198. Rothhammer V, Quintana FJ. The aryl hydrocarbon receptor: an environmental sensor integrating immune responses in health and disease. Nature reviews Immunology. 2019. doi: 10.1038/s41577-019-0125-8. PubMed PMID: 30718831.

199. Frericks M, Temchura VV, Majora M, Stutte S, Esser C. Transcriptional signatures of immune cells in aryl hydrocarbon receptor (AHR)-proficient and AHR-

deficient mice. Biological chemistry. 2006;387(9):1219-26. doi: 10.1515/BC.2006.151. PubMed PMID: 16972790.

200. Sekine H, Mimura J, Oshima M, Okawa H, Kanno J, Igarashi K, Gonzalez FJ, Ikuta T, Kawajiri K, Fujii-Kuriyama Y. Hypersensitivity of aryl hydrocarbon receptor-deficient mice to lipopolysaccharide-induced septic shock. Molecular and cellular biology. 2009;29(24):6391-400. doi: 10.1128/MCB.00337-09. PubMed PMID: 19822660; PubMed Central PMCID: PMC2786870.

201. Laupeze B, Amiot L, Sparfel L, Le Ferrec E, Fauchet R, Fardel O. Polycyclic aromatic hydrocarbons affect functional differentiation and maturation of human monocyte-derived dendritic cells. Journal of immunology. 2002;168(6):2652-8. PubMed PMID: 11884429.

202. van Grevenynghe J, Rion S, Le Ferrec E, Le Vee M, Amiot L, Fauchet R, Fardel O. Polycyclic aromatic hydrocarbons inhibit differentiation of human monocytes into macrophages. Journal of immunology. 2003;170(5):2374-81. PubMed PMID: 12594260.

203. Riemschneider S, Kohlschmidt J, Fueldner C, Esser C, Hauschildt S, Lehmann J. Aryl hydrocarbon receptor activation by benzo(a)pyrene inhibits proliferation of myeloid precursor cells and alters the differentiation state as well as the functional phenotype of murine bone marrow-derived macrophages. Toxicology letters. 2018;296:106-13. doi: 10.1016/j.toxlet.2018.07.050. PubMed PMID: 30099064.

204. Ghosn EE, Cassado AA, Govoni GR, Fukuhara T, Yang Y, Monack DM, Bortoluci KR, Almeida SR, Herzenberg LA, Herzenberg LA. Two physically, functionally, and developmentally distinct peritoneal macrophage subsets. Proceedings of the National Academy of Sciences of the United States of America. 2010;107(6):2568-

73. doi: 10.1073/pnas.0915000107. PubMed PMID: 20133793; PubMed Central PMCID: PMC2823920.

205. Singh NP, Singh US, Nagarkatti M, Nagarkatti PS. Resveratrol (3,5,4'-trihydroxystilbene) protects pregnant mother and fetus from the immunotoxic effects of 2,3,7,8-tetrachlorodibenzo-p-dioxin. Molecular nutrition & food research. 2011;55(2):209-19. doi: 10.1002/mnfr.201000206. PubMed PMID: 20715097; PubMed Central PMCID: PMC3061307.

206. Kerkvliet NI. Immunological effects of chlorinated dibenzo-p-dioxins. Environmental health perspectives. 1995;103 Suppl 9:47-53. doi: 10.1289/ehp.95103s947. PubMed PMID: 8635439; PubMed Central PMCID: PMC1518816.

207. Finnell JE, Lombard CM, Melson MN, Singh NP, Nagarkatti M, Nagarkatti P, Fadel JR, Wood CS, Wood SK. The protective effects of resveratrol on social stress-induced cytokine release and depressive-like behavior. Brain, behavior, and immunity. 2017;59:147-57. doi: 10.1016/j.bbi.2016.08.019. PubMed PMID: 27592314; PubMed Central PMCID: PMC5154920.

208. Uehara T, Eikawa S, Nishida M, Kunisada Y, Yoshida A, Fujiwara T, Kunisada T, Ozaki T, Udono H. Metformin induces CD11b+-cell-mediated growth inhibition of an osteosarcoma: implications for metabolic reprogramming of myeloid cells and anti-tumor effects. International immunology. 2019;31(4):187-98. doi: 10.1093/intimm/dxy079. PubMed PMID: 30508092; PubMed Central PMCID: PMC6440441.

209. Esser C, Rannug A. The aryl hydrocarbon receptor in barrier organ physiology, immunology, and toxicology. Pharmacological reviews. 2015;67(2):259-79. doi: 10.1124/pr.114.009001. PubMed PMID: 25657351.